UNIVERSITY OF COPENHAGEN
FACULTY OF SCIENCE

MASTER THESIS

On the Holographic Complexity of Janus Geometries

Kristian Toccacelo

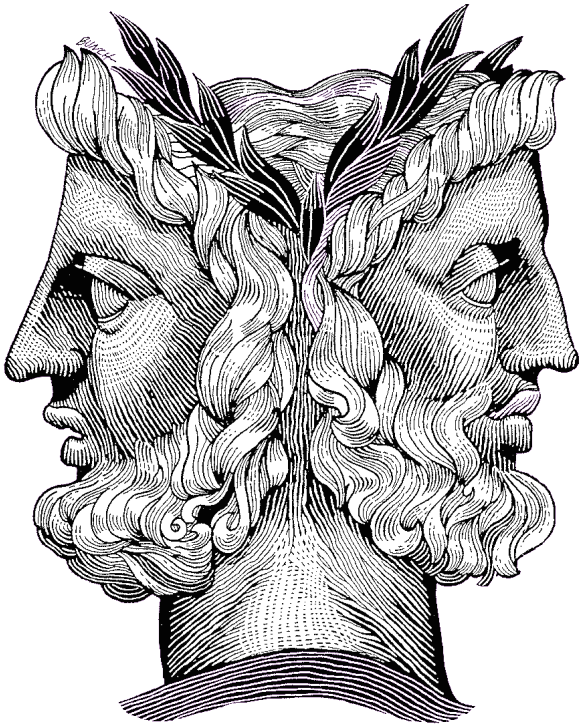

Advisors: Stefano Baiguera, Troels Harmark

Abstract

In this thesis we seek to investigate the Complexity = Volume conjecture in the context of Janus deformed geometries. This work is based on the arXiv submissions [1] and [2]. We discuss the case of Janus AdS_3 geometries, both at vanishing and finite temperature. The leading divergence of the volume complexity associated to the Janus interface is logarithmic, and its coefficient is a function of the deformation parameter. Contrarily to the BTZ background, the finite-temperature Janus deformation complexity is not topological and is therefore temperature-dependent. We also consider the time-evolution of the extremal-volume for the time-dependent Janus BTZ black hole. This background is dual to a pair of entangled CFTs with different couplings. The complexity rate for the early time out-of-equilibrium state is always smaller compared to the pure BTZ black hole. However, when the equilibrium is restored at late times, the CFT couplings don't influence the complexification rate. Finally, we compute the volume complexity for the AdS_5 Janus interface. In this case, the leading divergence is inversely proportional to the square of the cutoff parameter. Interestingly, when the boundary is separated into two subregions, a subleading logarithmic divergence appears. Similarly to entanglement entropy, this behavior my be ascribed to short range correlations entangling degrees of freedom across the dividing surface.

Contents

1 The AdS/CFT Correspondence **6**
- 1.1 Conformal Field Theories . . . 6
  - 1.1.1 Conformal Symmetry . . . 6
  - 1.1.2 Some Consequences of Conformal Invariance in QFTs . . . 7
- 1.2 Anti-de Sitter Spacetime . . . 8
  - 1.2.1 Maximally Symmetric Spaces: Euclidean Spheres and Euclidean AdS . . . 9
  - 1.2.2 Lorentzian AdS . . . 9
  - 1.2.3 Asymptotically AdS Spacetimes . . . 11
  - 1.2.4 Quantization of a Scalar Field in AdS_{d+1} . . . 11
- 1.3 Black Hole Thermodynamics and Holography . . . 13
  - 1.3.1 Black Hole Temperature . . . 13
  - 1.3.2 Black Hole Thermodynamics and the Holographic Principle . . . 15
- 1.4 AdS/CFT . . . 16
  - 1.4.1 Formulation of the Correspondence . . . 17
  - 1.4.2 Infrared vs. Ultraviolet . . . 18
  - 1.4.3 Mass Dimension Duality . . . 18
  - 1.4.4 AdS/CFT at Finite Temperature . . . 19

2 Holographic Entanglement Entropy **22**
- 2.1 Entanglement Entropy . . . 22
- 2.2 Entanglement Entropy in QFTs . . . 24
  - 2.2.1 Replica Trick . . . 25
- 2.3 Thermofield Double State . . . 26
  - 2.3.1 Eternal Black Holes and Thermofield Double States . . . 27
- 2.4 Holographic Entanglement Entropy . . . 28
  - 2.4.1 Heuristic Motivation of the RT Formula . . . 28
  - 2.4.2 An Example . . . 29
  - 2.4.3 Holographic Proof of Strong Sub-additivity . . . 30

3 Holographic Complexity **31**
- 3.1 Quantum Computational Complexity . . . 31
  - 3.1.1 Growth Rate of Complexity . . . 33
- 3.2 Complexity from Holgraphy . . . 34
  - 3.2.1 Growth of the Einstein-Rosen bridge: Complexity = Volume . . . 34
  - 3.2.2 Complexity = Action . . . 35
  - 3.2.3 Subregion Complexity . . . 37
- 3.3 Complexity in Quantum Field Theories . . . 37

4 Janus Geometries **39**
4.1 Three-dimensional Janus . . . 39
4.1.1 Conformal Diagram of the Janus Geometry . . . 41
4.1.2 Fefferman-Graham Expansion of the Janus AdS_3 Geometry . . . 43
4.1.3 Holographic Boundary Entropy of the AdS_3 Janus Solution . . . 44
4.2 Five-dimensional Janus Deformations . . . 45
4.2.1 Non-SUSY Janus AdS_5 . . . 45
4.3 BTZ-like Janus Solutions . . . 46
4.3.1 Static Janus BTZ Background . . . 47
4.3.2 Time-dependent Janus BTZ Background . . . 48

5 Volume Complexity for Three-dimensional Janus Geometries **51**
5.1 Regularization Schemes for AdS_d-Sliced Defect Geometries . . . 51
5.1.1 Fefferman-Graham Regularization . . . 52
5.1.2 Single Cutoff Regularization . . . 53
5.1.3 Double Cutoff Regularization . . . 54
5.2 Volume of Janus AdS_3 . . . 54
5.2.1 Remarks on Time-dependence . . . 57
5.3 Volume of the Static Janus BTZ Black Hole . . . 57
5.4 Volume of the Time-dependent Janus BTZ Geometry . . . 60
5.4.1 Volume at Vanishing Boundary Time . . . 60
5.4.2 Growth Rate of the Volume . . . 61

6 Volume Complexity for Janus AdS_5 **68**
6.1 Volume of the AdS_5 Janus Deformation . . . 68
6.1.1 Determination of the Cutoffs . . . 68
6.1.2 Computation of the Volume . . . 69
6.2 Subregion Volume for the Janus AdS_5 Geometry . . . 73
6.2.1 Ball-shaped Subregion on the Boundary . . . 73
6.2.2 Extremal Volume: Single Cutoff . . . 74

7 Closing Remarks **77**

A Useful Special Functions **81**
A.1 Jacobi Elliptic Functions and Elliptic Integrals . . . 81
A.2 Weierstrass Elliptic Functions . . . 82

B Alternative Regularizations **83**
B.1 Janus AdS_3 Volume: Fefferman-Graham Regularization . . . 83
B.1.1 Integration in the FG Patches . . . 83
B.1.2 Interpolation in the Middle Region . . . 84
B.2 Janus AdS_3 Volume: Double Cutoff Regularization . . . 85
B.3 Janus AdS_5: Double Cutoff Regularization . . . 85
B.3.1 Computation of the Volume . . . 86
B.3.2 Subregion Volume . . . 87

Opening Remarks

The idea that quantum gravity in an asymptotically AdS spacetime can be described through a conformal field theory living at the boundary [3], has been widely celebrated as one of the greatest achievements of early 21st century theoretical physics. As it stands, the AdS/CFT correspondence provides a powerful non-perturbative framework to investigate the properties of a subset of theories of quantum gravity.

Relatively recent progress in this field has unveiled remarkable connections between the theory of quantum information and quantum gravity. This all started back in the 70's, when Bekenstein and Hawking discovered that black holes can be treated as thermodynamic objects with an entropy proportional to the area of the horizon [4, 5]. Later, this idea was applied and generalized to the AdS/CFT correspondence. In fact, in holography the entropy of a spatial subsystem in the boundary CFT is realized through the Ryu-Takayanagi formula [6]; via this formula we can attain the entropy by computing the area of a codimension-1 surface embedded in the bulk spacetime and anchored to the subregion at the boundary.

Lately, another quantum information quantity has attracted a tremendous amount of attention: computational complexity. It was first introduced to explain the evolution in time of the Einstein-Rosen bridge [7], as this growth can't be accounted for by entanglement entropy since the wormhole keeps on growing long after the thermalization time. Or, as Susskind himself put it, *entanglement is not enough*.

Quantum complexity is usually defined in quantum circuits as the minimum number of $k-$local gates connecting a generic state in the Hilbert space to a reference state in the same Hilbert space. Two proposals have emerged as to what bulk quantity is dual to the complexity of states in the boundary. The first proposal, known as the CV conjecture (or the complexity = volume conjecture), states that complexity is dual to the maximal volume of a codimension-one sub-manifold attached to the boundary [7]. The other proposal is the so-called CA conjecture (or the complexity = action conjecture), which relates the complexity of states to the bulk action evaluated on a spacetime region known as the Wheeler-de Witt patch [8], that is, the bulk domain of dependence of a Cauchy surface anchored at the boundary state.

To this date, it is still not clear which conjecture should be favored, for this reason, it is crucial that we understand the differences between the conjectures. Despite exhibiting the same behavior at late times [9, 10], the two proposals differ in the early time behavior [11]. A more radical difference was discovered when considering a theory deformed by a defect. In fact, in [12] it was shown that for the AdS_3 Randall-Sundrum model the CV complexity features a logarithmic divergence coming from the defect whilst the CA complexity is devoid of such divergence. It was later shown in [13] that this is not always true, for in the $d > 2$ dimensional case the BCFT dual geometry does not distinguish CA from CV. However, this begs the question: what happens in different defect geometries? Particularly, what happens in interface theories?

This leads us neatly to the content of this master thesis. The starting point is a three-dimensional dilatonic deformation of AdS space known as the Janus geometry [14]. This geometry is known to have a clear holographic dual, since it can be embedded into type IIB supergravity in 10 dimensions over $AdS_3 \times \mathbf{S}^3 \times \mathcal{M}_4$, where $\mathcal{M}_4$ is a compact internal manifold. The resulting geometry is very similar to an AdS_2 foliation of AdS_3, the only difference is that the AdS_2 slices are multiplied by a non-trivial function of the remaining coordinate and

a deformation parameter γ. On the CFT side this geometry is dual to two CFTs with different couplings separated by an interface. Since the three-dimensional BTZ black hole is locally equivalent to vacuum AdS_3 space, there exist two generalizations of the Janus geometry where an horizon appears: the static Janus BTZ black hole, and the time dependent Janus BTZ black hole. The former is obtained by simply replacing the AdS_2 factor with a Rindler-like metric [15], whilst the latter represents a time dependent black hole geometry describing non-equilibrium physics [16]. The Janus deformation can also be implemented in $AdS_5 \times \mathbf{S}^5$, not only in a way that completely breaks supersymmetry [17] but also in a way that preserves $\mathbf{SO}(2,3) \times \mathbf{SU}(3)$ symmetry [18]. We will solely focus on the non-supersymmetric solution.

In this thesis we answer the question of how Janus interfaces affect complexity in the aforementioned CV conjecture. The thesis is structured in the following way. In chapters 1, 2, 3, and 4 all preliminary material is collected. In chapter 1 after having introduced CFTs, AdS spacetimes, and discussed black hole thermodynamics a lightning review of AdS/CFT is presented. In the chapters 2 and 3 we discuss respectively entanglement entropy and complexity from a holographic point of view. In chapter 4 we discuss the geometries which will be the object of study in the subsequent chapters. In chapter 5, which is based on the work [1], we apply CV in the context of three-dimensional Janus geometries, and in chapter 6, which is based on a work we will publish in the near future [2], we apply CV in the five-dimensional Janus geometry. Finally, we discuss our findings in chapter 7.

Chapter 1

The AdS/CFT Correspondence

1.1 Conformal Field Theories

Apart from being one of the two ingredients in the AdS/CFT correspondence, CFTs can be regarded as one of the hallmarks of modern theoretical physics. A conformal field theory is a theory (classical or quantum mechanical) that is invariant under the conformal group. We will soon see what this means in some detail, but one immediate consequence is that CFTs are scale-invariant theories. As such, CFTs characterize fixed points in renormalization group flows: CFTs are in some sense the only *true* QFTs. Conformal field theories are also very useful in modeling many body quantum systems near-criticality, that is, near or at a second order phase transition.

We will now summarize some of the most important facts about CFTs. This section follows the notes by F. Alday [19].

1.1.1 Conformal Symmetry

Consider a spacetime $\mathcal{M}$ equipped with metric $g_{\mu\nu}$, a conformal transformation is an invertible map $x \to x(x')$ that leaves the metric invariant up to a local rescaling factor, that is,

$$g'_{\mu\nu}(x') = \Lambda(x) g_{\mu\nu}(x). \tag{1.1}$$

The conformal group $\mathrm{Conf}(\mathcal{M})$ is the set of all such transformations.

When $\mathcal{M} = \mathbb{R}^d$ the conformal group can be easily classified by looking at infinitesimal conformal transformations, $x^\mu \to x^\mu + \epsilon^\mu(x)$. It turns out that in order for this to be a proper infinitesimal conformal transformation the function $\epsilon(x)$ can at most be a quadratic function of x, meaning that

$$\epsilon_\mu(x) = a_\mu + b_{\mu\nu} x^\nu + c_{\mu\nu\rho} x^\nu x^\rho, \tag{1.2}$$

with the following constraints:

- a_μ is free of constraints, and correspond to infinitesimal translations;
- $b_{\mu\nu} = \alpha \eta_{\mu\nu} + m_{\mu\nu}$, with $m_{\mu\nu} = -m_{\nu\mu}$. The trace b is the generator of infinitesimal dilations, while $m_{\mu\nu}$ is the generator of infinitesimal Lorentz transformations; and
- $c_{\mu\nu\rho} = \eta_{\mu\rho} b_\nu + \eta_{\mu\nu} b_\rho - \eta_{\nu\rho} b_\mu$, where $b_\mu \in \mathbb{R}^d$. These correspond to infinitesimal *special conformal* transformations.

From these infinitesimal transformations we can move to the finite versions, namely:

- translations

$$x^\mu \to x^\mu + a^\mu;$$

- rigid rotations
$$x^\mu \to M^\mu{}_\nu x^\nu;$$
- dilations
$$x^\mu \to \lambda x^\mu;$$
and
- special conformal transformations
$$x^\mu \to \frac{x^\mu - b^\mu x^2}{1 - 2b\cdot x + b^2 x^2}.$$

Any conformal transformation is either one of the above or a combination thereof. It is fairly straightforward to check that the set of conformal transformations possesses the structure of a group. In d-dimensions the nuber of generators is in total
$$\frac{(d+1)(d+2)}{2}. \tag{1.3}$$

One can at this point determine an explicit representation of these generators by examining the way a conformal transformation acts on a given field, and it turns out that:

- translations are generated by $P_\mu = -i\partial_\mu$;
- rigid rotations are generated by $L_{\mu\nu} = i(x_\mu\partial_\nu - x_\nu\partial_\mu)$;
- dilations are generated by $D = -ix^\mu\partial_\mu$; and
- SCT are generated by $K_\mu = -i(2x_\mu x^\nu\partial_\nu - x^2\partial_\mu)$.

One can quite readily determine the corresponding commutational relations which then define the so-called conformal algebra, that is, the Lie algebra corresponding to the conformal group,

$$\begin{aligned}
&[D, P_\mu] = iP_\mu\,, \quad [D, K_\mu] = iK_\mu\,, \quad [K_\mu, P_\nu] = 2i\left(\eta_{\mu\nu}D - L_{\mu\nu}\right)\\
&[L_{\mu\nu}, P_\rho] = -i\left(\eta_{\mu\rho}P_\nu - \eta_{\nu\rho}P_\mu\right)\,, \quad [L_{\mu\nu}, K_\rho] = -i\left(\eta_{\mu\rho}K_\nu - \eta_{\nu\rho}K_\mu\right)\\
&[L_{\mu\nu}, L_{\rho\sigma}] = -i\left(L_{\mu\rho}\eta_{\nu\sigma} - L_{\mu\sigma}\eta_{\nu\rho} - L_{\nu\rho}\eta_{\mu\sigma} + L_{\nu\sigma}\eta_{\mu\rho}\right)\,,\\
&[D, L_{\mu\nu}] = 0\,, \quad [P_\mu, P_\nu] = 0\,, \quad [K_\mu, K_\nu] = 0\,, \quad [D, D] = 0\,.
\end{aligned}$$

The conformal algebra in d dimensions is isomorphic to $\mathbf{SO}(d+1,1)$, or equivalently $\mathbf{SO}(d,2)$.

1.1.2 Some Consequences of Conformal Invariance in QFTs

In a quantum field theory, the degrees of freedom are local field operators, which we can be imagined as multi-component operators $\phi_\alpha(x)$, and the symmetries are realized by operators acting on these local operators. When we also have conformal invariance to play with we can classify the operators based on the way in which the generators of the stability group of $\mathbf{Conf}(\mathbb{R}^d)$ (i.e., the subgroup that leaves the origin invariant) act on the given field. We call a field $\phi_\alpha(x)$ that satisfies the following

$$[D, \phi_\alpha(0)] = i\Delta\phi_\alpha(0), \quad [L_{\mu\nu}, \phi_\alpha(0)] = i(S_{\mu\nu})^\beta_\alpha\phi_\beta(0), \quad [K_\mu, \phi_\alpha(0)] = 0, \tag{1.4}$$

a *primary operator* of scaling dimension Δ.

With the aid of the Heisenberg representation $\phi_\alpha(x) = e^{-iPx}\phi_\alpha(0)e^{iPx}$, it is possible to work out the way in which the generators of the conformal algebra act on a given operator, and from

there it's possible For example a spinless scalar primary field of scaling dimension Δ transforms under a conformal transformation $x \to x'$ as

$$\phi(x) \to \left|\frac{\partial x'}{\partial x}\right|^{-\Delta/d} \phi(x), \tag{1.5}$$

which can be written as

$$\phi(x) \to \Lambda(x)^{\Delta/2}\phi(x). \tag{1.6}$$

where we relabelled the jacobian as $|\partial x'/\partial x| = \Lambda(x)^{-d/2}$. By acting on a primary operator with derivatives we get a *descendant* operator, the scaling dimension of which is determined by the number of derivatives plus the scaling dimension of the primary it descended from.

Correlation functions are the main object of study of QFTs, these may be defined in the path integral formulation as

$$\langle \phi(x_1)\cdots\phi(x_n)\rangle = \frac{1}{Z}\int \mathcal{D}\phi\, \phi(x_1)\cdots\phi(x_n)e^{-S[\phi]}. \tag{1.7}$$

If the theory is invariant under some symmetry transformation $\phi'(x') = \mathcal{F}(\phi(x))$, then we have

$$\langle \phi(x_1')\cdots\phi(x_n')\rangle = \langle \mathcal{F}(\phi(x_1))\cdots\mathcal{F}(\phi(x_n))\rangle. \tag{1.8}$$

So, if the theory is invariant under the full conformal group, for correlators involving spinless primary fields transforming according to (1.5), we must have

$$\langle \phi(x_1')\cdots\phi(x_n')\rangle = \left|\frac{\partial x'}{\partial x}\right|^{-\Delta_1/d}_{x=x_1} \cdots \left|\frac{\partial x'}{\partial x}\right|^{-\Delta_n/d}_{x=x_n} \langle \phi(x_1)\cdots\phi(x_n)\rangle \tag{1.9}$$

This has some serious consequences on the general form of two- and three-point functions. In fact, it turns out that the most general two-point correlator is given by

$$\langle \phi_1(x_1)\phi_2(x_2)\rangle = \frac{1}{|x_{12}|^{2\Delta}} \tag{1.10}$$

if $\Delta_1 = \Delta_2 = \Delta$, and there are no correlations if the scaling dimensions differ. In the case of three-point correlation functions, we have

$$\langle \phi_1(x_1)\phi_2(x_2)\phi_3(x_3)\rangle = \frac{C_{123}}{|x_{12}|^{\Delta_1+\Delta_2-\Delta_3}|x_{23}|^{\Delta_2+\Delta_3-\Delta_1}|x_{13}|^{\Delta_3+\Delta_1-\Delta_2}}, \tag{1.11}$$

where C_{123} is a constant with non-trivial physical content.

A very important property of CFTs is the so-called *state/operator correspondence*, which states that: the set of all primary operators and descendants at any given point x is in a one-to-one correspondence with an eigenbasis of Hilbert space of the CFT quantized on $\mathbf{S}^{d-1}$.

1.2 Anti-de Sitter Spacetime

The other ingredient that makes up AdS/CFT is Anti-de Sitter spacetime. AdS is a maximally symmetric solution to the Einstein equation with negative cosmological constant, as opposed to dS (de Sitter) spacetime which is a maximally symmetric solution with positive cosmological constant. The positive cosmological constant solution was initially introduced by Willem de Sitter and has been used as a cosmological model for an expanding universe. This section borrows ideas from [20, 21].

1.2.1 Maximally Symmetric Spaces: Euclidean Spheres and Euclidean AdS

A manifold $\mathcal{M}$ is said to be maximally symmetric if it is homogeneous and isotropic. By homogeneous we mean that given two points p and q in $\mathcal{M}$, there exist an isometry ϕ belonging to the isometry group of $\mathcal{M}$ such that $\phi(p) = \phi(q)$; by isotropic we mean that for any point $p \in \mathcal{M}$, and for any two tangent vectors $v, w \in T_p(\mathcal{M})$, such that $v_\mu v^\mu = w_\mu w^\mu$, there exist an isometry ϕ belonging to the isometry group of $\mathcal{M}$ such that $\phi(p) = p$ and $\phi_*(v) = w$. It can be shown that an n-dimensional maximally symmetric space posseses exactly $n(n+1)/2$ Killing vectors, which is the largest possible number of linearly independent Killing vectors.

In a d-dimensional Euclidean space with ambient metric

$$ds^2 = dx_1^2 + \cdots + dx_{d+1}^2\,, \tag{1.12}$$

the maximally symmetric solution with positive curvature is a d-dimensional sphere, that is, $\mathbf{S}^d = \{x \in \mathbb{R}^d | x_1^2 + \cdots + x_{d+1}^2 = L^2\}$. The embedding is in this case said to be isometric, since the isometry group of $\mathbb{R}^{d+1}$, i.e., $\mathbf{SO}(d+1)$, leaves the sphere ivariant.

Likewise, a d-dimensional hyperboloid, is the maximally symmetric solution with negative curvature. However, if we wish to have an isometric embedding, we have to change the ambient metric to the Minkowski space

$$ds^2 = -dX_{d+1}^2 + dX_1^2 + \cdots + dX_d^2, \tag{1.13}$$

this is because the locus defining a d-dimensional hyperboloid, $\mathbf{H}^d = \{X \in \mathbb{R}^{d,1} | -X_{d+1}^2 + X_1^2 + \cdots + X_d^2 = -L^2\}$, is invariant under $\mathbf{SO}(d,1)$ transformations, which is the isometry group of d-dimensional Minkowski space. What we have just defined is the so-called Euclidean AdS space. One can find the induced metric on the Hyperboloid by introducing the global coordinates

$$x_{d+1} = L\cosh\rho, \quad x_i = L\Omega_i \sinh\rho, \tag{1.14}$$

where $\sum_i (\Omega_i)^2 = 1$. Using the fact that $\Omega_i d\Omega_i = 0$ we find

$$ds^2 = L^2(d\rho^2 + \sinh^2\rho\, d\Omega_{d-1}^2), \tag{1.15}$$

where $d\Omega_{d-1}^2$ is the metric on the unit $d-1$-dimensional sphere. As expected, the metric is invariant under transformations in $\mathbf{SO}(d,1)$ and is homogeneous, meaning that points can be mapped into each other via transformations in $\mathbf{SO}(d,1)$.

1.2.2 Lorentzian AdS

We can now define the spacetime we are really interested in, that is, the Lorentzian AdS_{d+1} spacetime. To do this, we have to consider the funny-looking embedding space

$$\eta_{ab} dX^a dX^b = -dX_0^2 + dX_1^2 + \cdots + dX_d^2 - dX_{d+1}^2. \tag{1.16}$$

We call AdS_{d+1} the spacetime defined by the hyperboloid

$$\eta_{ab} X^a X^b = -L^2 \subset \mathbb{R}^{d,2}. \tag{1.17}$$

Despite the fact that the embedding space has two time-like coordinates, the AdS space has only one time coordinate. The reason we need two time-like coordinates for the embedding space is so that the embedding is isometric, just as in the case of the Euclidean hyperboloid. This means that the AdS spacetime inherets the isometry group of $\mathbb{R}^{d,2}$, i.e., $\mathbf{SO}(d,2)$. Since the number of generators of $\mathbf{SO}(d,2)$ is $(d+1)(d+2)/2$, the same as the maxiaml number of killing vectors of a $d+1$-dimensional spacetime, we conclude that AdS is maximally symmetric.

As for the Euclidean AdS space, we can find the induced metric by considering the global coordinate

$$X_0 = L\cosh\rho\cos\tau, \quad X_i = L\Omega_i\sinh\rho, \quad X_{d+1} = L\cosh\rho\sin\tau, \tag{1.18}$$

where $\sum_i(\Omega_i)^2 = 1$, we thus find that the Lorentzian AdS metric is given by

$$ds^2 = L^2(-\cosh^2\rho\, d\tau^2 + d\rho^2 + \sinh^2\rho\, d\Omega_{d-1}^2). \tag{1.19}$$

For $\tau \in [0, 2\pi]$ and $\rho \in \mathbb{R}^+$ the hyperboloid is covered exactly once. We can avoid closed time-like curves by unrwrapping the τ coordinate and extend it to $\mathbb{R}$, this way we get the so-called universal cover. The metric in global coordinates is sometimes written using the coordinates

$$ds^2 = -\left(1+\frac{r^2}{L^2}\right)dt^2 + \left(1+\frac{r^2}{L^2}\right)^{-1} dr^2 + r^2\, d\Omega_{d-1}^2\,, \tag{1.20}$$

where $r \in [0,\infty)$ and $t \in \mathbb{R}$. The limit $r \to \infty$ corresponds to what is called the asymptotic boundary of AdS, which is a conformal boundary with topology $\mathbb{R}\times\mathbf{S}^{d-1}$.

Another set of coordinates which are extremely useful in practice are the so called Poincarè coordinates defined by

$$X^\mu = \frac{L}{z}x^\mu, \quad X_{d+1} + X_d = \frac{L}{z}, \quad -X_{d+1} + X_d = v, \tag{1.21}$$

so the metric takes the form

$$ds^2 = \frac{L^2}{z^2}(dz^2 - dt^2 + dx_1^2 + \cdots + dx_d^2). \tag{1.22}$$

These coordinates cover only a part of the AdS spacetime, and the geometry covered is referred to as the Poincarè patch. Note that for each z-slice, the spacetime appears to be flat Minkowski space $\mathbb{R}^{d-1,1} = \mathbb{M}_d$. In this case the boundary of AdS is reached in the limit $z \to 0$. On the other hand, $z \to \infty$ corresponds to a horizon, since the killing vector ∂_t has zero norm, and is referred to as the Poincarè horizon.

So far we have made no mention of gravity in defining this spacetime but it turns out that Lorentzian AdS is a solution to Einstein's equation

$$R_{\mu\nu} - \frac{1}{2}R\, g_{\mu\nu} = 8\pi G\, T_{\mu\nu}\,, \tag{1.23}$$

with the energy-momentum tensor given by

$$T_{\mu\nu} = \frac{d(d-1)}{16\pi G L^2} g_{\mu\nu}. \tag{1.24}$$

The causal structure of AdS_{d+1} is better understood if we comppactify the r coordinate in (1.20) by intruducing $\theta = \tan r \in (0, \pi/2)$, therefore,

$$ds^2 = \frac{1}{\cos^2\theta}(-dt^2 + d\theta^2 + \sin^2\theta\, d\Omega_{d-1}^2)\,. \tag{1.25}$$

The overall Weyl factor $1/\cos^2\theta$ does not influence the profile of null geodesics which implies that AdS_{d+1} is causally equivalent to a solid cylinder (see figure 1.1.)

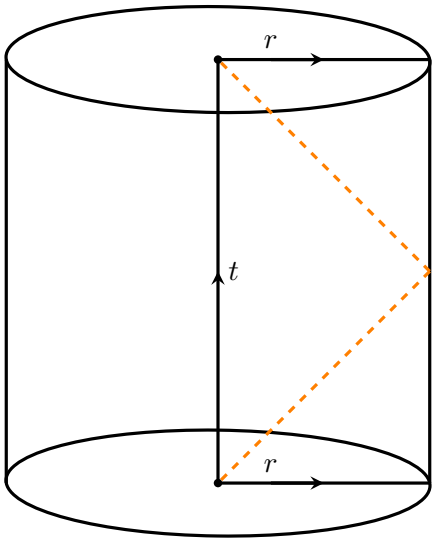

Figure 1.1: a light ray sent from $r = 0$ to the boundary bounces back to the center in a finite proper time. This is why we often think of AdS as being a finite box.

1.2.3 Asymptotically AdS Spacetimes

To discuss anything but the most trivial case in AdS/CFT, we need to discuss more than just AdS space. In fact, some of the most interesting examples of the duality involve spacetimes which deviate from the vacuum solution in a way or another. In general, the presence of non-trivial matter will inevitably cause some kind of perturbation, however, what seems essential for the correspondence to work is to require that the perturbations don't modify the asymptotic structure of AdS_{d+1}. It is then natural to define a set of asymptotically-AdS spacetimes, which posses a boundary topology equivalent to $\mathbb{R} \times \mathbf{S}^{d-1}$, and whose metric approaces

$$ds^2 = -\left(1 + \frac{r^2}{L^2}\right) dt^2 + \left(1 + \frac{r^2}{L^2}\right)^{-1} dr^2 + r^2\, d\Omega_{d-1}^2 \tag{1.26}$$

close to the boundary. It is sometimes interesting to discuss spacetimes which factorize into an asymptotically AdS_{d+1} part and a compact manifold $\mathcal{M}$ part.

A very interesting example (we'll come back to it later) is the AdS-Schwarzschild solution

$$ds^2 = f(r)d\tau^2 + \frac{1}{f(r)}dr^2 + r^2 d\Omega_{d-1}^2, \quad \text{where} \quad f(r) = 1 + \frac{r^2}{L^2} - \frac{\mu}{r^{d-2}}. \tag{1.27}$$

The parameter μ can be interpreted as a mass parameter, and the blackening function is defined so that in the limit $r \to \infty$ it approaces 1, which in turn means the metric approaces AdS_{d+1}. Interestingly, for finite r-values the AdS-Schwarzschild solution describes two asymptotically AdS boundaries connected by a wormhole.

1.2.4 Quantization of a Scalar Field in AdS_{d+1}

Let's consider the action governing the dynamics of a massive scalar field

$$S = -\frac{1}{2}\int \mathrm{d}^{d+1}x\, \sqrt{-g}\left(\partial_\mu\phi\, \partial_\nu\phi g^{\mu\nu} + m^2\phi^2\right), \tag{1.28}$$

with the background metric being AdS_{d+1}. The variation of this action leads to the following equation of motion

$$\frac{1}{\sqrt{-g}}\partial_\mu(\sqrt{-g}\, g^{\mu\nu}\partial_\nu\phi) - m^2\phi = 0. \tag{1.29}$$

In global coordinates it is convenient to solve the equation in the basis

$$f_{\omega\ell\vec{m}}(r,t,\Omega) = \psi_{\omega\ell}(r)e^{-i\omega t}Y_{\ell\vec{m}}(\Omega), \tag{1.30}$$

where $Y_{\ell\vec{m}}(\Omega)$ are spherical harmonics, and $\psi_{\omega\ell}(r)$ obeys the equation

$$(1+r^2)\psi'' + \left(\frac{d-1}{r}(1+r^2)+2r\right)\psi' + \left(\frac{\omega^2}{1+r^2} - \frac{\ell(\ell+d-2)}{r^2} - L^2m^2\right)\psi = 0. \tag{1.31}$$

This equation can be solved exactly $\forall r \in [0,\infty)$ with hypergeometric functions, however, one can gain lots of insight by focusing on the $r \to 0$ and $r \to \infty$ limits. Indeed, for small r we find

$$\psi'' + \frac{d-1}{r}\psi' + \frac{\ell(\ell+d-2)}{r^2}\psi = 0, \tag{1.32}$$

which is solved by

$$\psi_\ell(r) = N_\ell \cdot r^{-\left(\frac{d-2}{2} \pm \frac{1}{2}\sqrt{(d-2)^2+4\ell(\ell+d-2)}\right)}, \tag{1.33}$$

whilst close to the boundary the equation becomes

$$r^2\psi'' + (d+1)r\psi' - L^2m^2\psi = 0\,, \tag{1.34}$$

which is solved by

$$\psi_\ell(r) = \mathcal{N} \cdot r^{-\left(\frac{d}{2} \pm \frac{1}{2}\sqrt{d^2+4m^2L^2}\right)}. \tag{1.35}$$

For the small r solution, we have to choose the positive sign in the exponet, so that it is smooth at $r = 0$. The sign of the close-to-boundary solution is instead fixed by the boundary conditions we impose at the AdS boundary. When $m^2 \geq 0$ and $d \geq 2$ the only sign that preserves $\mathbf{SO}(d,2)$ symmetry and unitarity is the plus sign, thereby giving the solution

$$\psi_{\omega\ell}(r) \sim r^{-\Delta}\,, \tag{1.36}$$

where

$$\Delta = \frac{d}{2} + \frac{1}{2}\sqrt{d^2+4m^2L^2}. \tag{1.37}$$

This is what we call the standard quantization. In AdS/CFT the equation (1.37) is called the mass-dimensin relation. If $L^2m^2 < -d^2$ the negative sign solution can be allowed by unitarity, in that case we call it the alternate quantization. (Notice that even when $L^2m^2 < -d^2$ the standard quantization, meaning the positive sign solution, is still allowed by unitarity.)

Returning to the standard quantization, the restrictions imposed at $r = 0$ and $r = \infty$ imply that ω is quantized. In fact the exact solution shows that

$$\omega_{n\ell} = \Delta + \ell + 2n\,, \quad \text{where} \quad n \in \mathbb{N}. \tag{1.38}$$

This confirms the intuition that AdS, unlike Minkowski space, should be viewed as a finite box. We can now write the solution to our scalar field theory in terms of creation and annihilation operators

$$\phi(r,t,\Omega) = \sum_{n,\ell,\vec{m}} \left(f_{\omega\ell\vec{m}}\, a_{n\ell\vec{m}} + f^*_{\omega\ell\vec{m}}\, a^\dagger_{n\ell\vec{m}}\right). \tag{1.39}$$

The solutions ought to be normalized according to the Klein-Gordon norm

$$(f,g) = -i\int_{\Sigma_t} \mathrm{d}^d x\,\sqrt{-g}\,g^{tt}\left(g^*\partial_t f - g\partial_t f^*\right), \tag{1.40}$$

and the creation and annihilation operators ought obey the algebra

$$[a_{n\ell\vec{m}}, a^\dagger_{n'\ell'\vec{m}'}] = \delta_{nn'}\delta_{\ell\ell'}\delta_{\vec{m}\vec{m}'}\,. \tag{1.41}$$

1.3 Black Hole Thermodynamics and Holography

One of the most fascinating predictions of General Relativity is the existence of solutions characterized by regions of spacetime with such a strong gravitational "pull" that nothing, not even light, can escape! For most of the 20th century the great majority of people (inducing Einsein himself) believed these solutions to be unphysical and an unattractive feature of GR, something to be fixed. It wasn't until the end of the 20th century that a few people started to take these solutions seriously. From there on more and more people got convinced of the importance of these mysterious objects, until we finally got a glance of the unthinkable [22]. There are still a great number of mysteries hazing around these bizarre systems (information paradox, firewalls, islands... you name it!), also known as *black holes.*

There is one peculiarity about black holes which is central to the story we are telling in this thesis, that is, the realization that the entropy of a black hole scales with the area rather than the volume: this is what inspired the holographic principle.

1.3.1 Black Hole Temperature

There are a number of different black hole solutions to the Einstein equations, the simplest of which is the Schwarzschild solution

$$ds^2 = -f(r)dt^2 + f(r)^{-1}dr^2 + r^2(d\theta^2 + \sin^2\theta d\phi^2), \tag{1.42}$$

where $r \in [0, r_s) \cup (r_s, \infty]$, $t \in \mathbb{R}$, $\theta \in [0, \pi]$, $\phi \in [0, 2\pi]$, and $f(r) = 1 - r_s/r = 1 - 2GM/r$ is the blackening factor. The region in close proximity to the null hypersurface defined at $r = r_s$, i.e., the black hole event horizon, is of particular importance. That is because the horizon splits the spacetime into two distinct causal regions, and as is well known, whatever crosses the the horizon to go into the interior of the black hole cannot escape the interior. As we will now see, this has drastic consequences when we consider quantum fluctuations near the horizon.

Consider the near horizon expansion

$$f(r) = f'(r_s)(r - r_s) + \cdots, \tag{1.43}$$

for $r \in (r_s, r_s + \epsilon)$, and where ϵ is an infinitesimal. An observer in proximity of the horizon can measure the proper distance ρ from the horizon, according to

$$d\rho = \frac{dr}{\sqrt{f(r)}}. \tag{1.44}$$

Using the near horizon expansion of the blackening factor, and then integrating, we find

$$\rho \simeq \frac{2}{\sqrt{f'(r_s)}}\sqrt{r - r_s}, \tag{1.45}$$

plugging this back into the metric we get

$$ds^2 = -\left(\frac{1}{2}f'(r_s)\right)^2 \rho^2 dt^2 + d\rho^2 + r_s^2 d\Omega_2^2 = -\rho^2 d\eta^2 + d\rho^2 + r_s^2 d\Omega_2^2. \tag{1.46}$$

What we have just found is that in the near-horizon limit the geometry can be approximately described by Rindler $\times$ $\mathbf{S}^2$ (which is strictly speaking not a solution to the Einstein equation.)

The Rindler portion is described by the metric

$$ds^2_{\text{Rind}} = d\rho^2 - \rho^2 d\eta^2, \tag{1.47}$$

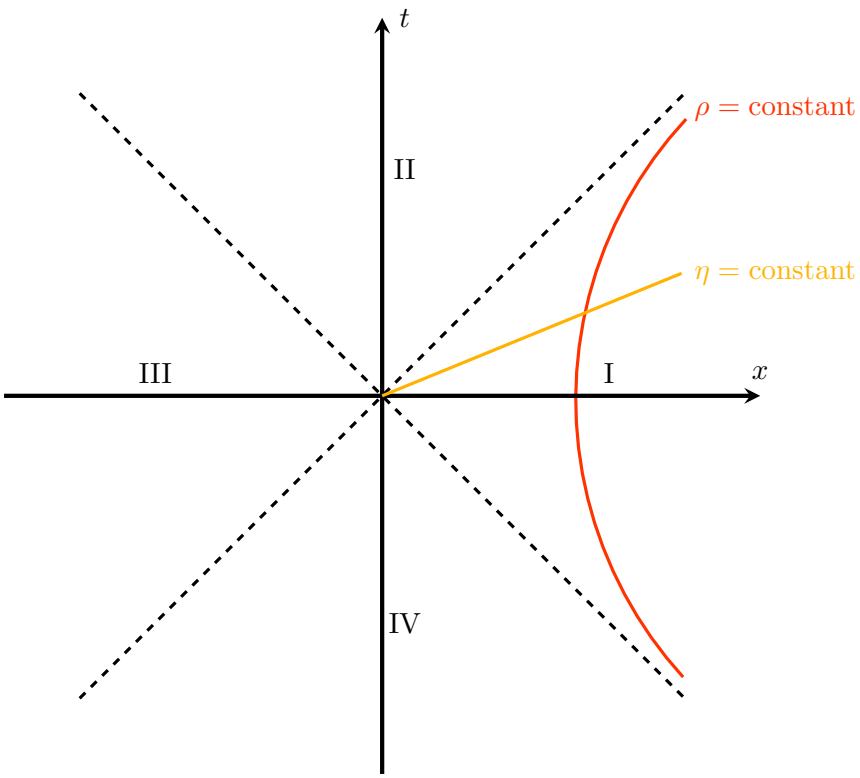

Figure 1.2: Rindler coordinates cover the region I of $\mathbb{R}^{1,1}$. One can extend the coverage to the regions II, III, and IV with Kruskal-like coordinates. The resulting space is akin to the maximally extended Schwarzschild solution with I and III being the asymptotic regions, and II and IV being the part and future interiors.

which by taking $\eta \to i\phi$ gives $\mathbb{R}^2$ in polar coordinates. Furthermore, with the coordinate transformation

$$x = \rho \cosh \eta, \quad t = \rho \sinh \eta, \tag{1.48}$$

we recover $\mathbb{R}^{1,1}$. Notice that the Rindler coordinates cover just a portion of $\mathbb{R}^{1,1}$, namely the patch $x > 0$ and $|t| < 0$ (see figure 1.2.)

A QFT at finite temperature is periodic under Euclidean time evolution, meaning that if we do a Wick rotation $t \to -i\tau$, then $\tau \sim \tau + \beta$, where β is the inverse temperature. This periodicity is for example exhibited in the thermal Green's function: $G_\beta(\tau, x) = G_\beta(\tau - \beta, x)$. So if we perform a Wick rotation in the near-horizon geometry above, namely $\eta \to i\phi$, we find that the Rindler portion of the metric becomes simply $\mathbb{R}^2$ in polar coordinates. Unless ϕ is periodic with period 2π, polar coordinates in $\mathbb{R}^2$ are singular when $\rho = 0$. Since the limit $\rho \to 0$ of the near-horizon geometry describes the the Schwarzchild horizon itself, which is non-singular, we conclude that ϕ must be periodic. This suggests that the Wick rotated near-horizon geometry describes a thermal QFT with temperature given by the periodicity. In particular, undoing the various coordinate transformations we find that

$$T = \frac{|f'(r_s)|}{4\pi}\,. \tag{1.49}$$

One interpretation of this result is that an accelerating observer in flat Minkowski space observes a thermal spectum of particles with temperature given by (1.49): this is known as the *Unruh effect* [23].

The other interpretation [5] is far more suggestive with far-reaching consequences: the Schwarzchild black hole we started with emits particles with a black body spectrum of temperature given by (1.49), known as the *Hawking temperature*. This argument might seem a little sketchy at first, but the conclusion is nonetheless correct, as confirmed by a more sophisticated account [5]. The conclusion hold for more complicated black holes as well.

1.3.2 Black Hole Thermodynamics and the Holographic Principle

We now know that black holes radiate particles in a thermal spectrum, with temperature (1.49). One immediate consequence is that we should be able to associate an entropy to a black hole

$$\frac{\mathrm{d}S}{\mathrm{d}T} = \frac{1}{T(E)}. \tag{1.50}$$

This makes sense; black holes are, after all, by definition perfect absorbers, and should therefore emit just like any other object in thermal equilibrium at temperature (1.49) with entropy (1.50). For a Schwarzschild black hole we can consider $E = M$, where M is the mass of the black hole, and therefore

$$S(E) = \int \frac{\mathrm{d}E}{T(E)} = \frac{4\pi r_s^2}{4G_N}.$$

Since the area of the event-horizon is given by

$$\mathcal{A} = \int \mathrm{d}^2x \sqrt{-\det \gamma} = 4\pi r_s^2,$$

with γ being the induced metric on the horizon, we conclude that

$$S = \frac{\mathcal{A}}{4G_N}\,, \tag{1.51}$$

which is the celebrated Bekenstein-Hawking entropy formula.

From the perspective of the *no-hair theorem*, which states that *a stationary black hole is fully described by its mass M, its angular momentum J, and its gauge charge Q,* black holes appear as fundamental objects with no internal structure. The fact that black holes have non-zero temperature and entropy might thereby come as a surprise. But from the perspective of the second law of thermodynamics it makes perfect sense, else: if a lump of matter with a certain entropy is ingurgitated by a black hole, an external observer would come to the conclusion that the this entropy simply disappeared from the universe, violating the second law. This goes hand in hand with the so-called *area theorem*, which states that *the event horizon area $\mathcal{A}$ of a black hole can never decrease with time*,

$$\delta\mathcal{A} \geq 0, \tag{1.52}$$

which is completely analogous to the second law $\delta S \geq 0$.

We should by now be convinced that black holes are thermodynamic systems. As such, we should, at least in principle, be able to apply the Boltzmann formula

$$S = k_B \log \mathcal{N}, \tag{1.53}$$

which relates the entropy S of a system to the number of microscopic degrees of freedom $\mathcal{N}$, to black holes. What the underlying microstates are in the case of black holes is still an open question, related to the so-called *information paradox*. As it stands, the Bekenstein formula for the entropy of a black hole may catch an eye or two. Indeed, that the entropy is proportional to the area is a remarkable feature. Since entropy is tied to the number of degrees of freedom of

a system through the Boltzmann formula – more generally the Vonn-Neumann formula, see 2 – we should come to the conclusion that for black holes the number of degrees of freedom scales as the area. This is in stark contrast to ordinary QFTs on a lattice, where the number of degrees of freedom scales as the volume. It turns out that if taken seriously, this apparent contradiction can teach us something deep and valuable about gravity.

In fact, let's consider an isolated system of mass M, entropy S, and let's suppose the whole system is contained inside a spherical surface of area $\mathcal{A}$. Let $M_{\mathcal{A}}$ be the mass of the black hole whose horizon area is $\mathcal{A}$. Clearly we must have $M \leq M_{\mathcal{A}}$. Keeping $\mathcal{A}$ fixed we may add $M_{\mathcal{A}} - M$ energy to the system; this will inevitably turn the system into a black hole of mass $M_{\mathcal{A}}$ and horizon area $\mathcal{A}$. Hence, according to the second law of thermodynamics, the following inequality must hold for the subsystems

$$S_{\text{BH}} \geq S + S', \tag{1.54}$$

where S_{BH} is the entropy of the black hole with horizon area $\mathcal{A}$, and S' the entropy of the matter added subsequently. This implies the following:

$$S \leq S_{\text{BH}}, \tag{1.55}$$

that is, the maximal entropy inside a region bounded by a surface of area $\mathcal{A}$ is

$$S_{\text{max}} = \frac{\mathcal{A}}{4G_N}.$$

This heuristic argument (for a more detailed account see [24]) indicates that not only all the information stored within the interior of a black hole is fully encoded on the surface of the event horizon but also that the amount of information stored by any physical system in a region cannot exceed the area of the boundary surface of said region. This is what sparked the idea of holography.

The *holographic principle* states that: *in a quantum theory of gravity, given a region of spacetime, the degrees of freedom are fully localized on the boundary surface of the region so that the number of degrees of freedom inside the region is no more than one per unit of Planck area.*

As alluded to earlier, this principle is violated in non-gravitational systems such as ordinary QFTs. In a three-dimensional spin chain lattice with lattice spacing a, for instance, the number of degrees of freedom scales as $V/a^3 \gg A/\ell_P^2$. So according to the holographic principle, quantum gravity leads to a huge reduction in the number of degrees of freedom.

1.4 AdS/CFT

We are now ready to turn our attention to the AdS/CFT correspondence.

At the most basic level AdS/CFT states the equivalence between the language of quantum field theory and the langauge of (super)gravity, via a so-called *dictionary*. As we will see in moment, the quantum field theory lives on the boundary of the spacetime on which the gravitational theory is defined, thus making the correspondence a realization of the holographic principle. This fact alone should be reason enough to be interested in AdS/CFT, but the range of potential applications goes way beyond holography, from condensed matter theory (AdS/CMT) to the quark-gluon plasma (fluid/gravity duality.)

We won't introduce the duality in a historically accurate way, we will rather treat it as a truth handed to us by some deity (perhaps by the Roman god Janus) and from there discuss the implications. We will closely follow the approach of [25, 26, 21]. For a more in-depth and historically accurate introduction [27, 28] are great references.

1.4.1 Formulation of the Correspondence

Without further ado, let's introduce the glorious AdS/CFT correspondence.

Statement 1: *any conformal field theory defined on* $\mathbb{R} \times \mathbf{S}^{d-1}$ *is dynamically equivalent to a semiclassical theory of gravity in asymptotically* $AdS_{d+1} \times \mathcal{M}$*, where* $\mathcal{M}$ *is a compact manifold*[1]*.*

This statement on its own is quite cryptic and vague, so we need to contextualize it a bit.

The first question one might ask is what is meant by *dynamically equivalent*. By this we mean that observables on the two sides of the correspondence are in a one-to-one map through the *holographic dictionary*, in this sense, the duality can be viewed as an isomorphism between the Hilbert spaces on each side: $\phi : \mathcal{H}_{\text{AdS}} \to \mathcal{H}_{\text{CFT}}$. The holographic dictionary, much like ordinary dictionaries, is expanding, and occasionally new entries are introduced. Much of this thesis will be dedicated to one of the most recent additions to the dictionary, the CV-duality. More on that later.

We implicitly already know the first line of the dictionary. Indeed, since the conformal group in d dimensions and the isometry group of AdS_{d+1} are both isomorphic to $\mathbf{SO}(d, 2)$ we claim that the generators implementing these symmetries on each sides are related by the isomorphism ϕ,

$$\phi \circ U_{\text{AdS}} = U_{\text{CFT}} \circ \phi \,. \tag{1.56}$$

This implies that the spectrum of the Hamiltonians is equivalent on either side, and that any operator on one side can be transformed into an operator on the other side throug ϕ. It is generally convenient to choose a basis in which $\phi = \mathbb{I}$.

To formulate more entries to the dictionary we need an additional statement.

Statement 2: *a d-dimensional CFT whose spectrum is spanned by a complete set of primary operators* O_i *has a semiclassical dual near the vacuum if there exist a local bulk action* $S[\phi_i, \Lambda]$*, where* Λ *is a UV cutoff and* ϕ_i *are a finite set of bulk fields that satisfy the bulk equations of motion and (scalar fileds, gauge fields, metric, etc.) such that*

$$\int \mathcal{D}\phi_i \, e^{iS[\phi_i,\Lambda]} \, O_{i_1}(x_1) \cdots O_{i_n}(x_n) \simeq \langle O_{i_1}(x_1) \cdots O_{i_n}(x_n) \rangle_{CFT} \,, \tag{1.57}$$

to all orders in $\frac{1}{L\Lambda}$*. Here* x_i *are coordinates on the boundary, and the* O_i *on the left are given by*

$$\lim_{r\to\infty} r^{\Delta_i} \phi_i(r, x) = O_i(x) \,, \tag{1.58}$$

where Δ_i *is the scaling dimension of* O_i*, and* r *the radial AdS coordinate.*

The equation (1.58) is the analogous of the LSZ formula in flat QFT and is referred to as the *extrapolate dictionary*. This relation is of utmost importance in AdS/CFT as it provides a prescription for relating bulk fields to boundary operators. For instance, it allows to relate the bulk metric g_{MN} to the boundary stress tensor $T_{\mu\nu}$.

However, statement 2 is still not enough, after all, as we alluded to earlier, we expect the most interesting bulk geometries to be described by a CFT somewhat far from the vacuum. Black holes are a perfect example of such scenario. Therefore we need one more statement.

Statement 3: *a* CFT_d *has a semiclassical dual if in addition to having a semiclassical dual near the vacuum, the relation* (1.57) *holds for a more general set of asymptotically-AdS boundary conditions which allow for a fixed but arbitrary boundary metric.*

[1] $\mathcal{M}$ is usually a trivial manifold so we will act as if it doesen't exist.

In practice AdS/CFT is telling us that the boundary value of a bulk field $\phi(x) = \lim_{r\to\infty}\phi(r,x)$ acts as a source in the CFT, that is,

$$\mathcal{L}_{\text{CFT}} \to \mathcal{L}_{\text{CFT}} + \int \mathrm{d}^d x\, \phi(x) O(x). \tag{1.59}$$

This implies that correlation functions in the boundary are completely specified by the generating functional

$$Z_{\text{CFT}} = e^{W[\phi]} = \left\langle e^{\int \mathrm{d}^d x \phi(x) O(x)} \right\rangle_{\text{CFT}}, \tag{1.60}$$

and its derivatives

$$\langle O(x_1)\cdots O(x_n)\rangle = \left.\frac{\delta^n W}{\delta\phi^n}\right|_{\phi=0}. \tag{1.61}$$

AdS/CFT may therefore be summarized in a single line:

$$Z_{\text{CFT}}[\phi(x)] = Z_{\text{AdS}}[\phi(r,x)|_{\partial\text{AdS}} = \phi(x)]\,. \tag{1.62}$$

This is the celebrated Gubser, Klebanov, Polyakov, Witten dictionary [29, 30].

1.4.2 Infrared vs. Ultraviolet

The extra dimension on the gravity side turns out to have a very important interpretation within the correspondence. Recall that the AdS metric in Poicarè coordinates is given by

$$ds^2 = \frac{L^2}{z^2}(dz^2 + dx^\mu dx_\mu).$$

where the coordinates on the boundary are given by $x^\mu = (\vec{x}, t)$. If we express the local bulk proper time and proper distance with respect to the boundary coordinates we find,

$$\mathrm{d}\tau = \frac{L}{z}\,\mathrm{d}t, \quad \text{and} \quad \mathrm{d}\ell = \frac{L}{z}\,\mathrm{d}x,$$

which, if inverted, implies that from the boundary point of view we will have

$$E_{\text{CFT}} = \frac{L}{z}E_{\text{local}}, \quad \text{and} \quad d_{\text{CFT}} = \frac{z}{L}d_{\text{local}}.$$

This suggests the following: identical processes in the bulk theory at different values of the radial coordinate z (that is, processes with same E_{local} and same d_{local}) are mapped to processes in the boundary theory with energy $E_{\text{CFT}} \sim 1/z$, and $d_{\text{CFT}} \sim z$. The factor $1/z$ should therefore be identified with an energy scale in the CFT. This also means that the limits $z \to \infty$ and $z \to 0$ correspond respectively to UV and IR regimes in the boundary theory.

This relation is at the heart of AdS/CFT. In fact, it tells us that in the semiclassical limit the correspondence is a *strong/weak* duality. This is practically very important, since it allows us to treat strong coupling regimes in the boundary, which are computationally prohibitive, with weak coupling regimes in the semiclassical bulk.

1.4.3 Mass Dimension Duality

In section 1.2.4 we found the solutions of the AdS equations of motion and quantized the corresponding bulk fields. In light of AdS/CFT we can give a holographic interpretation to the relation (1.37).

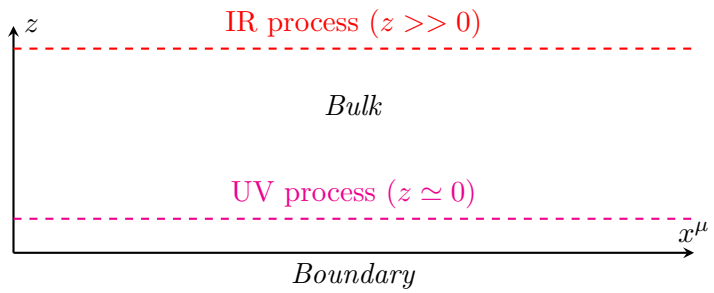

Figure 1.3: degrees of freedom deep in the bulk correspond to IR processes in the boundary, vice versa, degrees of freedom close to the boundary correspond to UV physics in the boundary.

Assuming that the bulk metric is expressed in Poincarè coordinates, the solutions to the bulk equations of motion close to the boundary are

$$\phi(z,x) = A(x)z^{d-\Delta} + B(x)z^{\Delta}\,, \tag{1.63}$$

where Δ is given by (1.37), and x is a boundary coordinate. Let's further assume$m^2L^2 \geq -d^2/4$ and that we are in standard quantization.

As discussed in 1.2.4, the modes corresponding to z^{Δ} are normalizable, and as such are used to build up the bulk Hilbert space. Since, according to AdS/CFT, the bulk Hilbert space is equivalent to the boundary Hilbert space, the normalizable modes will be dual to boundary primary operators. On the other hand, non-normalizable modes are not part of the bulk Hilbert space, so if present should be interpreted as defining the background, that is, from the boundary perspective they deform the theory as sources. So, if $A(x) = \phi_0(x)$, that is,

$$\phi_0(x) = \lim_{z\to 0} z^{\Delta-d}\phi(z,x), \tag{1.64}$$

we will have the deformation

$$\mathcal{L}_{\text{CFT}} \to \mathcal{L}_{\text{CFT}} + \int \mathrm{d}^d x\, \phi_0(x) O(x) \tag{1.65}$$

in the boundary theory. This also suggests that Δ is precisely the scaling dimension of the boundary operator $O(x)$. This becomes clear if we act with the bulk isometry $(z,x) \to (\lambda z, \lambda x)$, which results in

$$O(x) \to \lambda^{-\Delta} O(x). \tag{1.66}$$

Interestingly, this means that, in standard quantization, we can classify the boundary operators through (1.37) in the following way:

- if $m = 0$, $\Delta = d$, that is, $O(x)$ is a *marginal* operator;
- if $m^2 < 0$, $\Delta < d$, that is, $O(x)$ is a *relevant* operator; and
- if $m^2 > 0$, $\Delta > d$, that is, $O(x)$ is an *irrelevant* operator.

1.4.4 AdS/CFT at Finite Temperature

According to AdS/CFT, when the bulk geometry is pure AdS the dual boundary theory is in a vacuum state. On the other hand, when the bulk geometry deviates from pure AdS, we expect

the boundary theory to be in an excited state. In general we can define deformations of the bulk that maintain the correct boundary structure[2] as

$$ds^2 = \frac{L^2}{z^2}\left(dz^2 + \Gamma_{\mu\nu}(x,z)dx^\mu dx^\nu\right), \tag{1.67}$$

where for $z \to 0$,

$$\Gamma_{\mu\nu}(x^\mu, z) = \eta_{\mu\nu} + O(z^d). \tag{1.68}$$

It is extremely interesting to understand which bulk geometry describes a thermal state in the CFT side. Let's for simplicity we consider the AdS_5/CFT_4 duality, and we start with the case in which the thermal CFT is defined on $\mathbb{R}^{d-1} \times \mathbf{S}^1_\beta$, where $\mathbf{S}^1_\beta$ is a circle of radius β. Two candidates could come to mind as to what geometry is dual to the thermal state: a thermal gas in AdS, or an Euclidean black hole in AdS. Both solutions look in principle promising, since thy both are:

- asymptotically AdS;
- finite T theories that satisfy the laws of thermodynamics; and
- translationally and rotationally invariant along the boundary directions.

However, the thermal gas solution, which is defined by Wick rotating pure AdS and requiring smoothness at the origin, is unstable and must therefore be ruled out. We are left with the black hole solution.

The black hole solution is a solution of Einstein's equation with an event horizon whose topology is $\mathbb{R}^{d-1}$. To describe it, we can start by considering the ansatz in Lorentzian signature

$$ds^2 = \frac{L^2}{z^2}\left(-f(z)dt^2 + d\vec{x}^2\right) + \frac{L^2}{z^2}g(z)dz^2, \tag{1.69}$$

which solves Einstein's equation if

$$f(z) = \frac{1}{g(z)} = 1 - \left(\frac{z}{z_0}\right)^d. \tag{1.70}$$

The constant z_0 describes the position of the event horizon. Going to Euclidean signature, and requiring regularity at the origin, we find the thermodynamic temperature $\beta = 4\pi z_0/d$. This is the temperature of the boundary theory, and we again see the IR/UV connection since $T \sim z_0^{-1}$. So in this simple case, the holographic dual of a thermal CFT state in $\mathbb{R}^{d-1} \times \mathbf{S}^1_\beta$ is a black brane solution in AdS.

The story becomes more interesting when we consider a CFT defined on $\mathbf{S}^{d-1} \times \mathbf{S}^1_\beta$. In this case we have two dimensionful parameters, namely T, and R (the radius of $\mathbf{S}^{d-1}$), which means that the physics will depend on the product RT. Now the thermal solution in AdS is allowed, so there are two possibilities.

- One possibility is global AdS_{d+1} with the Euclidean metric

$$ds^2 = \left(1 + \frac{r^2}{L^2}\right)d\tau^2 + \left(1 + \frac{r^2}{L^2}\right)^{-1} dr^2 + r^2 d\Omega^2_{d-1}. \tag{1.71}$$

  We require $\tau \sim \tau + \beta$, so that the temperature is the inverse of the compactified time τ. Note that, since there is no horizon, there is no further restriction on the value of β, and therefore the temperature is just a free parameter in this solution.

[2] We discuss this in section 1.2.3, but essentially we want the geometry to asymptotically resemble AdS.

- The other possibility is AdS-Schwarzschild with the Euclidean metric

$$ds^2 = f(r)d\tau^2 + \frac{1}{f(r)}dr^2 + r^2 d\Omega_{d-1}^2, \quad \text{where} \quad f(r) = 1 + \frac{r^2}{L^2} - \frac{\mu}{r^{d-2}}. \tag{1.72}$$

  We can interpret μ as some sort of chemical potential related to the size of the black hole. The temperature in this case is $\beta = 4\pi/f'(r_0)$, where r_0 is the value for which the blackening factor vanishes. In particular we find

$$\beta = \frac{4\pi r_0 L^2}{dr_0^2 + (d-2)L^2} \implies T(r_0) = \frac{dr_0^2 + (d-2)L^2}{4\pi r_0 L^2}. \tag{1.73}$$

Taking a closer look the profile of (1.73), one realizes that the AdS-Schwarszchild solution only exists above the temperature $T_{min} = \sqrt{d(d-2)}/2\pi L$, and that above this temperature it actually corresponds to two solutions with different horizon radii. We refer to the geometry of the smallest of the two radii as the "small" black hole solution, while the larger one as the "large" black hole solution. The two solutions are degenerate when we reach T_{min}. Moreover, the small solution is of negative specific heat, since for decreasing r_0 the temperature increases, contrarily, the large solution is of positive specific heat.

We therefore have the following situation:

1. for temperatures below T_{min}, thermal AdS is the only solution; and
2. for temperatures above T_{min}, we have three possible solutions, namely, thermal AdS, the small black hole, and the large black hole.

Since the small black hole solution is characterized by negative specific heat, it has to be ruled out: no sensible CFT has negative specific heat. We are thus left with the thermal AdS solution, and the large black hole solution. To decide which of these two solutions dominates at a given temperature, we have to compare the free energies. The solution which dominates will minimize the free energy, and since $e^{-\beta F} \sim e^{-S_E[\Phi_c]}$, where $S_E[\Phi_c]$ is the euclidean action evaluated on a classical on-shell solution, the dominant solution will be the one with largest $S_E[\Phi_c]$. It turns out that there exist a temperature T_c, below which the thermal AdS solution dominates, and above which the large black hole solution dominates. Furthermore, at T_c there is a first order phase transition, since at this point the derivative of F is not continuous. This transition was studied by Hawking and Page years before anyone cared about AdS spacetime, and is therefore referred to as the Hawking-Page transition.

To summarize:

- a thermal CFT state in $\mathbb{R}^{d-1} \times \mathbf{S}^1_\beta$ is dual to the black brane solution (i.e., a black hole solution whose horizon is topologically $\mathbb{R}^{d-1}$) in AdS; and
- a thermal CFT state in $\mathbf{S}^{d-1} \times \mathbf{S}^1_\beta$ is dual to the thermal AdS solution up to a transition temperature T_c after which it becomes dual to the large AdS-Schwarzschild solution.

When the dual geometry is characterized by the presence of a horizon, we naturally expect the entropy to be non-zero, and it seems not so unreasonable to associate this entropy to the entropy of the thermal CFT state. This connection between geometry and entropy shouldn't come as a surprise given what we know about classical black holes; it emerges effortlessly if we accept that black holes are thermodynamic systems and that the horizon area is (up to constants) the entropy of the black hole. Given AdS/CFT, it seems that we now have some hope of understanding the microscopic origin of the black hole entropy. In the next chapter we will come back to this connection between geometry and entropy and we will further generalize this aspect of the duality.

Chapter 2

Holographic Entanglement Entropy

In this chapter, we review some developments in AdS/CFT that came about in the 00s and that sparked enormous interest around the idea that gravity and quantum information could be one and the same. A slogan that has emerged from these developments is that *gravity is quantum entanglement* [31].

First we review the basics of *entanglement entropy* for ordinary quantum mechanical systems, then we will move to quantum field theories, and, finally, we will make full circle by discussing the holographic interpretation of boundary entanglement entropy.

2.1 Entanglement Entropy

In quantum mechanics physical systems are described by states defined on a Hilbert space$\mathcal{H}$. Let's suppose that this space can be factorized into the tensor product of two subspaces $\mathcal{H}_A$ and $\mathcal{H}_B$, namely $\mathcal{H} = \mathcal{H}_A \otimes \mathcal{H}_B$.

Definition (1): *given a state $|\Psi\rangle \in \mathcal{H}$ in the full Hilbert space, we say that this state has quantum entanglement if and only if it can't be decomposed into a direct product of states in $\mathcal{H}_A$ and states in $\mathcal{H}_B$, that is, $|\Psi\rangle \neq |\psi\rangle_A \otimes |\psi\rangle_B$, where $|\psi\rangle_A \in \mathcal{H}_A$ and $|\psi\rangle_B \in \mathcal{H}_B$.*

We can equivalently phrase this definition in terms of the density matrix.

Definition (2): *given a state $|\Psi\rangle \in \mathcal{H}$ we say that this state is entangled if and only if the density matrix $\rho = |\Psi\rangle\langle\Psi|$ is not separable, i.e., if it cannot be written as*

$$\rho = \sum_k p_k \rho_A^{(k)} \otimes \rho_B^{(k)}, \tag{2.1}$$

where $\sum_k p_k = 1$ and $p_k > 1$.

It is easy to prove the equivalency of the two definition. The orthodox example of an entangled state, is that of a two-qubit system in the state

$$|\Psi\rangle = \frac{1}{\sqrt{2}} \left(|1\rangle_A|0\rangle_B - |0\rangle_A|1\rangle_B\right) = \frac{1}{\sqrt{2}}(|10\rangle - |01\rangle). \tag{2.2}$$

Conversely, the two-qubit state

$$|\Phi\rangle = \frac{1}{\sqrt{2}}(|0\rangle_A + |1\rangle_A) \otimes \frac{1}{\sqrt{2}}(|0\rangle_B + |1\rangle_B), \tag{2.3}$$

is not entangled. The simplest way to quantify the amount of entanglement in a given state is through the Entanglement Entropy. In a bipartite system $\mathcal{H} = \mathcal{H}_A \otimes \mathcal{H}_B$, we define the reduced

density matrix

$$\rho_A = \mathrm{Tr}_B \rho = \sum_k \langle \psi_k^{(B)} | \rho | \psi_k^{(B)} \rangle, \tag{2.4}$$

where $|\psi_k^{(B)}\rangle$ form a basis in $\mathcal{H}_B$, and the Von-Neumann entanglement entropy may be defined as

$$S_A = -\mathrm{Tr}(\rho_A \log \rho_A). \tag{2.5}$$

This quantity satisfies a few key properties:

- $S_A = 0$ if and only if ρ is separable;
- if ρ is a pure state density matrix then $S_A = S_B$;
- if ρ is a mixed state density matrix with entropy $S(\rho)$, then

  $$|S_A - S_B| \leq S(\rho) \leq S_A + S_B, \tag{2.6}$$

  where th second inequality is often called sub-additivity;
- suppose the Hilbert space can be decomposed into a tensor product of sub-spaces of the kind $\mathcal{H} = \mathcal{H}_A \otimes \mathcal{H}_B \otimes \mathcal{H}_C \otimes \mathcal{H}_D \otimes \cdots$, then the following inequality holds

  $$S_{AB} + S_{BC} \geq S_B + S_{ABC}, \tag{2.7}$$

  which is called strong sub-addititvity.

Going back to the two-qubit example, we can consider the maximally-entangled state

$$|\chi\rangle = \frac{1}{\sqrt{2}} \left(|0\rangle_A |0\rangle_B + |1\rangle_A |1\rangle_B \right), \tag{2.8}$$

for which the Vonn-Neumann entropy reads

$$S_A = -2 \cdot \frac{1}{4} \log \frac{1}{4} = \log 2 \,. \tag{2.9}$$

This simple example provides an interpretation of entanglement entropy: *it is a measure of how entangled a system is.* In fact, for a system split in to two k-qubit subspaces, a maximally entangled state has $S_A = k \log 2$. So S_A counts the number of entangled bits between the two subsystems.

The logarithm that appears in the definition of Vonn-Neumann entropy makes it difficult to compute for more complicated systems (particularly in quantum field theory). Fortunately we can define a related quantity,

$$S_A^{(n)} = -\frac{1}{n-1} \log \mathrm{Tr} \rho_A^n. \tag{2.10}$$

known as Renyi entropy. If all n Renyi entropies are known we can recover the VN entropy in the limit

$$S_A = \lim_{n \to 1} S_A^{(n)}. \tag{2.11}$$

This is a non-trivial statement that can be proven rigorously.

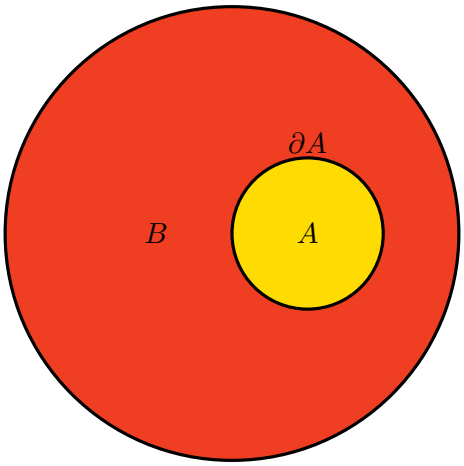

Figure 2.1: a time-slice of the Lorentzian manifold $\mathcal{M}$ divided into two regions, A and B. The regions are drawn as circles, but they could be any shape.

2.2 Entanglement Entropy in QFTs

Consider a quantum field theory defined on a Lorentzian manifold $\mathcal{M}$ with Hilbert space $\mathcal{H}$. Consider then a fixed time-slice on the manifold, and divide the induced space-like surface into two distinct regions, A and B (see fig. 2.1.) The codimension-2 surface separating the two regions is what we call the enatngling surface.

We may be tempted to then define entanglement entropy mirroring what we discussed for ordinary quantum mechanics and call it a day. But in contrast to ordinary quantum mechanics, in QFT it is in general not possible to separate the Hilbert space into a tensor product $\mathcal{H}_A \otimes \mathcal{H}_B$. This is because of diverging UV modes appearing at arbitrarily small scales across the boundary surface ∂A, i.e., the entangling surface. In any event, we can still define EE but we must also handle the divergences.

We can deal with these diverging modes, as usual, by placing the quantum field theory on a lattice with lattice spacing ϵ. With the theory on a lattice, the Hilbert space of a finite region is finite-dimensional, and we are thus able to associate a tensor factor $\mathcal{H}_A$ to a region A on the spatial manifold. Now we can define EE as per the definition in the section above. The notion of entanglement entropy in a QFT acquires a geometrical meaning. We can for example ask questions like how entangled a spatial region A is with respect to the complement of A, and so forth.

Computing the entanglement entropy in a QFT can be a daunting task, but the general structure is usually dominated by short-range correlations across the entangling surface, that is,

$$S_A \sim \int_{\partial A} \mathrm{d}^{d-2}\sigma \sqrt{h}\, \mathcal{F}[K_{ab}, h_{ab}]\,, \tag{2.12}$$

where $\mathcal{F}$ is a theory-dependent functional, K_{ab} is the extrinsic curvature, and h_{ab} the induced metric on the entangling surface. The previous expression can be expanded in powers of resulting in the so-called *area law*,

$$S_A = N \frac{\mathrm{Area}(\partial A)}{\epsilon^{d-2}} + \cdots\,, \tag{2.13}$$

where N is a constant that depends on the details of the theory, and $d > 2$. This captures only the leading divergence and is telling us something quite interesting: the vacuum state of any QFT in $d > 2$ dimensions is a highly entangled state. In $1+1$ dimensions the entanglement entropy of a spatial region of length L can be computed exactly in the case of a CFT, the result

is found to be

$$S_A = \frac{c}{3}\log\frac{L}{\epsilon}. \tag{2.14}$$

There are a plethora of ways to prove this, and one of them involves the so-called *replica trick*.

2.2.1 Replica Trick

The replica trick is a procedure to compute the Von-Neumann entanglement entropy from the path integral formalism [32, 33, 34]. The trick relies on the fact that it's generally easier to compute the quantity $\mathrm{Tr}\rho_A^n$, as opposed to $\mathrm{Tr}\rho_A \log \rho_A$, and this quantity can be computed naturally from the Euclidean path integral. In the end the Von-Neumann entropy will be determined by

$$S_A = -\frac{\partial}{\partial n}\log \mathrm{Tr}_A \rho_A^n|_{n=1}. \tag{2.15}$$

In complete analogy to wave functions in ordinary quantum mechanics, it is possible to define wave functionals in quantum field theory. In QM the wave function corresponding to a state $|\Psi\rangle$ is given by projecting the state onto the continuous "eigenvectors" defined by the position operator, namely $\Psi(x) = \langle x|\Psi\rangle$. Similarly, in a QFT the dynamical degrees of freedom are field operators $\phi(x)$ (in the position representation), so for a state $|\Psi\rangle$ in this QFT we can define the wave functional by projecting the state onto the eigenbasis defined by the field operators in position representation, that is,

$$\Psi[\phi(x)] = \langle\phi(x)|\Psi\rangle. \tag{2.16}$$

If we consider the wave functional corresponding to the vacuum of the theory, this will be given by the Euclidean path integral

$$\Psi_0[\phi(x)] = \int_{\tau<0}^{\phi(\tau=0,x)=\phi(x)} \mathcal{D}\phi(\tau,x)e^{-S_E[\phi]}. \tag{2.17}$$

We can also represent density matrices in the Euclidean path integral language. Density matrices are operators that act on the space of two fields to the complex numbers, meaning that density matrices can be understood, up to an overall normalization factor, as Euclidean path integrals with two open cuts (i.e., two unspecified boundary conditions.) The matrix elements of the density matrix will be given by

$$\rho(\phi_1(x_A),\phi_2(x_A)) = \langle\phi_1(x)|\rho|\phi_2(x)\rangle = \Psi_0[\phi_1(x)]\Psi_0^*[\phi_2(x)]. \tag{2.18}$$

Since we are interested in the entanglement entropy of a spatial sub-region A, we will have to trace out the degrees of freedom outside of A, this is in practice realized by integrating over all the fields localized in the complement of A, which we call B, thus

$$\langle\phi_1(x_A)|\rho_A|\phi_2(x_A)\rangle = \int \mathcal{D}\phi(x_B)\Psi_0[\phi_1(x)]\Psi_0^*[\phi_2(x)], \tag{2.19}$$

where x_A stands for $x \in A$, and x_B stands for $x \in B$. Using the path integral representation of the wave functionals we arrive at the following

$$\langle\phi_1(x_A)|\rho_A|\phi_2(x_A)\rangle = \frac{1}{Z_1}\int \mathcal{D}\phi(\tau,x)e^{-S[\phi]}\prod_{x\in A}\delta(\phi(\tau=0^+,x)-\phi_1(x))\cdot\delta(\phi(\tau=0^-,x)-\phi_2(x)), \tag{2.20}$$

where Z_1 represents the vacuum partition function. If we were considering, for example, a $(1+1)$-dimensional CFT in the Euclidean space $\mathbb{R}^2$, Z_1 would be the vacuum partition function

of $\mathbb{R}^2$. At this point we take n copies of (2.20) gluing each copy to the subsequent one along the cut A, this allows us to compute the trace of ρ_A^n as

$$\mathrm{Tr}\rho_A^n = \frac{1}{(Z_1)^n}\int \mathcal{D}\phi_1(x_A)\cdots\mathcal{D}\phi_n(x_A) \tag{2.21}$$

$$\times\, \rho(\phi_1(x_A),\phi_2(x_A))\rho(\phi_2(x_A),\phi_3(x_A))\cdots\rho(\phi_n(x_A),\phi_1(x_A)), \tag{2.22}$$

which can be rewritten as a path integral over a Riemann surface $\mathcal{R}_n$ with n sheets, that is,

$$\mathrm{Tr}\rho_A^n = \frac{1}{(Z_1)^n}\int_{(\tau,x)\in\mathcal{R}_n}\mathcal{D}\phi(\tau,x)e^{-S[\phi]} = \frac{Z_n}{(Z_1)^n}. \tag{2.23}$$

Thus, we find that the entanglement entropy can be computed as

$$S_A = -\frac{\partial}{\partial n}\left[\log\frac{Z_n}{(Z_1)^n}\right]_{n=1}. \tag{2.24}$$

2.3 Thermofield Double State

In QFT a thermal mixed state $\rho = e^{-\beta H}$ can always be treated as a pure state in a bigger Hilbert space, through a very useful procedure called *purification*. The idea is the following.

Suppose that the mixed state is defined in some Hilbert space $\mathcal{H}_1$, which is spanned by the energy eigenbase of some Hamiltonian H. Firstly, we double the degrees of freedom of this quantum system, so that we have two exact copieas of the original Hilbert space $\mathcal{H}_1$. We dub the second copy $\mathcal{H}_2$ and the total Hilbert space spanned by the tensor product of the two copies $\mathcal{H} = \mathcal{H}_1\otimes\mathcal{H}_2$. Note that at the level of Lagrangians and field operators, we have two exact copies of the original QFT, so that for every field operator in the original Lagrangian we have two fields in the doubled QFT, which live in separate spacetimes and are not coupled in the Lagrangian in any way at all. Say the Hamiltonian H is characterized by the spectrum of eigensates $H|n\rangle = E_n|n\rangle$, then, the second step is to construct the state

$$|\mathrm{TFD}\rangle = \frac{1}{\sqrt{Z(\beta)}}\sum_n e^{-\beta\frac{E_n}{2}}|n,1\rangle|n,2\rangle, \quad \text{where} \quad |n,i\rangle\in\mathcal{H}_i, \tag{2.25}$$

which is the so-called *thermofield double state*. Clearly $|\mathrm{TFD}\rangle$ is a pure state in $\mathcal{H}$. This is actually a particular instance of what is known as a *Smith decomposition*. We can define the corresponding density matrix $\rho_{\mathrm{TFD}} = |\mathrm{TFD}\rangle\langle\mathrm{TFD}|$, and by tracing out the degrees of freedom of the second copy we see that

$$\rho_1 = \mathrm{Tr}_2\rho_{\mathrm{TFD}} \tag{2.26}$$

$$= \sum_m\langle m,2|\left(\sum_{n,n'}e^{-\beta\frac{E_n+E_{n'}}{2}}|n,1\rangle|n,2\rangle\langle n',1|\langle n',2|\right)|m,2\rangle \tag{2.27}$$

$$= e^{-\beta H}. \tag{2.28}$$

We therefore conclude that, by ignoring the degrees of freedom contained in the second copy, the thermofield double state is indistinguishable from a thermal mixed state in $\mathcal{H}_1$.

For local operators O_1 in $\mathcal{H}_1$, we have

$$\langle\mathrm{TFD}|O_1|\mathrm{TFD}\rangle = \frac{1}{Z(\beta)}\mathrm{Tr}_1 e^{-\beta H_1}O_1. \tag{2.29}$$

If consider the local operators $O_1\in\mathcal{H}_1$, and $O_2\in\mathcal{H}_2$, the expectation value $\langle\mathrm{TFD}|O_1O_2|\mathrm{TFD}\rangle$ may in general be non-vanishing, despite there being no correlations at the level of Lagrangians. This is an interesting quantum effect due to entanglement.

2.3.1 Eternal Black Holes and Thermofield Double States

In AdS/CFT, when the gravitational side is pure AdS, states in the bulk are dual to vacuum states in the boundary. However, when the boundary theory is in a highly energetic thermal state, the geometry in the bulk theory is characterized by a horizon: a black hole in AdS is dual to a greatly excited thermal state in the boundary. This opens the possibility of studying the properties that define the spacetime of a black hole through the thermal state of the dual CFT.

In 2001 Maldacena proposed that the geometry of an eternal (two-sided) black hole in AdS is dual to two copies of the CFT in a *temofield double* state [35]. This seemingly bold proposal, makes sense if we think about the maximally extended geometry of a Schwarzschild black hole in AdS. Indeed, as depicted in the picture 2.2, for a maximally extended AdS-Schwarzschild black hole there are two distinct asymptotic regions, and it is only natural to assume that there is a dual CFT description in each boundary (say CFT_R and CFT_L). The boundaries are causally disconnected, but we can still define a classical geometry connecting the two regions. This geometry is what we refer to as a wormhole, or Einstein-Rosen bridge. As we know, a thermofield double state describes two correlated but uncoupled systems; meaning that the two boundary CFTs, although not interacting at the level of the lagrangian, can have non-vanishing expectation values $\langle \text{TFD}|O_L O_R|\text{TFD}\rangle$, where O_L is an operator in CFT_L, and O_R is an operator in CFT_R. This correlation is purely quantum mechanical, and is due to the fact that the two theories are entangled. In this sense we can argue that the geometry of the Einstein-Rosen bridge is created by entangling the two conformal field theories at the boundaries of the maximally extended geometry.

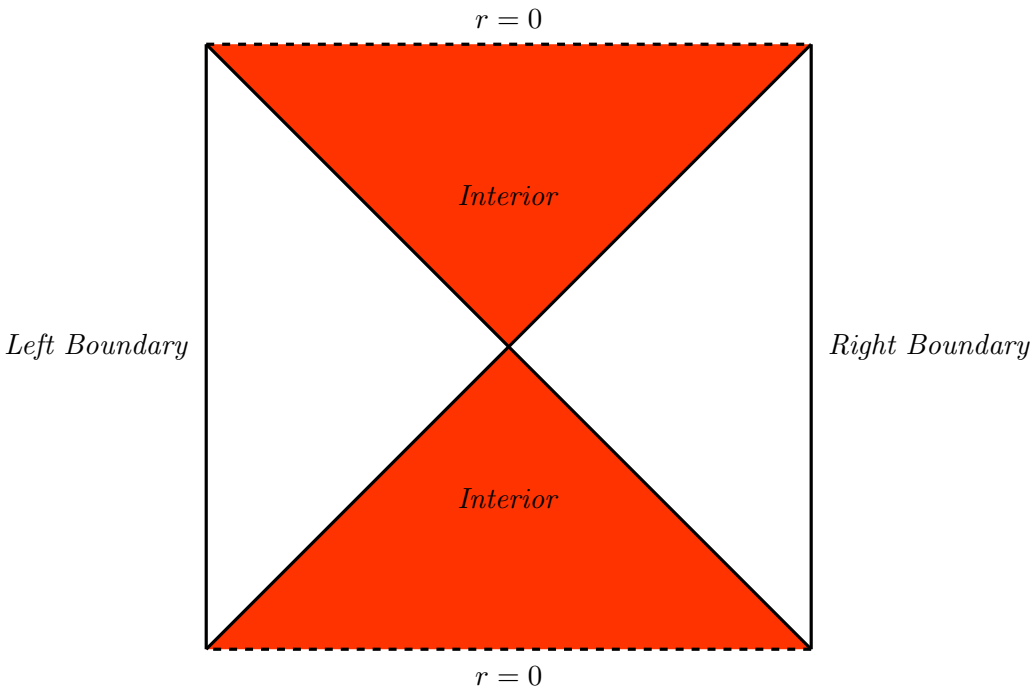

Figure 2.2: Penrose diagram of an eternal AdS black hole. The region shaded in red represents the interior.

The "total" Hamiltonian $H = H_L - H_R$ acting on the doubled Hilbert space $\mathcal{H} = \text{CFT}_L \otimes \text{CFT}_R$, has an interesting interpretation according to this picture. On the CFT side, the termofield double state is left invariant under the time evolution dictated by H:

$$e^{-iHt}|\text{TFD}\rangle = \frac{1}{\sqrt{Z(\beta)}} \sum_n e^{-\beta \frac{E_n}{2}} e^{-i(H_L - H_R)t}|n, L\rangle|n, R\rangle = |\text{TFD}\rangle\,. \tag{2.30}$$

From the bulk prospective, H can be viewed as the dual to the generator of time isometries ∂_t.

This proposal relating termofield double states to AdS black holes can be motivated formally via path integrals, and its generalizations have been given the slogan ER=EPR. This conjecture has only been quantitatively motivated at a semiclassical level, but, depending on who is interrogated, is believed to be true in a more general and fundamental sense; it is believed to be a property of any UV complete theory of quantum gravity.

2.4 Holographic Entanglement Entropy

As we have seen in this chapter, in the context of quantum mechanics and QFT the concept of entanglement entropy naturally arises when we consider subdivisions of the Hilbert space. Particularly, in QFTs this subdivision acquires a geometric "flare". As such, given the AdS/CFT correspondence it would be interesting to understand how this subdivision on the boundary is reflected in the bulk. The precise bulk interpretation of boundary entanglement entropy was first found by Ryu and Takayanagi [6] and was later generalized by Hubeny, Rangamani, and Takayanagi [36]. Ever since, a vast literature has emerged trying to explore the connection between quantum information and holography.

Let's consider a holographic theory whose bulk manifold is described by a static metric. Given a spatial subregion A on the boundary spacetime and a codimension-2 surface Γ_A embedded in the bulk, such that $\partial\Gamma_A = A$ and such that Γ_A is homologous to A, then the Ryu-Takayanagi proposal states that

$$S_A = \mathrm{Min}_{\Gamma_A}\left[\frac{\mathrm{Area}(\Gamma_A)}{4G_N}\right]. \tag{2.31}$$

This ansatz can be generalized to the case in which the bulk geometry is time dependent. In that case we must consider a foliation of the bulk manifold, pick a time slice Σ, and extremize the area of a codimension-2 surface bulk surface $\Gamma_A(t)$ (which, again, has to be homologous to the spatial subregion A, and share the same boundary as A) before proceeding with the minimization. That is,

$$S_A = \mathrm{Min}_{\Gamma_A(t)}\left[\mathrm{Extr}_{\Gamma_A(t)}\left(\frac{\mathrm{Area}(\Gamma_A(t))}{4G_N}\right)\right]. \tag{2.32}$$

2.4.1 Heuristic Motivation of the RT Formula

We can sketch a proof of the Ryu-Takayanagi formula using the replica trick presented earlier. In holography this means making n copies of the bulk manifold, sew them together cyclically, and evaluate the gravitational partition function on the resulting manifold. This should in principle yield the boundary entanglement entropy via (2.24) [6, 33], that is, if we believe one of the fundamental principles of AdS/CFT, namely

$$Z_{\mathrm{AdS}} = Z_{\mathrm{CFT}}\,. \tag{2.33}$$

Suppose the replicated bulk geometry is $\mathcal{B}_n$, from the above we expect

$$Z[\mathcal{M}_n] = e^{-S[\mathcal{B}_n]}\,, \tag{2.34}$$

where $\mathcal{M}_n$ is the n-sheeted manifold that implements the replica trick entanglement entropy for the boundary region A. For simplicity we restrict ourselves to the AdS_3 case. The three-dimensional case is particularly simple since we can assume that the back-reacted geometry $\mathcal{B}_n$ that approaches $\mathcal{M}_n$ on the boundary is an n-sheeted AdS_3 geometry. The manifold $\mathcal{M}_n$ and $\mathcal{B}_n$ are both characterized by a deficit angle $\delta = 2\pi(1-n)$: in the former case the deficit appears

along the boundary ∂A, whilst in the latter it appears along some surface (curve) Γ_A. The Ricci scalar in conical spaces is given by [37]

$$R = 4\pi\,(1-n)\,\delta(\Gamma_A) + R_{\text{AdS}}\,, \tag{2.35}$$

where the support of the delta-function is defined along the surface (curve) Γ_A, and R_{AdS} is the Ricci scalar of empty AdS_3. Plugging this into the gravitational action and evaluating the integral, one finds

$$S = -\frac{1-n}{4G}\text{Area}(\Gamma_A) + \text{terms linear in } n\,, \tag{2.36}$$

hence, by plugging the gravitational partition function in (2.24), we find

$$S_A = -\frac{\partial}{\partial n}\left[\frac{1-n}{4G}\text{Area}(\Gamma_A)\right]_{n=1} = \frac{\text{Area}(\Gamma_A)}{4G}\,. \tag{2.37}$$

The last step consists in the realization the the area is minimal: this is because of the action principle applied to (2.36).

This argument can be applied in higher dimensions as well, with all the caveats that come from having more dimensions [6, 33].

2.4.2 An Example

Let's see the holographic entanglement entropy formula in action with a simple example. Consider a $2d$ CFT and the spatial subregion $A = [-\frac{\ell}{2}, \frac{\ell}{2}]$ in its vacuum state. The semiclassical dual geometry is pure AdS_3, and the metric reads

$$ds^2 = \frac{L}{z^2}(-dt^2 + dx^2 + dz^2). \tag{2.38}$$

This geometry is obviously static, meaning that we can set $t = 0$ and express x as a function of z so that on the time-slice $t = 0$ the induced metric reads

$$dl^2 = \frac{L^2}{z^2}\left(1 + x'(z)\right)dz^2. \tag{2.39}$$

The area of the induced codimension-2 surface (in this case a curve) is obtained by integrating the determinant of the induced metric. If we parametrize the curve so that $x(0) = \ell/2$, we find that the lenght of the curve is given by

$$\text{Area}(\Gamma_A) = 2\int_\epsilon^{z_0} \text{d}z\frac{L}{z}\sqrt{1 + \left(\frac{\text{d}x}{\text{d}z}\right)^2}. \tag{2.40}$$

We have introduced a cutoff parameter ϵ since the lenght of a curve reaching the boundary at $z = 0$ is infinite. This is equivalent to stating that the entanglement entropy in the boundary CFT is a UV divergent quantity. At this point we must find the curve that minimizes the action, i.e., the geodesic. This is a simple variational problem, and it turns out that the geodesic is given by

$$x(z) = \sqrt{\frac{\ell^2}{4} - z^2}. \tag{2.41}$$

Plugging this in the Ryu-Takayanagi formula we arrive at

$$S_A = \frac{1}{3}\frac{3L}{2G_N}\log\frac{\ell}{\epsilon}\,. \tag{2.42}$$

If we identify the central charge c with the factor $3L/2G_N$ we recover the expected result from CFT_2

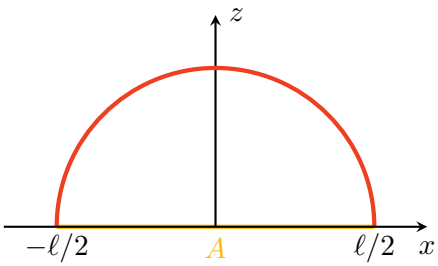

Figure 2.3: the geodesic in empty AdS_3 connecting the boundaries of the boundary subregion is a semicircle penetrating into the bulk.

2.4.3 Holographic Proof of Strong Sub-additivity

If the holographic prescription for computing entanglement entropy is correct, then we must confirm that basic properties of entanglement entropy are not violated. We can for example check whether or not strong sub-additivity is violated.

For simplicity, let's consider the static case with AdS_3 geometry in the bulk, and let's consider the spatial bondary regions A and B. The RT surfaces are geodesic lines parametrized by (2.41). We denote with γ_A the RT surface of region A, with γ_B the RT surface of region B, with $\gamma_{A\cup B}$ the RT surface of region $A \cup B$, and finally with $\gamma_{A\cap B}$ the RT surface of region $A \cap B$. The RT surfaces are drawn in the figure 2.4 below. A quick glance at the figure allows us to conclude that:

$$S(A) + S(B) \geq S(A \cup B) + S(A \cap B).$$

The same proof in QFT is quite technical and not at all straight forward, so it is quite remarkable that we were able to do it with such ease in the holographic setting! With some care one can extend this result to the time dependent case and to higher dimensional correspondences.

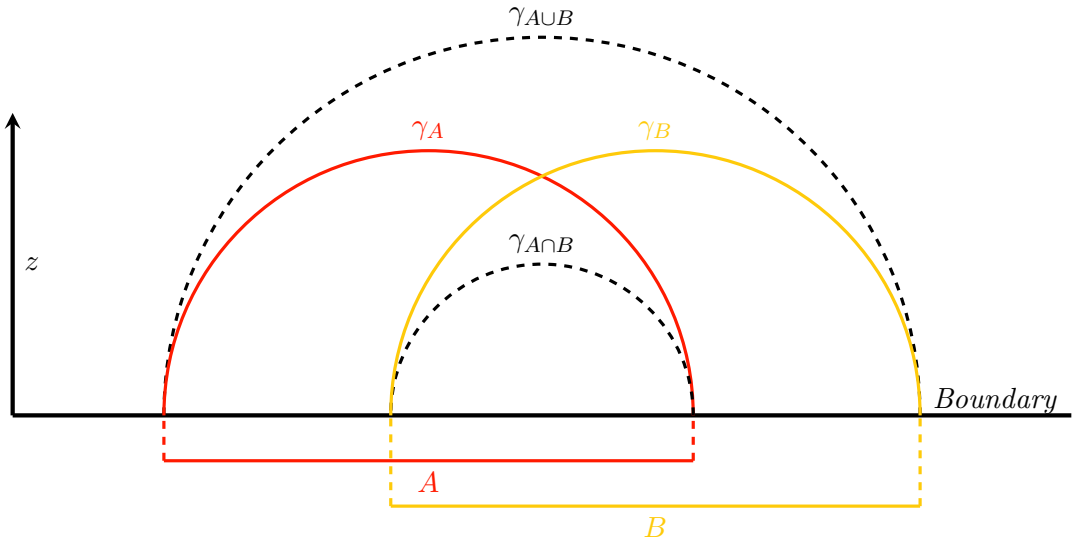

Figure 2.4: graphical proof of strong subadditivity of entanglement entropy in holography.

Chapter 3

Holographic Complexity

In this chapter we explore a quantum information quantity which has recently made its way into the realm of inquiry of high energy physics: quantum complexity.

3.1 Quantum Computational Complexity

In the field of information theory the notion of complexity, or hardness, is a fundamental one. Broadly speaking, given a computational problem the complexity is a measure of the inherent difficulty in carrying out such computation. This notion naturally carries over to the sub-field of quantum information theory, where computations can be viewed in therms of quantum circuits [38].

A quantum circuit is a collection of quantum gates and wires connected to each other so as to form an a-cyclic network. The gates are represented by operators and the wires are the qubits the gates act on. When the gates are represented by unitary operators the circuit is said to be unitary. We will focus on the unitary case, as this choice does not result in a loss of generality. The circuit will have a certain number of input qubits and a certain number of output qubits, and when the circuit is unitary these coincide. At last, we say that a gate is k-local if the gate acts on no more than $k \in \mathbb{N}$ qubits. We can now give a rudimentary definition of what we mean by quantum complexity.

Definition: *given a reference state $|\psi_r\rangle$ and a target state $|\psi_t\rangle$ in a K-qubit system, where $K \in \mathbb{N}$, we define the complexity of $|\psi_t\rangle$ with respect to the reference state as the minimal number of k-local gates necessary in a circuit that has $|\psi_r\rangle$ as input and $|\psi_t\rangle$ as output.*

It may be noted that this definition is ambiguous with respect to K: relative complexity of two states depends in on the number of qubits on which a gate can act. This kind of ambiguity is what we call a *multiplicative ambiguity*, since a k-local gate can always be reproduced by a certain number of $(k-1)$-local gates.

One can also define the relative complexity of states in a slightly different way, which is useful when trying to extend the notion of complexity to quantum field theories;

definition: *given a reference state $|\psi_r\rangle$ and a target state $|\psi_t\rangle$ in a K-qubit system, where $K \in \mathbb{N}$, and a small tolerance parameter $\epsilon > 0$, we define the complexity of $|\psi_t\rangle$ with respect to the reference state and with tolerance ϵ as the minimal number of k-local gates necessary in a circuit such that*

$$\|g_n \cdots g_1 |\psi_r\rangle - |\psi_t\rangle\|^2 \leq \epsilon \,, \tag{3.1}$$

where $\{g_1, \cdots, g_n\}$ are the gates that make up the circuit, and $\|\cdot\|$ a norm in $\mathbf{CP}(2^K - 1)$.

This last definition introduces an additional ambiguity, namely the tolerance parameter, which is what we call an additive ambiguity. The reason is that with such definition an additive logarithmic term appears in the complexity (see [39]).

Finally, complexity may also be defined via the unitary operators that act on the qubits. The definition is a simple extension of the above definitions,

definition: *given a unitary operator $U \in \mathbf{SU}(2^K)$, where $K \in \mathbb{N}$, we define the complexity of U as the minimal number of k-local gates necessary in a circuit such that*

$$U = g_n \cdots g_1 \cdot \mathbb{I}\,, \tag{3.2}$$

where $\{g_1, \cdots, g_n\}$ are the gates that make up the circuit.

If one replaces the identity operator in (3.2) with a generic unitary operator $V \in \mathbf{SU}(2^K)$, one gets the definition of relative complexity of two unitaries $\mathcal{C}(U, V)$. One can show that this quantity satisfies the conditions to be a right-invariant[1] metric on the group manifold $\mathbf{SU}(2^K)$.

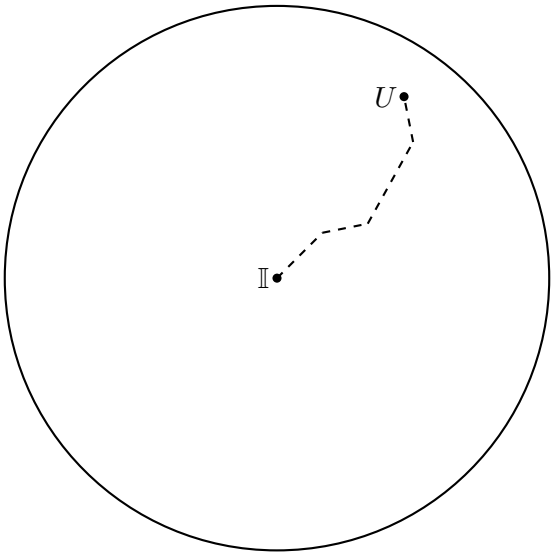

Figure 3.1: Complexity of a unitary in $\mathbf{SU}(2^K)$.

The fact that the relative complexity is a metric suggests that perhaps quantum complexity can be understood as a right-invariant geometry. In this sense, the circuit complexity of a unitary operator can be related to a geodesic problem in a particular curved geometry. This elegant idea was initially suggested by Michael Nielsen et al. [40, 41]. In this framework, the problem of finding the minimal size quantum circuit that implements a given unitary K-qubit operation $U \in \mathbf{SU}(2^K)$ is translated to a Hamiltonian control problem. In other words, we look for a time-dependent Hamiltonian $H(t)$ that generates U under time evolution,

$$U(t) = \mathcal{P} \exp\left[\int_0^{t'} \mathrm{d}t'\, H(t')\right], \quad \text{where} \quad H(t') = \sum_i Y^i(t') M_i\,, \tag{3.3}$$

M_i are the generalized Pauli matrices, and $\mathcal{P}$ implements a time ordering of the Hamiltonian so that the circuit is built form the right to the left, and then we minimize the so-called *cost*

[1] To be right-invariant means that if $W \in \mathbf{SU}(2^K)$ is another unitary then $\mathcal{C}(U, V) = \mathcal{C}(UW, VW)$. One can easily check that this is the case with the relative complexity. On the other hand, the relative complexity is not left-invariant, meaning that $\mathcal{C}(U, V) \neq \mathcal{C}(WU, WV)$.

functional, defined as

$$\mathcal{F}(U(t)) = \int_0^1 \mathrm{d}t\, F(U(t), \dot{U}(t)) \tag{3.4}$$

with the boundary conditions $U(0) = \mathbb{I}$ and $U(1) = 1$. The function $F(U, v)$ needs to satisfy various conditions and there are a number of possible choices examined in [42].

3.1.1 Growth Rate of Complexity

Let's assume we are given a Hilbert space constructed with K qubits. A seemingly natural question to ask, given that we have just defined complexity, is: how "complex" can a given state be?

To answer this question, we may start by writing down the most general state in this 2^K-dimensional Hilbert space,

$$|\psi\rangle = \sum_{i=1}^{2^K} \alpha_i |i\rangle\,. \tag{3.5}$$

There are of course infinite possible states in this space, since we can pick a from continuous infinity of possible parameters α_i. Nonetheless, we can give an estimate of "how infinite" by regularizing the infinity. In fact, if for some reason our choice was restricted to a set of discrete values, say there are m such values[2], we could in principle count the number of possible states. In fact, with this restriction the number of possible states $\mathcal{C}_m$ is

$$\mathcal{C}_m = m^{2^K} = \exp(2^K \log m). \tag{3.6}$$

Note how the dependence on m is weaker relative to the number of qubits K. The maximal complexity is for this qubit system exponential in k. (It should be noted that almost all states in this Hilbert space are exponentially complex.)

It is interesting to compare (3.6) with the classical counterpart. Classically, a similar counting procedure for a K-bit system allows to conclude that the maximal complexity is proportional to K. The difference is enormous.

Further, the time it takes for a K-qubit system to reach thermal equilibrium is polynomial in K whilst the time it takes to reach maximal complexity is exponential in K. These time-scales are vastly separated different from a quantum-mechanical perspective. A K-qubit system complexifies in a linear fashion: the complexity grows linearly for a long time, until it saturates at $\log \mathcal{C} \simeq K$. It was argued by Susskind [39], that the slope of the curve during the linear growth regime is given by

$$\frac{\mathrm{d}\mathcal{C}}{\mathrm{d}t} = TS, \tag{3.7}$$

where T is the temperature and S the entropy. This guess is based on two basic observations. Firstly, complexity is an extensive quantity: it is proportional to the number of degrees of freedom in the system. Therefore, entropy may be used to estimate the size of the system, hence, the growth rate should be proportional to S. Second of all, the slope should have units of inverse time. The rate could therefore be proportional to the energy of the system, however, the ground states of systems such as extremal black holes have non-vanishing entropy and energy, but no matter what complexity they have is constant in time. Temperature seems to be the only reasonable quantity.

The claim that complexity grows linearly with time can be Justified using Nielsen's approach [42], but that this happens all the way to $t_{\mathcal{C}} = e^K$ is a conjecture.

[2] We can think of m as our regulator.

3.2 Complexity from Holgraphy

When a gravitational system collapses to form a black hole the horizon grows monotonically until a final value is reached. If we believe that black holes follow the laws of thermodynamics, the growth of the event horizon can be traced back to the second law of thermodynamics: entropy increases until thermal equilibrium is reached. This is a well-known phenomenon that in principle can be observed by an asymptotic observer.

There is another similar phenomenon that takes place within the bounds set by the event horizon, and which cannot be traced to the irreversibility of thermodynamics: the growth in time of the interior of the black hole. The reason we cannot describe this evolution with the second law of thermodynamics, is that the growth continues for times much greater than the thermalization time (which is the time it takes to reach thermal equilibrium.)

Motivated by the Holographic principle, Susskind and others have proposed that this growth can be accounted for by the growth of complexity in the dual boundary description. There are two competing conjectures as to what bulk quantity is dual to the complexity of states in the boundary: the complexity = volume (CV) and the complexity = action (CA) conjectures.

3.2.1 Growth of the Einstein-Rosen bridge: Complexity = Volume

Consider an eternal black hole geometry which, as we know, is dual to the thermofield double state introduced in section 2.3. To track the evolution of the region beyond the horizon we have to choose a foliation of the geometry. We imagine that for each $t = t_L = t_R$ a space-like surface is attached to the two boudaries, moreover, we restrict to only slices of maximal spatial volume. In principle one could choose different times at the two boundaries, but the symmetry properties of this gravitational setup, namely the invariance under the shifts $t_L \to t_L + \Delta t$ and $t_R \to t_R - \Delta t$, allow us to choose $t_L = t_R$. From the boundary theory perspective this symmetry is manifested through the invariance of the thermofield double state under the time evolution of the Hamiltonian $H = H_R - H_L$.

The metric describing the geometry of interest is given by

$$ds^2 = -f(r)dt^2 + f(r)^{-1}dr^2 + r^2 d\Omega_{d-2}^2, \tag{3.8}$$

where the blackening factor is

$$f(r) = \frac{r^2}{L^2} + 1 - \frac{\mu^2}{r^{d-3}}, \tag{3.9}$$

and where L is the AdS radius. It is particularly easy to show that the volume of the Einstein-Rosen bridge grows in the limit $t \to \infty$. For a given time-slice the volume reads

$$\mathcal{V}(t) = \int \mathrm{d}t \sqrt{|f(r)| r^{2(d-2)}}, \tag{3.10}$$

subject to the condition $\delta\mathcal{V} = 0$. In the limit $t \to \infty$ the maximal slices are simply given by constant r curves, since the system is translationally and rotationally invariant. The value of r in this late time limit is therefore is found by maximizing the integrand, that is,

$$\frac{\partial}{\partial r}\sqrt{|f(r)| r^{2(d-2)}} = 0 \implies r_f = \frac{\mu}{\sqrt{2}}. \tag{3.11}$$

The maximal volume for late times is then given by

$$\mathcal{V}(t) = 2\Omega_{d-2}\, r_f^{d-2}\sqrt{|f(r_f)|}\, t\,. \tag{3.12}$$

From (3.12) we can determine the rate of growth of the maximal volume at late times, i.e.,

$$\frac{\mathrm{d}\mathcal{V}}{\mathrm{d}t} = 2\omega_{d-2} r_f^{d-2} \sqrt{|f(r_f)|}, \tag{3.13}$$

which can be expressed as

$$\frac{\mathrm{d}\mathcal{V}}{\mathrm{d}t} = \frac{2L}{d-1} \mathcal{A}_H \kappa \,. \tag{3.14}$$

Having used the explicit expression for $f(r)$ and then related all to the surface gravity κ and the area of the event horizon $\mathcal{A}_H$. We can then compare this with the growth rate of complexity

$$\frac{\mathrm{d}\mathcal{C}}{\mathrm{d}t} \sim ST. \tag{3.15}$$

If, motivated by the holographic principle, we relate S to the area of the event horizon and T to the surface gravity, we get

$$\frac{\mathrm{d}\mathcal{C}}{\mathrm{d}t} \sim \frac{\mathcal{A}_H \kappa}{8\pi G}, \tag{3.16}$$

in this sense, by comparing (3.14) and (3.16), we can conclude that the growth rate of complexity is proportional to the growth rate of the volume. This is the essence of the CV conjecture.

CV conjecture: *in a holographic theory the complexity of a state in the boundary theory is dual to the extremal volume of a time-slice $\mathcal{B}$ anchored to the boundary state at time t,*

$$\mathcal{C}_{\mathcal{V}} = \frac{\mathcal{V}(\mathcal{B})}{G_N \ell}, \tag{3.17}$$

where ℓ is a length scale associated with the bulk geometry, G_N Newton's constant, and $\mathcal{V}(\mathcal{B})$ the maximal volume of the time-slice $\mathcal{B}$.

The maximal volume slice in an eternal AdS black hole geometry looks something like the yellow curve in fig. 3.2. It should be clear that such volume diverges when we approach the boundaries of the spacetime, so some kind of regularization is needed. We will see later how this is done in practice, for now, it suffices to say that the structure of the UV divergences was found in [43],

$$\mathcal{C}_{\mathcal{V}} = \frac{L^{d-1}}{(d-1)G_N} \int \mathrm{d}^{d-1}\sigma \sqrt{h} \left[\frac{1}{\delta^{d-1}} - \frac{(d-1)}{2(d-2)(d-3)\delta^{d-3}} \left(R^a{}_a - \frac{1}{2}R - \frac{(d-2)^2}{(d-1)^2} K^2 \right) + \cdots \right], \tag{3.18}$$

where $h_{\alpha\beta}$ is the induced metric on the bulk extremal surface. When $d = 3$ the first sub-leading divergence appears as a logarithmic term,

$$\mathcal{C}_{\mathcal{V}}^{\log} = \log\left(\frac{\delta}{L}\right) \frac{L^2}{8G_N} \int \mathrm{d}^2\sigma \sqrt{h} (4R^a{}_a - 2R - K^2) \,. \tag{3.19}$$

We only commented on the late-time behavior of the volume of the ERB, but a comprehensive analysis for all times in the case of AdS black holes was carried out in [11].

3.2.2 Complexity = Action

The complexity = volume conjecture has since its conception passed a number of tests which seem to corroborate the proposal. First of all, the maximal volume slice naturally reproduces the growth rate of complexity, for the quantity ST provides a rough estimate of the rate of

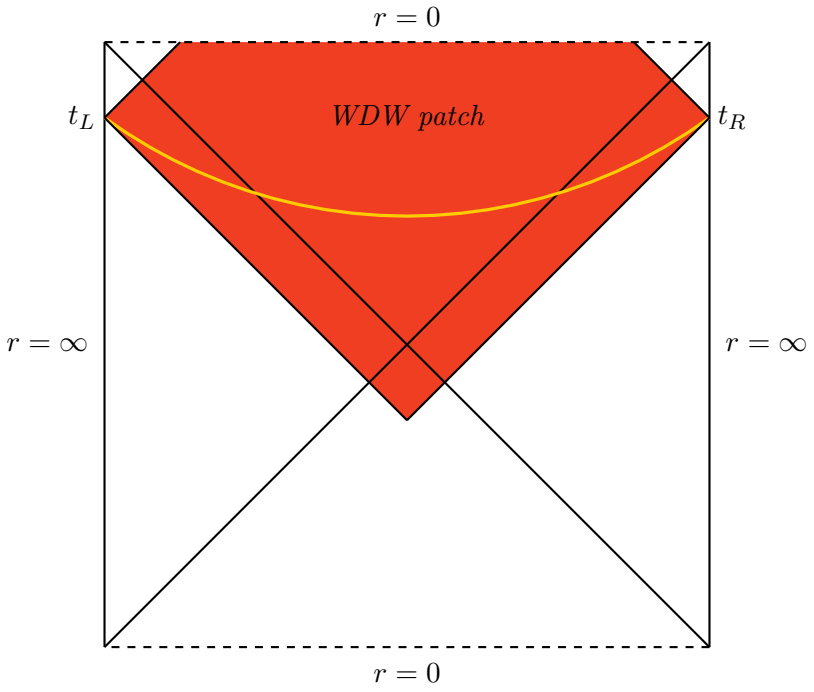

Figure 3.2: Penrose diagram of an eternal AdS black hole. The region shaded in red represents the WDW patch, while the yellow curve represents the maximal volume slice.

complexification of a strongly coupled system. Secondly, shock wave geometries have proven that in the maximal volume slice construction correctly captures cancellations that are expected from complexity [9].

Despite it being a quite robust proposal, the CV-duality presents some undesirable features. One of these features is related to the length-scale ℓ, which has to be picked by hand depending on the geometry, in an seemingly arbitrary manner. Moreover, it is not clear why the maximal slice should be preferred over any other slice. In an attempt to construct the bulk dual of complexity that inherits the niceties of the CV-duality but excludes these unsatisfactory elements, the CA-duality was introduced [8, 10].

CA conjecture: *in a holographic theory the complexity of a state in the boundary theory is dual to the bulk action evaluated on the spacetime region formed by the union of all spacelike surfaces anchored at the boundary at time t (also known as the Wheeler-DeWitt patch),*

$$\mathcal{C}_{\mathcal{A}} = \frac{\mathcal{I}_{\text{WDW}}}{\pi}\,, \tag{3.20}$$

where $\mathcal{I}_{\text{WDW}}$ is the gravitational action evaluated on the WDW patch.

The Wheeler-DeWitt patch of an AdS black hole is depicted in the figure 3.2. By integrating over the Wheeler-DeWitt patch we circumvent the problem of singling out an extremal time-slice as the domain of dependence of the maximal slice selected by the CV-duality coincides with the WDW patch. Furthermore, no arbitrary length scale is needed in (3.20).

We can motivate the CA-duality by looking at the geometry dual to the thermofield double state. We pick the boundary state at times t_R and t_L on the left and right boundaries of the eternal black hole geometry,

$$|\psi(t_L, t_R)\rangle = e^{-i(H_L t_L + H_R t_R)} \frac{1}{\sqrt{Z}} \sum_{\alpha} e^{\frac{\beta E_\alpha}{2}} |E_\alpha\rangle_L |E_\alpha\rangle_R. \tag{3.21}$$

The geometry behind the horizon can be viewed as a d-dimensional world-volume $\mathcal{W}$ approximated by a d-dimensional cylinder of length $t_L + t_R$. Cross sections of this world-volume have spatial area $G_N S$ on a time interval roughly equal to L_{AdS} so that the world volume of the tube is $|\mathcal{W}| \sim G_N S L_{\text{AdS}}$. Since the maximal volume of the wormhole is $\mathcal{V} \sim G_N S$, the complexity equals volume formula my be rewritten as

$$\frac{\mathcal{V}(t_L, t_R)}{G_N L_{\text{AdS}}} \sim \frac{|\mathcal{W}(t_L, t_R)|}{G_N L_{\text{AdS}}^2}, \tag{3.22}$$

and since the cosmological constant is proportional to $-1/L_{\text{AdS}}^2$ the above expression can be expressed in terms of the classical action of the world-volume $\mathcal{W}$. This is what inspired the CA-duality.

As for the maximal volume, the gravitational action diverges when approaching the boundary. The general structure of the UV divergences is slightly more complicated than the one found for the volume and can be found in [43].

3.2.3 Subregion Complexity

It is possible to extend the holographic complexity proposals above so that the complexity is calculated for a mixed state on the boundary. Mixed states are produced by restricting boundary states on subregions, in particular, holographic mixed states are encoded in the bulk by the entanglement wedge relative to the subregion [44, 45]. As such, we expect that the prescription for holographic complexity of mixed states will involve the entanglement wedge.

This problem was first picked up in [46], where a CV-like duality was proposed for time independent geometries. Later, the proposal was generalized to non-static geometries [43] and a CA counterpart was also introduced.

Subregion CV-duality states that: *given a subregion A on a boundary time slice Σ, the subregion complexity corresponding to A is given by the maximal volume of a bulk timeslice $\mathcal{R}_A$ bounded by A and the HRT surface atached to ∂A, that is*

$$\mathcal{C}_{\mathcal{V}}(A) = \frac{\mathcal{V}(\mathcal{R}_A)}{G_N \ell} \tag{3.23}$$

where $\mathcal{V}$ is the above-mentioned volume, G_N Newton's constant, and ℓ is a length-scale associated to the bulk geometry.

Similarly, **subregion CA-duality** states that: *given a subregion A on a boundary time slice Σ, the subregion complexity for A is given by the bulk action evaluated on the intersection of the entanglement wedge corresponding to the subregion A and the Wheeler-DeWitt patch corresponding to the boundary slice Σ, that is*

$$\mathcal{C}_{\mathcal{A}}(A) = \frac{\mathcal{I}(\mathcal{W})}{\pi} \tag{3.24}$$

where $\mathcal{I}$ is the above-mentioned action, and $\mathcal{W}$ is the intersection of the Wheeler-DeWitt patch and the entanglement wedge.

3.3 Complexity in Quantum Field Theories

At the time Ryu and Takayanagi came up with a proposal for how entanglement entropy should be understood in holography we had a good understanding of how to define entanglement entropy in many body quantum systems. The same cannot be said of Coplexity. We are in fact far from having a clear picture, and in some sense we are working backwards: starting from the bulk geometry and working our way towards the boundary theory. Nevertheless, some progress has

been made using Nielsen's geometric approach, particularly for free theories [47] and weakly interacting theories [48]. In [47] the authors considered the free field theory defined by

$$H = \int \mathrm{d}^{d-1}x \left[\pi(x)^2 + \partial^\mu\phi(x)\partial_\mu\phi(x) + m^2\phi(x)^2\right], \tag{3.25}$$

which on a lattice looks like

$$H = \frac{1}{2}\sum_{\vec{n}} \left\{ \frac{p(\vec{n})^2}{\delta^{d-1}} + \delta^{d-1}\left[\frac{1}{\delta^2}\sum_i [\phi(\vec{n}) - \phi(\vec{n}-\hat{x}_i)]^2 + m^2\phi(\vec{n})^2\right]\right\}. \tag{3.26}$$

As for the cost function defining the Hamiltonian control problem, they chose

$$\mathcal{F}(U) = \int_0^1 \mathrm{d}s \sqrt{G_{IJ}Y^I(s)Y^J(s)}\,, \tag{3.27}$$

which geometrically corresponds to looking for geodesics in a Riemannian geometry. In this setup they found that the leading divergence of the complexity of the ground state relative to a Gaussian reference state is given by

$$\mathcal{C} \sim \left(\frac{V}{\delta^{d-1}}\right)^{\frac{1}{2}}. \tag{3.28}$$

In holography we expect the leading divergence to be $\mathcal{C}_{\text{holo}} \sim V/\delta^{d-1}$, therefore, the free theory computation differs by the power of $1/2$ appearing in (3.28). In [47] it was noted that with a different cost function, hence a different norm, the correct power can be attained. Another possibility, pointed out in [49], is that the discrepancy is a result of strong couplings. In fact, whereas the result (3.28) is valid for a free theory, the holographic quantity we are comparing it to arises from a strongly coupled boundary theory.

Further developments along these lines can be found in, e.g., [50, 51, 52]. A different approach is that of path integral optimization, where computational complexity is associated to an optimization problem for Euclidean path-integrals [53]. In particular, the problem is reduced to the minimization of a functional, which in two dimensions reduces to the *Liouville* action.

Chapter 4

Janus Geometries

Conformal field theories have over the years proven to be remarkably important in the quest to understand quantum field theories. The large number of symmetries inherent to CFTs is what make them so powerful. In fact, these symmetries are often all we need to completely constrain correlation functions, making CFTs the perfect playground to investigate non-perturbative aspects of QFTs. Most notably, CFT appear to be the natural endpoints of RG flows, and therefore characterize the UV and IR limits of ordinary QFTs.

However, if we wish to apply CFTs to *the real-world* it would seem that we find ourselves at an impasse. Indeed, real-world systems are characterized by impurities, *defects*, *domain walls*, and are generally finite in size (that is to say there are boundaries.) All these features conspire to break symmetries, most notably translational and rotational symmetries. This is one of the may reasons why it is interesting to study conformal field theories with boundaries and defects (DCFT and BCFT respectively.)

Janus solutions are dilatonic deformations of AdS that holographically describe interface conformal field theories. While it was originally found as a non-supersymmetric dilatonic deformation of $\mathrm{AdS}_5 \times \mathbf{S}^5$ [17], it was later discovered that a similar non-supersymmetric deformation could be performed on $\mathrm{AdS}_3 \times \mathbf{S}^2 \times \mathcal{M}_4$ [14]. $\mathrm{AdS}_5 \times \mathbf{S}^5$ can also be deformed preserving $\mathbf{SO}(2,3) \times \mathbf{SU}(3)$ symmetry [18]; here we will only consider the non-supersymmetric deformations. On the bulk side, these solutions feature a thick AdS_{d-1}-sliced domain wall in AdS_d with a non-trivial dilaton field that, as we'll soon see, approaches different constant boundary values on each side of the geometry. On the boundary, the $\mathcal{N} = 4$ SYM theory is deformed by an exactly marginal operator dual to the dilaton, so that the Yang-Mills coupling jumps discontinuously at the interface between the two asymptotic regions [54].

Interestingly, Janus black hole-like solutions can also be found [14, 15, 55]. Here we'll discuss the *time dependent Janus BTZ solution* and the *static Janus BTZ solution.*

4.1 Three-dimensional Janus

This section is dedicated to the study of the Janus deformation of $\mathrm{AdS}_3 \times \mathbf{S}^3 \times \mathcal{M}_4$, where $\mathcal{M}_4$ is a compact manifold. The starting point is an ansatz for a dilatonic deformation of $\mathrm{AdS}_3 \times \mathbf{S}^3 \times \mathcal{M}_4$ in the Einstein frame, namely

$$ds^2 = e^{\frac{\phi}{2}} f(\mu) \left(d\mu^2 + ds^2_{\mathrm{AdS}_2}\right) + e^{\frac{\phi}{2}} ds^2_{\mathbf{S}^3} + e^{-\frac{\phi}{2}} ds^2_4 \,, \tag{4.1}$$

where $\phi(\mu)$ is a non trivial dilaton field. From this ansatz one can write down the ten-dimensional IIB supergravity equations of motion, but it turns out that the same equations can be derived from a dimensionally reduced action. The ansatz for the dimensional reduction is

$$ds^2 = e^{\frac{\phi}{2}} g_{ab} dx^a dx^b + e^{\frac{\phi}{2}} ds^2_{\mathbf{S}^3} + e^{-\frac{\phi}{2}} ds^2_4, \tag{4.2}$$

where the metric $g_{ab}(x)$ and the dilaton $\phi(x)$ are general functions of the three-dimensional coordinates x^a. The equations of motion of interest are derived from the three-dimensional action

$$I = \frac{1}{16\pi G_3}\int \mathrm{d}^3x\,\sqrt{g}\,\left(R_3 - g^{ab}\partial_a\phi\partial_b\phi + \frac{2}{L^2}\right)\,, \tag{4.3}$$

where L is the AdS radius and G_3 the three-dimensional Newton constant, which couples three-dimensional Einstein gravity with negative cosmological constant to a non-trivial scalar field.

The resulting EOMs can be solved exactly and lead to the Janus AdS_3 geometry

$$ds_3^2 = L^2(f(y)ds^2_{\mathrm{AdS}_2} + dy^2)\,, \quad \text{where} \quad f(y) = \frac{1}{2}\left(1+\sqrt{1-2\gamma^2}\cosh 2y\right)\,, \tag{4.4}$$

and with the dilaton field given by

$$\phi(y) = \phi_0 + \frac{1}{\sqrt{2}}\log\left(\frac{1+\sqrt{1-2\gamma^2}+\sqrt{2}\gamma\tanh y}{1+\sqrt{1-2\gamma^2}-\sqrt{2}\gamma\tanh y}\right)\,. \tag{4.5}$$

It is clear that the solution depends on the parameter γ which is defined in the interval $[-1/\sqrt{2}, 1/\sqrt{2}]$. Plugging $\gamma = 0$ in (4.4) and (4.5), we get

$$ds_3^2 = L^2(\cosh^2 y\, ds^2_{\mathrm{AdS}_2} + dy^2) \quad \text{and} \quad \phi(y) = \phi_0\,, \tag{4.6}$$

therefore, given that the instanton field assumes a constant value, we expect the geometry to be that of pure AdS_3. For this reason, we will henceforth refer to γ as the deformation parameter.

As a matter of fact, the geometry described in (4.6) is precisely that of vacuum AdS_3, albeit expressed in an unusual way. This can be explicitly seen if we turn to the the usual Poincarè representation of AdS_3,

$$ds^2_{\mathrm{AdS}_3} = \frac{L^2}{\xi^2}(-dt^2 + d\xi^2 + d\eta^2), \tag{4.7}$$

where $\xi \in [0,\infty]$ is the radial coordinate. With the coordinate transformation

$$\tanh y = \frac{\eta}{\sqrt{\xi^2+\eta^2}}\,, \quad \text{and} \quad \xi = \sqrt{\xi^2+\eta^2}, \tag{4.8}$$

where $y \in \mathbb{R}$ and $z \in [0,\infty]$, we obtain

$$ds^2_{\mathrm{AdS}_3} = L^2\left(dy^2 + \cosh^2 y\,\frac{dz^2-dt^2}{z^2}\right) \tag{4.9}$$

$$= L^2\left(dy^2 + \cosh^2 y\, ds^2_{\mathrm{AdS}_2}\right)\,, \tag{4.10}$$

which is precisely the metric found in (4.6). The resulting AdS_3 geometry is written in terms of AdS_2 slices. At first glance it might seem as there are three boundary components to the AdS_2 sloced geometry: two $(1+1)$-dimensional half-spaces that are reached in the limits $y \to \pm\infty$, and the AdS_2 boundary of each slice reached in the limit $z \to 0$. However, these seemingly disconnected components are glued continuously along the $(0+1)$-dimensional worldline at $z = 0$. The picture 4.1 should hopefully provide some more context.

In light of this, the AdS_3 Janus deformation can be viewed as an AdS_2 foliation of AdS_3 where each slice is warped by a non-trivial function of the y coordinate and the deformation parameter γ. The AdS_3 Janus geometry is therefore an AdS_2 sliced domain wall solution [56].

The Janus geometry can also be expressed using the coordinate

$$\mathrm{d}\mu = \frac{\mathrm{d}y}{\sqrt{f(y)}}\,, \tag{4.11}$$

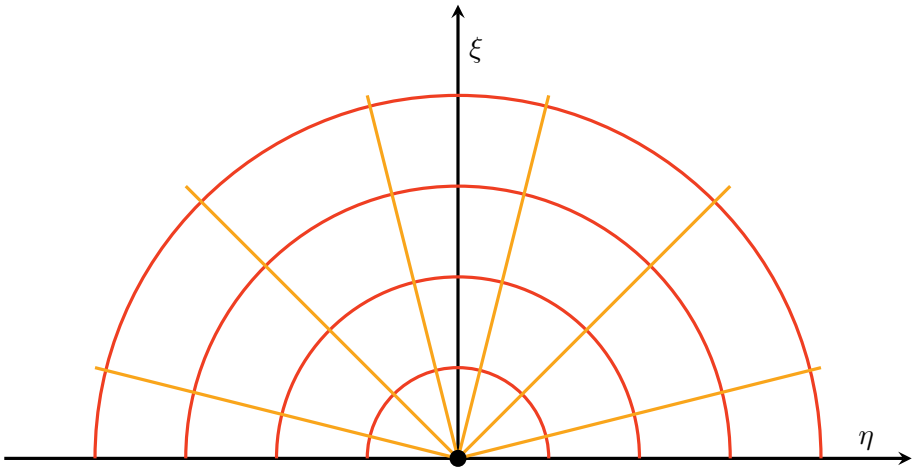

Figure 4.1: foliation of the AdS_3 geometry in terms of AdS_2 slices, where red lines correspond to constant z-values and the yellow lines correspond to constant y-values.

which is defined on the interval $[-\mu_0, \mu_0]$, where

$$\mu_0 = \int_0^\infty \frac{\mathrm{d}y}{\sqrt{f(y)}} = \frac{1}{\kappa_+}\mathbb{K}\left(\frac{\kappa_-}{\kappa_+}\right), \tag{4.12}$$

$\mathbb{K}(x)$ is the first kind of complete elliptic integral, and $\kappa_\pm^2 = 1/2\left(1 \pm \sqrt{1-2\gamma^2}\right)$. In the μ-coordinate system the three-dimensional Janus metric reads

$$ds^2 = L^2 f(\mu)\left(d\mu^2 + ds^2_{\mathrm{AdS}_2}\right), \tag{4.13}$$

where

$$f(\mu) = \frac{\kappa_+^2}{\mathrm{sn}^2\left(\kappa_+(\mu+\mu_0), \frac{\kappa_-}{\kappa_+}\right)}, \tag{4.14}$$

and the dilaton field is expressed by

$$\phi(\mu) = \phi_0 + \sqrt{2}\log\left[\mathrm{dn}\left(\kappa_+(\mu+\mu_0), \frac{\kappa_-}{\kappa_+}\right) - \frac{\kappa_-}{\kappa_+}\,\mathrm{cn}\left(\kappa_+(\mu+\mu_0), \frac{\kappa_-}{\kappa_+}\right)\right]. \tag{4.15}$$

The dual interpretation of this system is a two-dimensional CFT deformed by an exactly marginal operator $O(x)$ (dual to the bulk massless dilaton ϕ) with terms $J_+ \int d^2x\, O(x)$ and $J_- \int d^2x\, O(x)$ in the two sides of the boundary. Notably, we have $J_\pm = \lim_{y\to\pm\infty}\phi(y)$, meaning that the Janus deformation connects two theories with different coupling constant. Since the Janus deformation is associated with a marginal operator, it does not change the central charge of the CFT.

4.1.1 Conformal Diagram of the Janus Geometry

In order to understand the causality properties of the Janus space, it is useful to build the conformal diagram. This can be obtained if we manage to rewrite the metric in such a way that a conformal factor appears. If we parametrize the (4.13) metric using Poincaré coordinates along the AdS_2 slices, we obtain

$$ds^2 = \frac{L^2}{z^2} f(\mu)\left(z^2 d\mu^2 + dz^2 - dt^2\right). \tag{4.16}$$

This has the structure $ds^2 = \Omega^2 ds^2_{\mathbb{M}_3}$, with conformal factor $\Omega = \sqrt{f}L/z$ and boundary metric given simply by three-dimensional Minkowski space, where the spatial part is written in polar coordinates with angle μ and radius $z > 0$. The resulting conformal diagram is depicted in Fig. 4.2.

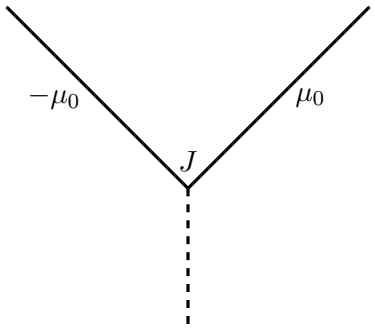

Figure 4.2: conformal diagram (taken from [17]) for the Janus AdS_3 geometry with Poincaré coordinates on the AdS_2 slices. The polar angle corresponds to the coordinate $\mu \in [-\mu_0, \mu_0]$ and the radial coordinate is $z \in [0, \infty]$. The joint J corresponds to the place where the two parts with the topology of half $\mathbb{R}^2$ meet. It can be seen as a domain wall on the boundary.

In particular, the boundary contains two halves of $\mathbb{R}^2$ defined by $\mu = \pm\mu_0$, so that the total boundary becomes full $\mathbb{R}^2$. Since $\mu_0 \geq \pi/2$, the junction between the half-boundaries meets at a joint[1] J with an obtuse angle.

We can also choose global coordinates on the slicing. In that case resulting metric reads

$$ds^2 = \frac{L^2}{\cos^2\lambda}\left(-dt^2 + \cos^2\lambda\, d\mu^2 + d\lambda^2\right), \tag{4.17}$$

and the associated conformal diagram is given in Fig. 4.3.

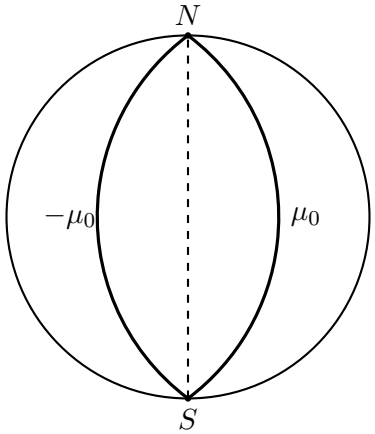

Figure 4.3: conformal diagram (again, taken from [17]) for the Janus AdS_3 geometry with global coordinates on the AdS_2 slices.

We notice again that the boundary consists of two parts, defined by $\mu = \pm\mu_0$, which topologically correspond to two halves of $\mathbf{S}^1$ joined through the north and south poles.

[1] While this joint seems singular, it can be shown that it is only an artifact of the coordinate system and there isn't any irregularity.

4.1.2 Fefferman-Graham Expansion of the Janus AdS$_3$ Geometry

The gravitational observables that come into play in holographic computations, such as in the CV conjecture, present divergent results and need to be regularized. A standard procedure for regularizing an asymptotically AdS metric is to introduce a constant cutoff along the radial direction in a Fefferman-Graham expansion of the metric (a good reference for the Fefferman-Grahm procedure is Appendix B of [57], and [58] for the case we will be interested in.) This requires finding a coordinate transformation (the so-called Fefferman-Grahm frame) in which the metric takes the form

$$ds^2 = \frac{L^2}{\xi^2}\left(d\xi^2 + g_{ij}(x,\xi)dx^i dx^j\right), \tag{4.18}$$

close to the boundary. Here $\xi \in [0,\infty)$, and $g_{ij}(x,\xi)$ can be expanded in ξ around 0. We will now implement this procedure to regularize the AdS$_3$ Janus geometry.

Let's start by considering the AdS$_2$-sliced metric for the pure AdS$_3$ geometry, given by

$$ds^2 = L^2\left(dy^2 + \cosh^2 y\,\frac{dz^2 - dt^2}{z^2}\right). \tag{4.19}$$

In this case, since the metric is related to the vacuum AdS$_3$ geometry in Poincarè coordinates through the coordinate transformation we examined earlier, the Fefferman-Grahm coordinates are simply given by

$$\tanh y = \frac{\eta}{\sqrt{\xi^2+\eta^2}}, \quad \text{and} \quad \xi = \sqrt{\xi^2+\eta^2}. \tag{4.20}$$

If we now turn to the Janus geometry, we can see that in the boundary regions $y \to \pm\infty$ the metric reduces to

$$ds^2_{\pm\infty} = L^2\left(dy^2 + \frac{\sqrt{1-2\gamma^2}}{4}e^{\pm 2y}\frac{dz^2-dt^2}{z^2}\right). \tag{4.21}$$

We can shift the y coordinate so that the constant is absorbed, that is,

$$\tilde{y} = y \pm \frac{1}{2}\log\sqrt{1-2\gamma^2}, \quad ds^2_{\pm\infty} = L^2\left(d\tilde{y}^2 + \frac{1}{4}e^{\pm 2\tilde{y}}\frac{dz^2-dt^2}{z^2}\right). \tag{4.22}$$

At this point we can introduce the Fefferman-Graham coordinates:

- when $\tilde{y} \to \infty$, $\xi \to 0$, and $\eta > 0$ we have

$$e^{-2\tilde{y}} = \frac{1}{4}\frac{\xi^2}{\eta^2}, \quad z = \eta\left(1 + \frac{1}{2}\frac{\xi^2}{\eta^2}\right); \tag{4.23}$$

- and when $\tilde{y} \to -\infty$, $\xi \to 0$, and $\eta < 0$ we have

$$e^{2\tilde{y}} = \frac{1}{4}\frac{\xi^2}{\eta^2}, \quad z = |\eta|\left(1 + \frac{1}{2}\frac{\xi^2}{\eta^2}\right). \tag{4.24}$$

The metric then becomes

$$ds^2_{\pm\infty} = \frac{L^2}{\xi^2}\left(d\xi^2 + d\eta^2 - dt^2\right) + O(\xi). \tag{4.25}$$

This is valid when we are far from the interface located at $\eta = 0$. When we get close to the interface the coordinate transformation defined above is no longer valid – as can be seen from the coordinate transformations (4.23) and (4.24). A different cutoff must be introduced in proximity to the interface. We will deal with this problem later on in section 5.1.

The regime where the FG expansion is valid corresponds to $\xi/\eta \ll 1$, which implies that at lowest order $\eta \simeq z$. By setting the cutoff at $\xi = \varepsilon$ and considering finite $\eta \simeq z = z_0$, we get

$$\varepsilon = \frac{2\,z_0}{(1-2\gamma^2)^{\frac{1}{4}}}e^{-y_\infty}. \tag{4.26}$$

4.1.3 Holographic Boundary Entropy of the AdS_3 Janus Solution

In the next chapter we will be concerned with the computation of the extremal volume of Janus AdS_3. As a preparation to this computation, and to see in practice the regularization procedure we just discussed, we now consider the computation of the holographic entanglement entropy [58, 59].

We can start by considering an entangling region $\mathcal{A}$ on the boundary CFT which crosses the interface symmetrically. Following the Ryu-Takayanagi prescription, to compute the entropy we must evaluate the length of a geodesic curve connecting the two boundaries of the region $\mathcal{A}$. In this case the geodesics are incredibly simple: they are the curves at constant z. We chose the constant so that the entangling region becomes the interval $[-z_0, z_0]$, in this way the geodesic length is given by

$$\Gamma(\gamma) = L \int_{-y_\infty}^{y_\infty} \mathrm{d}y = 2L\, y_\infty, \tag{4.27}$$

therefore, using the Fefferman-Grahm coordinates found in the previous section, we arrive at

$$\Gamma(\gamma) = 2L \left(-\log \epsilon - \frac{1}{2} \log \sqrt{1 - 2\gamma^2} + \log(2z_0) \right). \tag{4.28}$$

The entanglement entropy of the boundary defect theory is then found by subtracting the geodesic length in AdS_3 and dividing by Newton's constant, that is,

$$S = \frac{\Gamma(\gamma) - \Gamma(0)}{G_3} = -\frac{L}{4G_3} \log \sqrt{1 - 2\gamma^2}. \tag{4.29}$$

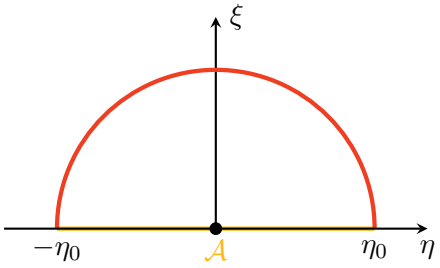

Figure 4.4: constant $z = z_0$ curve connecting the boundaries of the entangling region $\mathcal{A}$.

We can also consider the case in which the entangling region lies entirely on one side of the defect [60]. The appropriate embedding of the $t = 0$ curve is in this case $y = y(z)$. For this choice the geodesic length reads

$$\Gamma(\gamma) = \int \mathrm{d}z \sqrt{\frac{f(y)}{z^2} + \left(\frac{\mathrm{d}y}{\mathrm{d}z}\right)^2}, \tag{4.30}$$

which if extremized leads to the following Euler-Lagrange equation

$$f'(y) \left(\frac{1}{z^2} + \frac{(\partial_z y)^2}{f(y) + z^2(\partial_z y)^2} \right) - \frac{2}{z} \frac{f(y)(\partial_z y + z\partial_z^2 y)}{f(y) + z^2(\partial_z y)^2} = 0. \tag{4.31}$$

A simple solution to this equation, which corresponds to an absolute minimum of the functional (4.30), is given by $y = 0$. This solution correspond to having the entangling region entirely on one side of the interface as depicted in fig. 4.5.

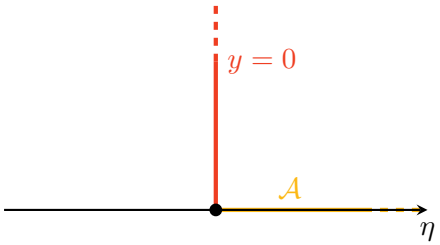

Figure 4.5: the red curve represents the RT surface corresponding to the entangling region $\mathcal{A}$ placed on one side of the interface.

In this case the holographic entanglement entropy is given by

$$S(\gamma) = \frac{L}{4G_3}\sqrt{f(0)}\int_{\epsilon}^{z_{IR}}\frac{\mathrm{d}z}{z} \tag{4.32}$$

$$= \frac{L}{4\sqrt{2}G_3}\sqrt{1+\sqrt{1-2\gamma^2}}\log\frac{z_{IR}}{\epsilon}, \tag{4.33}$$

where z_{IR} is an infrared regulator and ϵ a UV regulator. If we subtract the vacuum result we find that

$$S = S(\gamma) - S(0) = \frac{c}{6}\left(\sqrt{\frac{1+\sqrt{1-2\gamma^2}}{2}} - 1\right)\log\frac{L}{\epsilon}, \tag{4.34}$$

where $c = 3L/2G_3$, and we have identified z_{IR} with the AdS radius.

4.2 Five-dimensional Janus Deformations

The Janus deformation considered in the previous section can also be performed in $\mathrm{AdS}_5 \times \mathbf{S}^5$. In this case it is possible to deform the space without breaking $\mathbf{SO}(2,3)\times\mathbf{SU}(3)\times\mathbf{U}(1)_\beta\times\mathbf{SL}(2,\mathbb{R})$ symmetry, resulting in a super-symmetric solution [18]. We will restrict our interest to the non-supersymmetric solution.

The non-supersymmetric Janus deformation of $\mathrm{AdS}_5 \times S^5$ is a solution of type IIB supergravity with a non-trivial dilaton profile, which is regular and classically stable against all small and a certain class of large perturbations [17, 56]. The CFT dual is given by $\mathcal{N} = 4$ Super Yang-Mills (SYM) theory on both sides of a planar codimension-one interface, whose coupling constant varies discontinuously across the interface where the half-spaces are glued together [18]. The two different values of the gauge coupling correspond to the two asymptotic values of the dilaton in the Janus solution. The $\mathrm{SO}(2,3)$ symmetry of the Janus solution maps to the conformal symmetry preserved by the interface on the CFT side. This symmetry is manifest at the classical level, but was also shown to persist at the first non-trivial quantum level. The $\mathrm{SO}(6)$ symmetry of the Janus solution maps to an (accidental) internal symmetry[2] on the CFT side. It should be noted that the interface in the Janus solution carries no degrees of freedom in addition to the ones inherited from $\mathcal{N} = 4$ SYM.

4.2.1 Non-SUSY Janus AdS_5

The non-SUSY five-dimensional Janus solution [18, 61] is a one-parameter deformation of AdS_5 described in terms of the metric

$$ds^2 = L^2\left[(\gamma)^{-1}h^2(w)dw^2 + h(w)ds^2_{\mathrm{AdS}_4}\right], \tag{4.35}$$

[2]Since the Janus solution breaks all the supersymmetries, the global $\mathrm{SO}(6)$ symmetry is no longer an R-symmetry.

where γ is the deformation parameter, with range $3/4 \leq \gamma \leq 1$, and the four-dimensional AdS slice is written in Poincaré coordinates according to Eq. (5.3). The warp factor $h(w)$ is defined as [18, 61]

$$h(w) = \gamma \left(1 + \frac{4\gamma - 3}{\wp(w) + 1 - 2\gamma}\right) = \gamma \left(1 + \frac{4\gamma - 3}{\wp(w) - \wp(w_0)}\right) , \tag{4.36}$$

and $\wp(w)$ is the Weierstrass elliptic $\wp$–function[3]. The elliptic invariants (g_2, g_3) of the Weierstrass $\wp-$function are

$$g_2 = 16\gamma(1-\gamma) , \qquad g_3 = 4(\gamma - 1) , \tag{4.37}$$

and w_0 is defined as the positive solution of

$$\wp(w_0) = 2\gamma - 1 . \tag{4.38}$$

The dilaton of the non-SUSY Janus solution is

$$\phi(w) = \phi_0 + \sqrt{6(1-\gamma)} \left(w + \frac{4\gamma - 3}{\wp'(w)} \left(\ln \frac{\sigma(w + w_1)}{\sigma(w - w_1)} - 2\zeta(w_1) w\right)\right) , \tag{4.39}$$

where σ and ζ denote the Weierstrass functions defined in Eq. (A.13) of Appendix A.2, ϕ_0 is a real constant and w_1 is defined by the equation

$$\wp(w_1) = 2(1-\gamma) . \tag{4.40}$$

When $\gamma = 1$, the solution reduces to AdS_5 with constant dilaton $\phi = \phi_0$, while $\gamma = 3/4$ leads to a linear dilaton solution.

The Janus solution is defined in the interval $-w_0 < w < w_0$. The function $h(w)$, introduced in Eq. (4.36), has simple poles at $w = \pm w_0$. As $w \to \pm w_0$, the Janus solution asymptotes to AdS_5 with constant dilaton $\phi_\pm = \phi(\pm w_0)$, where $\phi_+ \neq \phi_-$ unless $\gamma = 1$. In other words, for generic γ the Janus solution has two asymptotically AdS_5 regions in which the dilaton takes two different values.

The conformal structure of the Janus AdS_5 solution is easily determined by means of the change of variables

$$d\mu = \sqrt{\frac{h(w)}{\gamma}}\, dw , \tag{4.41}$$

which brings the metric into the form

$$ds^2 = L^2\, h(\mu) \left(d\mu^2 + ds^2_{AdS_4}\right) . \tag{4.42}$$

Up to a conformal factor, the boundary metric is four-dimensional Minkowski spacetime. In other words, the conformal structure is the same as for the three-dimensional Janus solution, and is shown in Fig. 4.2.

4.3 BTZ-like Janus Solutions

It is possible to obtain a gravity solution similar to the Janus deformation of AdS_3 geometry by replacing the factor of empty AdS space in three-dimensional Janus metric with the BTZ black hole metric. This procedure is allowed because the BTZ solution is simply a discrete quotient of AdS space [62] and still satisfies $R_{ab} = -2g_{ab}$. This can also be recognized in the fact that AdS_3 and the BTZ background are locally isomorphic, so it is possible to get the BTZ geometry by means of a coordinate transformation in AdS_3.

[3] We refer the reader to Appendix A.2 for more details on the Weierstrass elliptic function.

4.3.1 Static Janus BTZ Background

We explain in more detail how to perform the Janus deformation of the BTZ black hole while retaining a static solution, following [15, 55]. Starting from the Janus AdS metric

$$ds^2 = L^2 \left(dy^2 + f(y)\, ds^2_{\mathrm{AdS}_2}\right) = L^2\, f(\mu) \left(d\mu^2 + ds^2_{\mathrm{AdS}_2}\right) , \tag{4.43}$$

one can parametrize the two-dimensional AdS slices using global coordinates

$$ds^2_{\mathrm{AdS}_2} = \frac{1}{\cos^2 \lambda} \left(d\lambda^2 - d\tau^2\right) . \tag{4.44}$$

In this coordinate system, $\lambda \in (-\lambda_\infty, \lambda_\infty)$ with $\lambda_\infty \in [0, \pi/2)$ and the two half-boundaries are located at $y = \pm\infty$.

At this point, one can perform the coordinate change

$$w = \frac{\cos\tau}{\cos\lambda} , \qquad \tanh \frac{r_h\, t}{L^2} = \frac{\sin\tau}{\sin\lambda} , \tag{4.45}$$

which brings the AdS_2 factor to the form

$$ds^2_{\mathrm{AdS}_2} \to ds^2_{\mathrm{Rindler}} = -\frac{(w^2-1)\, r_h^2}{L^4} dt^2 + \frac{dw^2}{w^2-1} . \tag{4.46}$$

This is a Rindler-AdS metric which corresponds to the case of a hyperbolic geometry and allows to get a black hole solution where the horizon is located at $w = 1$ and has size r_h. Plugging this back into the Janus metric we find

$$ds^2 = L^2 f(\mu) \left[d\mu^2 + f(\mu) \left(-\frac{(w^2-1) r_h^2}{L^4} dt^2 + \frac{dw^2}{w^2-1}\right)\right] , \tag{4.47}$$

which is the so-called static Janus BTZ solution. For vanishing deformation parameter the above metric reduces to the ordinary BTZ solution in three-dimensions (see fig. 4.6).

This can be seen by using the coordinate transformation

$$\frac{r_h}{r} = \frac{\cos\mu}{\sqrt{w^2 - \sin^2\mu}} , \qquad \sinh \frac{r_h x}{L^2} = \frac{\sin\mu}{\sqrt{w^2 - \sin^2\mu}} , \tag{4.48}$$

which brings the combination of Eq. (4.43) with (4.46) to

$$ds^2_{\mathrm{BTZ}} = -\frac{r^2 - r_h^2}{L^2} dt^2 + \frac{L^2 dr^2}{r^2 - r_h^2} + \frac{r^2}{L^2} dx^2 . \tag{4.49}$$

With the identification $x \sim x + 2\pi$, the above describes the BTZ black hole with vanishing angular momentum. The horizon is at $r = r_h$ and $r = 0$ corresponds to a singularity of the orbifold type. When γ is non-vanishing, this periodic indentification is forbidden for translational invariance is broken along the x direction. On the other hand, time-translation invariance is not broken by the deformation, and, as for the undeformed BTZ geometry, the killing vector in the Kruskal extension corresponds to the time translations

$$t_L \to t \pm \Delta t , \qquad t_R \to t_R \mp \Delta t , \tag{4.50}$$

which on the boundary equates to evolving in time with the Hamiltonian $H_L - H_R$.

From the point of view of the AdS slicing of the black hole metric (described in fig. 4.6), it may appear that there are many disconnected boundaries. However, a careful analysis shows that the regions $x \to -\infty$ and $x \to \infty$ both merge to a point at the spatial section of the global AdS_3 geometry, and then the left (right) boundary is a connected region. The only causal disconnected regions are the left boundary with respect to the right one.

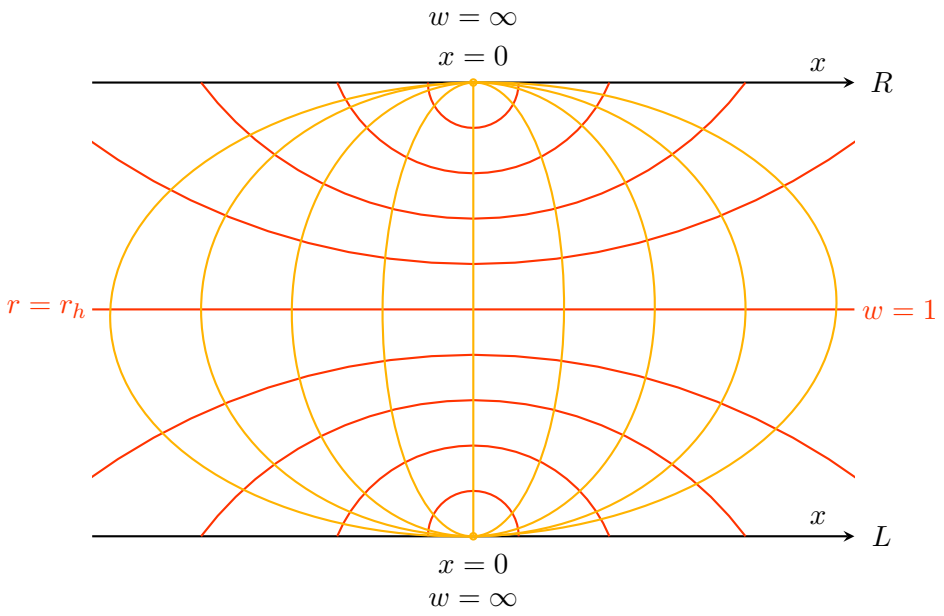

Figure 4.6: picture representing the AdS slicing of the BTZ black hole at constant time. The lines at constant w are depicted in red, while the curves at constant μ in orange. The coordinate x runs along the left (L) and right (R) disconnected boundaries. The coordinate r covers the region outside the horizon and runs on the vertical axis: starting from the middle line located at $r = r_h$, it increases towards the L and R boundaries.

For generic γ the asymptotic region of the solution can be mapped to the BTZ spacetime using the coordinate change

$$\frac{r}{r_h} \simeq \sqrt{(w^2-1)f(y)+1}\,, \qquad \sinh\frac{r_h x}{L^2} \simeq \text{sign}(x)\sqrt{\frac{f(y)-1}{(w^2-1)f(y)-1}}\,. \tag{4.51}$$

It is important to observe that while this black hole solution is a deformation of the BTZ background, it still has many common features with the original solution. Indeed, the left and right CFTs on the boundaries are described by a thermofield (TFD) double state

$$|\psi(t_L,t_R)\rangle = e^{-i(t_L\, H\otimes\mathbf{1}+t_R\,\mathbf{1}\otimes H)}|\psi(0,0)\rangle\,, \qquad |\psi(0,0)\rangle = \frac{1}{\sqrt{Z}}\sum_n e^{-\frac{\beta}{2}E_n}|n\rangle\otimes|n\rangle\,, \tag{4.52}$$

and in particular the case where $t_L = -t_R$ is time-independent, corresponding to the timelike Killing symmetry of the geometry. Due to this invariance, it is not restrictive to consider a case where the boundary time is $t_L = t_R = t_B/2$.

4.3.2 Time-dependent Janus BTZ Background

The case considered in Section 4.3.1 is not the only possibility to introduce a Janus deformation inside a black hole geometry. Contrarily to the above-mentioned scenario, here we will consider a solution whose horizon size and the dilaton value at the horizon will vary with time.

The starting point for constructing the time dependent Janus BTZ black hole is the BTZ metric

$$ds^2_{\text{BTZ}} = -\frac{r^2-r_h^2}{L^2}dt^2 + \frac{L^2dr^2}{r^2-r_h^2} + \frac{r^2}{L^2}dx^2\,. \tag{4.53}$$

The Janus deformation is obtained by imposing

$$\tan\mu = \pm\cosh(r_h t)\sqrt{\left(\frac{r}{r_h}\right)^2 - 1}\,. \tag{4.54}$$

This identification is the responsible for the time-dependence of the final configuration, since it relates the μ coordinate with time and radial distance.

We can cover the whole region of the geometry by introducing the Kruskal variables

$$V = e^{r_h(t+r_*)}\,, \qquad U = -e^{-r_h(t-r_*)}\,, \tag{4.55}$$

with tortoise coordinate

$$r_*(r) = \frac{1}{2r_h}\log\left(\frac{r-r_h}{r+r_h}\right)\,, \tag{4.56}$$

which brings the metric to the form

$$ds^2 = \frac{f(\mu)}{(1+U^2)(1+V^2)}(-4dUdV + r_0^2(1-UV)^2 d\theta^2)\,. \tag{4.57}$$

This is the metric for the time dependent Janus deformation of the BTZ black hole. It is useful to compactify by introducing the coordinates

$$V = \tan w_1\,, \qquad U = \tan w_2\,, \tag{4.58}$$

and, finally, go back from null coordinates to timelike and spacelike ones defining

$$\tau = w_1 + w_2\,, \qquad \mu = w_1 - w_2\,. \tag{4.59}$$

After performing these transformations and using the condition (4.54), we obtain [14, 16]

$$ds_3^2 = f(\mu)\left(-d\tau^2 + d\mu^2 + r_h^2\cos^2\tau d\theta^2\right)\,, \tag{4.60}$$

which, according to the $\mathrm{d}\mu = \mathrm{d}y/\sqrt{f(y)}$ change of variable, can be written as

$$ds_3^2 = dy^2 + f(y)\left(-d\tau^2 + r_h^2\cos^2\tau d\theta^2\right)\,, \tag{4.61}$$

with the same dilaton solution given in Eq. (4.5). The metric describes a time dependent configuration with two disconnected boundaries separated by event horizons; the Pensrose diagram of this multi-boundary solution is depicted in 4.7.

The coupling on the two sides of the diagram is given by e^{ϕ_+} and e^{ϕ_-}, respectively ond the left and right, and the two CFTs are correlated through the bulk in a non-trivial way. In fact, the dilaton does not divide each boundary component into two halves, rather, it takes one value in one component of the boundaries and the other in the other component. It is important to observe that the TFD state defined on the two CFTs living at the boundaries are different from the standard BTZ and also from the Janus deformation discussed in Section 4.3.1. Indeed, the initial state is determined by

$$|\psi(0,0)\rangle = \frac{1}{\sqrt{Z}}\sum_{m,n}\langle E_m^L|E_n^R\rangle\, e^{-\frac{\beta}{4}(E_m^L+E_n^R)}|E_m^L\rangle\otimes|E_n^R\rangle\,. \tag{4.62}$$

This expression reduces to the usual one in Eq. (4.52) only if the Hamiltonian defined on the two sides of the spacetime satisfy $H_L = H_R$.

Notice that if we take the metric in Eq. (4.60) and we set $\gamma = 0$, we can recover the standard metric for the stationary BTZ black hole. In fact, if the parameter γ is vanishing, the function $f(\mu)$ defined in equation (4.14) reduces to

$$f(\mu) = \frac{1}{\cos^2\mu}\,. \tag{4.63}$$

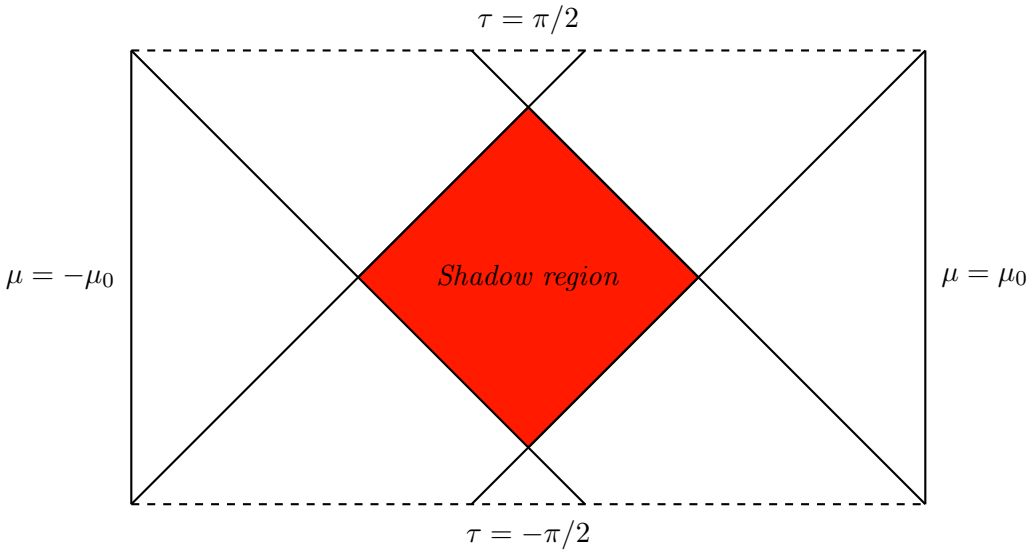

Figure 4.7: Penrose diagram of the Janus deformation of the BTZ black hole. The μ variable runs along horizontal lines from $-\mu_0$ to μ_0, while τ runs vertically from $-\pi/2$ to $\pi/2$. The shaded region represents the so-called *shadow region*.

The Penrose diagram for this case becomes a square which locally is just AdS space, and the metric reduces to

$$ds_3^2 = \frac{1}{\cos^2\mu}\left(-d\tau^2 + d\mu^2 + r_h^2\cos^2\tau d\theta^2\right) \tag{4.64}$$

which describes the static BTZ black hole.

Chapter 5

Volume Complexity for Three-dimensional Janus Geometries

In this chapter we apply the CV conjecture to the three-dimensional defect geometries considered in the previous chapter, that is, we consider an extremal spacelike codimension-one slice attached to the boundary and we evaluate the induced volume for Janus AdS_3, static Janus BTZ, and time-dependent Janus BTZ. This chapter centers around the arXiv submission [1].

Since the maximal volume slice extends all the way to the boundary, the corresponding holographic complexity will be divergent and it will be necessary to regularize the UV modes. In the case of entanglement entropy, divergences arise due to the arbitrarily short correlations between degrees of freedom on each side of the entangling region. The leading divergence scales with the area law and either the finite term (in odd spacetime dimensions) or the coefficient of the logarithmic divergence (in even spacetime dimensions) have a universal interpretation which is not sensitive to the ambiguities in the choice of the regulator. As discussed in the section 3.2.1, in the case of CV-duality, the outcome of a similar classification is a leading divergence proportional to the bondary volume of the time slice, and a set of subleading terms defined in terms of integrals over the same slice [43]. However, this structure may change when defects, interfaces, or boundaries are present. This problem was already addressed in some specific cases [12, 13, 63]. Interestingly, it was found that in the case of the three-dimensional Randall-Sundrum model the structure of the divergences is modified by the defect only in CV-duality [12], suggesting that defects could possibly distinguish CA from CV. From what is known to date, it seems that this is an artifact of three-dimensional geometries [13]. As we will see in a bit, the Janus AdS_3 volume features a logarithmic divergence akin to the one found for the three-dimensional Randall-Sundrum model.

The chapter is structured in the following way. In section 5.1 we discuss three different prescription for regularizing divergences in general AdS_d-sliced domain wall geometries. In section 5.2 and 5.3, we compute the subregion volume complexity at vanishing boundary time for the AdS_3 Janus deformation and the BTZ static Janus deformation respectively. Finally, the time-dependent BTZ Janus solution is considered in section 5.4.

5.1 Regularization Schemes for AdS_d-Sliced Defect Geometries

In order to deal with the UV divergences that arise when considering an extremal surface hanging from the boundary, we introduce three regularization prescriptions. As a cross check, we compute the volume with the three different prescriptions and we show that they only differ by finite terms in the three-dimensional case we are about to consider (see appendix B.) Each regularization is equally valid to describe the relevant physics of the system.

For later purposes, we consider a general interface theory described by a codimension-one defect embedded in a AdS_{d+1} bulk geometry, whose isometries get reduced from the conformal

group $\mathbf{SO}(d,2)$ to the subgroup $\mathbf{SO}(d-1,2)$. The natural way to parametrize this geometry is to perform a slicing of spacetime in terms of AdS_d slices. The metric takes the form [61, 64]

$$ds^2 = L^2\left(A^2(y)ds^2_{\mathrm{AdS}_d} + \rho^2(y)dy^2\right)\,, \tag{5.1}$$

with y being a non-compact coordinate such that when $y \to \pm\infty$

$$A(y) \to \frac{L_\pm}{2}e^{\pm y \pm c_\pm}\,, \qquad \rho(y) \to 1\,. \tag{5.2}$$

Here $L_\pm$ and $c_\pm$ are constants (which can take two different values at the boundaries $y = \pm\infty$), and we are assuming that there isn't any other internal direction in the spacetime. We parametrize the AdS_d slices using Poincaré coordinates

$$ds^2_{\mathrm{AdS}_d} = \frac{1}{z^2}\left(dz^2 - dt^2 + d\vec{x}^2_{d-2}\right)\,, \tag{5.3}$$

where (t,z) are the time and radial coordinates on each slice and $\vec{x}$ collects all the other orthogonal directions. In the following, we will introduce three regularization techniques inspired by the similar discussion for the entanglement entropy developed in [64]. In all the computations of this Section, the volume will be determined from

$$\mathcal{V} = \int \mathrm{d}z \int \mathrm{d}y \int \mathrm{d}\vec{x}\,\sqrt{h}\,, \tag{5.4}$$

where $\sqrt{h}$ is the determinant of the induced metric. The integration along the orthogonal spatial directions $\vec{x}$ is usually trivial, while the part along the (y,z) coordinates contains the relevant information about the defect.

5.1.1 Fefferman-Graham Regularization

We perform the Fefferman-Graham (FG) expansion of the geometry near the asymptotically AdS_{d+1} region of spacetime, which brings the metric to the form

$$ds^2 = \frac{L^2}{\xi^2}\left[d\xi^2 + g_1(\xi/\eta)\,\left(-dt^2 + d\vec{x}^2\right) + g_2(\xi/\eta)\,d\eta^2\right]\,, \tag{5.5}$$

where ξ is a radial coordinate for the asymptotic AdS region in Poincaré coordinates, η is a field theory direction orthogonal to the defect, and g_1, g_2 are two functions encoding the change of coordinates from the original metric (5.1) with slicing (5.3) to this one. The transformation consists in a change of coordinates $(z,y) \to (\xi,\eta)$. We perform an expansion of Eq. (5.5) such that the asymptotic metric reads

$$ds^2 = \frac{L^2}{\xi^2}\left(d\xi^2 + d\eta^2 + d\vec{x}^2 - dt^2 + \mathcal{O}(\xi)\right)\,. \tag{5.6}$$

The natural prescription to regularize divergences using the FG form of the metric is to introduce a UV cutoff by cutting the spacetime with the surface located at $\xi = \delta$, and expand all the results in a series around $\delta = 0$. The problem of this procedure is that in the region where $\xi/\eta \ll 1$, the FG expansion breaks down and the coordinates (ξ,η) are ill-defined [57] (as we mentioned in section 4.1.2.)

For this reason, the defect geometry is characterized by the existence of two patches, defined away from the region of the defect on the left and right sides of the spacetime, where the FG expansion is valid: we call them FG patches. We do not have access to a natural UV cutoff in the middle region close to the defect. To overcome the problem, the original proposal from [61] is to interpolate the cutoff determined by requiring $\xi = \delta$ in the left and right FG patches

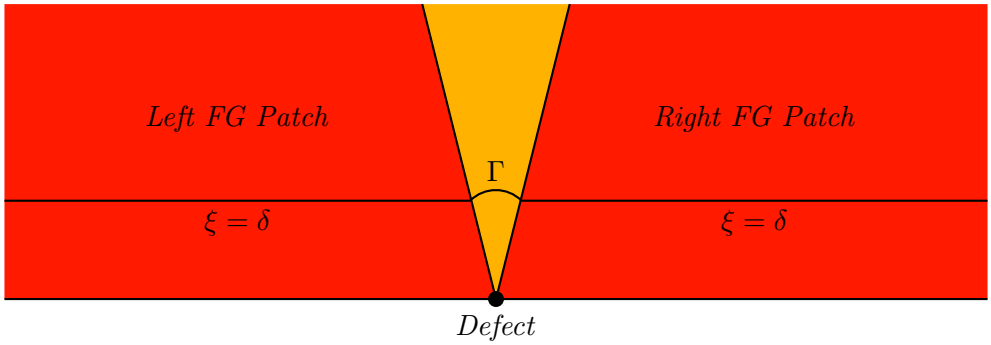

Figure 5.1: interpolation between two FG patches with a continuous curve Γ.

with an arbitrary curve in the middle region. The only constraint is that the curve should be continuous at the value $y = y_0$ where the FG expansion breaks down. The corresponding curve is pictorially represented in Fig. 5.1.

This method was later applied in [12], with the additional requirement that the interpolation is smooth, i.e., the curves in the middle region are perpendicular to the surface which delimits the FG patches. We apply this procedure to the case of Janus AdS_3 geometry in Appendix B.1.

5.1.2 Single Cutoff Regularization

This technique is inspired by the Fefferman-Graham method, but has the advantage of not introducing any arbitrary interpolating curve in the middle region. Instead, it uses the FG map to induce a minimal value on the z coordinate, in such a way that the integration does not reach the region $z \to 0$ where the expansion breaks down. We explain how the procedure works starting from empty AdS_{d+1} space, which can be written using the slicing (5.1) if we choose $A(y) = \cosh y$ and $\rho(y) = 1$. In this case, the FG coordinate transformation which brings the metric to the Poincaré form in Eq. (5.6) is exact and reads

$$\eta = z \tanh y \,, \qquad \xi = \frac{z}{\cosh y} \,. \tag{5.7}$$

If we placethe cutoff surface at $\xi = \delta$, we get the condition

$$\delta = \frac{z}{\cosh y} \,, \tag{5.8}$$

which selects a maximal value of $y = y^*(z)$ for the first non-trivial integration in Eq. (5.4). On the other hand, reversing this formula gives a constraint on the minimal value of the integration along z, determined by

$$z_{\min} = \delta \min_{y \in \mathbb{R}} (\cosh y) = \delta \,. \tag{5.9}$$

In this way, we observe that the choice of a single cutoff δ from the FG expansion restricts the integration along both the (y, z) coordinates and regularizes the volume.

In the presence of a defect, the procedure is the same, except that the conditions determined from the FG representation of the metric get modified to

$$\delta = \frac{z}{A(y)} \,, \qquad z_{\min} = \delta \min_{y \in \mathbb{R}} [A(y)] \,. \tag{5.10}$$

At the end of the procedure, we will perform a Laurent expansion of the result in powers of δ/z. We apply this technique for all the computations in the main text.

5.1.3 Double Cutoff Regularization

The previous techniques regularized all the integrals with the choice of a single UV cutoff inspired by the FG expansion. On the other hand, we can consider the two directions (y, z) separately and a cutoff along each of them. This method is based on the observation that, after the subtraction of the vacuum geometry, we should obtain a holographic quantity intrinsic to the defect: for this reason, a natural cutoff can be imposed on the AdS_d slicing at $z = \delta$, instead of selecting the asymptotic radial direction in the AdS_{d+1} bulk geometry. This choice by itself is not sufficient to regularize the full integral (5.4), since the metric factor $A(y)$ is still singular at infinity: for this reason we also determine a maximum value of y where the integration ends by requiring

$$A(y) = \frac{1}{\varepsilon}\,. \tag{5.11}$$

Notice that while the δ cutoff has a physical meaning, the ε cutoff is a mathematical artifact introduced at intermediate steps, and the result, after the vacuum subtraction, should therefore be ε-independent. As a consequence, we are allowed to remove the ε cutoff at the end of the computation by taking the limit $\varepsilon \to 0$. We elaborate on this procedure in Appendix B.2.

5.2 Volume of Janus AdS_3

Before we dive into the computation of the volume, a comment is in order. It turns out that in addition to the diverging UV modes, the volume is characterized diverging IR modes. We could regularize this divergence by introducing an IR cutoff at some constant value of the Fefferman-Graham (FG) coordinates, however, this approach is not very practical for Janus geometries, since the FG coordinates are known just as an expansion near the boundary. Another possibility, which turns out to be more convenient, is to consider a particular limit of subregion complexity. Subregion volume complexity [46] is on the bulk side defined as the volume of an extremal slice delimited by a Ryu-Takayanagi surface anchored to a boundary subregion. The precise meaning of subregion complexity in the dual CFT is still an open question. Some proposals, such as fidelity, purification complexity, and basis complexity, were in discussed [46, 65]. In any event, the RT surface that defines the subregion volume can effectively be used as an infrared regulator: the total complexity will then be identified by the limit in which the subregion covers the entire boundary.

The natural choice of boundary subregion for Janus AdS_3 is an interval of length ℓ centered around the interface. The total complexity can then be defined as the $\ell \to \infty$ limit of the subregion volume, with the length ℓ playing the role of IR regulator.

The interval is located at the FG radial coordinate $\xi = \delta$ and placed symmetrically along the orthogonal direction to the interface, i.e., $\eta \in [-\ell/2, \ell/2]$. There is an ambiguity in the regularization of the UV divergences: we can either put the subregion on the cutoff surface $\xi = \delta$ and build the corresponding RT surface, or we can put the interval on the real boundary $\xi = 0$ and then cut the RT surface with the line at $\xi = \delta$. Since the difference between the two cases results in a difference in the finite term, we will only focus on the former case.

As as argued by Gutperle et al. in [64], on a fixed time slice the Janus geometry features a particularly simple class of geodesics given by curves at constant z. Using the FG expansion in Eq. (4.23) and putting the boundary conditions $\xi = \delta$ and $\eta = \frac{\ell}{2}$, we determine the constant $\bar{z}$ value where the surface is located:

$$\bar{z} = \frac{\ell}{2}\left(1 + \frac{2\delta^2}{\ell^2}\right)\,. \tag{5.12}$$

Notice that the limit $\delta \to 0$ is completely regular, which means that we can also make it vanish in the above expression without affecting the divergent and the finite structure of the result.

The prescription for the extremal volume tells us to consider a solution at $t = 0$ anchored at the boundary and delimited by the RT surface.

The UV divergencies will be regularised according to the single cutoff prescriptions described in section 5.1. The correspondence between the generic form (5.1) of the metric with a conformal defect and the Janus background is

$$A^2(y) = f(y)\,, \qquad \rho(y) = 1\,, \qquad L_\pm^2 = \sqrt{1-2\gamma^2}\,, \qquad c_\pm = 0\,. \tag{5.13}$$

In this way the requirement in Eq. (5.10) to regularize the UV divergences becomes

$$\frac{z}{\sqrt{f(y)}} = \delta\,. \tag{5.14}$$

This single condition identifies both a maximum value of the coordinate $y = y^*(z)$, obtained by inverting the previous expression, and a minimum value of the coordinate $z = z_{\min}$, determined from the second identity in Eq. (5.10). Concretely, they are given by

$$y^*(z) = f^{-1}\left(\frac{z^2}{\delta^2}\right), \qquad z_{\min} = H(\gamma)\,\delta\,, \qquad H(\gamma) = \sqrt{f(0)} = \sqrt{\frac{1+\sqrt{1-2\gamma^2}}{2}}\,. \tag{5.15}$$

The integral which computes the subregion volume in Eq. (5.4) takes the form

$$\mathcal{V}(\gamma,\ell) = 2L^2 \int_{z_{\min}}^{\bar{z}} \frac{\mathrm{d}z}{z} \int_0^{y^*(z)} \mathrm{d}y\, \sqrt{f(y)}\,. \tag{5.16}$$

With the change of variables

$$\tau = \frac{f(y)}{H^2}\,, \qquad \zeta = \frac{z^2}{H^2\delta^2}\,, \qquad \bar{\zeta} = \frac{\bar{z}^2}{H^2\delta^2}\,, \tag{5.17}$$

we can express the integral as

$$\mathcal{V}(\gamma,\ell) = \frac{L^2H^3}{\sqrt{2}} \int_1^{\bar{\zeta}} \frac{\mathrm{d}\zeta}{\zeta} \int_1^{\zeta} \frac{\sqrt{\tau}\,\mathrm{d}\tau}{\sqrt{\gamma^2 + 2H^2\tau(H^2\tau - 1)}} \tag{5.18}$$

$$= \frac{L^2H^3}{\sqrt{2}} \int_1^{\bar{\zeta}} \mathrm{d}\tau \int_\tau^{\bar{\zeta}} \frac{\mathrm{d}\zeta}{\zeta} \frac{\tau^{1/2}}{\sqrt{\gamma^2 + 2H^2\tau(H^2\tau - 1)}}\,. \tag{5.19}$$

It is useful to introduce

$$m = \frac{1-\sqrt{1-2\gamma^2}}{1+\sqrt{1-2\gamma^2}}\,. \tag{5.20}$$

Since $0 \le \gamma \le 1/\sqrt{2}$, we have $1/\sqrt{2} \le A \le 1$ and $0 \le m \le 1$. We can directly evaluate the ζ-integral, which leads us to

$$\mathcal{V}(\gamma,\ell) = \frac{L^2H}{2} \int_1^{\bar{\zeta}} (\log\bar{\zeta} - \log\tau) \sqrt{\frac{\tau}{(\tau-1)(\tau-m)}}\,\mathrm{d}\tau\,. \tag{5.21}$$

This integral contains two terms. The $\log\bar{\zeta}$ term is trivial and can be evaluated promptly. Conversely, the $\log\tau$ term is non-trivial and needs to be expanded for slamm δ. To expand in δ we do the following: we first determine the leading divergence of the integrand at infinity, and then we proceed to split the integral by adding and subtracting said leading term. In this way, we end up with a renormalized finite part and a purely diverging part. Hence

$$\mathcal{V}(\gamma,\ell) = \frac{L^2H}{2} \int_1^{\bar{\zeta}} \mathrm{d}\tau\, \sqrt{\tau}\,(\log\bar{\zeta} - \log\tau) \left[\left(\frac{1}{\sqrt{(\tau-1)(\tau-m)}} - \frac{1}{\tau}\right) + \frac{1}{\tau}\right] \tag{5.22}$$

$$= L^2\left[\frac{\ell}{\delta} + \eta(\gamma)\log\left(\frac{\ell}{2H\,\delta}\right) + \chi(\gamma)\right], \tag{5.23}$$

where

$$\eta(\gamma) = H\left[\int_1^\infty \tau^{1/2}\left(\frac{1}{\sqrt{(\tau-1)(\tau-m)}} - \frac{1}{\tau}\right)\mathrm{d}\tau - 2\right] = 2A\left(\mathbb{K}(m) - \mathbb{E}(m)\right)\,, \tag{5.24}$$

$$\chi(\gamma) = H\left[-2 - \frac{1}{2}\int_1^\infty \tau^{1/2}\log\tau\left(\frac{1}{\sqrt{(\tau-1)(\tau-m)}} - \frac{1}{\tau}\right)\mathrm{d}\tau\right]\,. \tag{5.25}$$

At this point we can subtract the volume of undefomed AdS_3, which is recovered by setting $\gamma = 0$. Since

$$\eta(0) = 0\,, \quad \text{and} \quad \chi(0) = -\pi\,, \tag{5.26}$$

the vacuum volume is

$$\mathcal{V}(0,\ell) = L^2\left(\frac{\ell}{\delta} - \pi\right)\,. \tag{5.27}$$

As a cross-check, we can perform the AdS_3 computation directly. The cutoff now reads

$$y^* = \operatorname{arccosh}\left(\frac{z}{\delta}\right)\,, \qquad z_{\min} = \delta\,, \tag{5.28}$$

and therefore

$$\mathcal{V}(0,\ell) = 2L^2\int_\delta^{\bar{z}}\frac{\mathrm{d}z}{z}\int_0^{\operatorname{arccosh}(z/\delta)}\mathrm{d}y\,\cosh y = L^2\left(\frac{\ell}{\delta} - \pi\right)\,. \tag{5.29}$$

The difference between the regularised volumes of the Janus geometry and AdS_3 is

$$\Delta\mathcal{V}(\gamma,\ell) \equiv \mathcal{V}(\gamma,\ell) - \mathcal{V}(0,\ell) = L^2\left[\eta(\gamma)\,\log\left(\frac{\ell}{2H\,\delta}\right) + \chi(\gamma) + \pi\right]\,. \tag{5.30}$$

The only divergence in Eq. (5.30) is logarithmic, which is interpreted as the contribution from the defect, and it is proportional to the function $\eta(\gamma)$. Note that for small γ

$$\eta(\gamma) \approx \frac{\pi}{4}\gamma^2\,, \tag{5.31}$$

and that η is divergent for $\gamma \to 1/\sqrt{2}$, which corresponds to the linear dilaton limit. A plot of $\eta(\gamma)$ is shown in figure 5.2. It is interesting to compare $\eta(\gamma)$ with the Janus ground state degeneracy g, computed in [59]

$$\log g = \frac{L}{4G}\kappa(\gamma)\,, \qquad \kappa(\gamma) = \log\frac{1}{\sqrt{1-2\gamma^2}}\,. \tag{5.32}$$

Interestingly, we have that with good approximation $\eta \approx \kappa\,\pi/4$, see figure 5.2. The log divergencies of complexity have a very similar (but not identical) functional dependence on γ as $\log g$.

Note that the ℓ-dependent part of eq. (5.30) is proportional to the entanglement entropy of the segment without the defect, i.e.,

$$S_{\mathrm{AdS}} = \frac{c}{3}\log\left(\frac{\ell}{\delta}\right)\,. \tag{5.33}$$

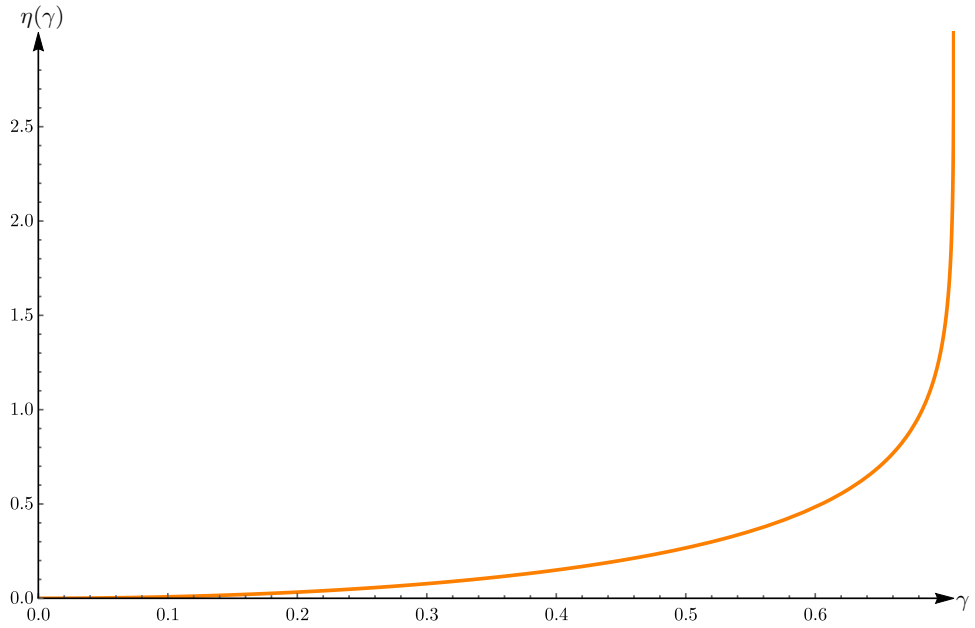

Figure 5.2: plot of $\eta(\gamma)$ as defined in Eq. (5.24), which is the coefficient of the log divergencies due to the defect.

5.2.1 Remarks on Time-dependence

We want to show that it is not restrictive to study the CV conjecture in the Janus AdS_3 background using a time slice at constant boundary time. One could be tempted to assign different time arrows on each of the two $y = \pm\infty$ boundaries (as customary for the left and right side of the Kruskal diagram). However, this is not consistent because the two boundaries are not causally disconnected. We are then forced to evolve the time in a unique way according to the asymptotic Killing vector of the metric. This forces us to take the boundary condition of the extremal volume at constant time t. This is true also for the RT surface that is needed for the subregion, which is also time independent.

Let us now show that the whole solution is at constant t. Let us parametrize the codimension-one slice expressing the time as a function $t(y, z)$. From the metric in eq. (4.4), the volume functional is

$$\mathcal{V} = L^2 \int \mathrm{d}z\, \mathrm{d}y\, \mathcal{L}\,, \qquad \mathcal{L} = \frac{\sqrt{f(y)}}{z} \sqrt{1 - (\partial_y t)^2 - \frac{f(y)}{z^2}\, (\partial_z t)^2}\,. \tag{5.34}$$

The $t = t_0$ function, where t_0 is a constant, is a solution of the Euler-Lagrange equation. Moreover, this solution has the property to maximize the volume functional.

5.3 Volume of the Static Janus BTZ Black Hole

In this Section we compute the subregion complexity for a symmetric interval with length ℓ centered around the defect of the static Janus BTZ geometry at vanishing boundary time. The metric is

$$ds^2 = L^2 \left[dy^2 + f(y) \left(-\frac{(w^2-1) r_h^2}{L^4} dt^2 + \frac{dw^2}{w^2-1} \right) \right], \tag{5.35}$$

which is obtained by substituting the Rindler-like metric (4.46) in (4.43), and performing the μ–to–y change of variable $\mathrm{d}\mu = \mathrm{d}y/\sqrt{f(y)}$.

The RT surface on a constant time slice lies at a constant value $w = \bar{w}$ [55]. We locate the interval along the coordinate $x \in [-\frac{\ell}{2}, \frac{\ell}{2}]$ orthogonal to the defect and at the radial distance $r = L^2/\delta$ determined by the FG expansion. The value of $\bar{w}$ can be obtained by combining the two equations (4.51) with $r = L^2/\delta$, $x = \ell/2$ and solving for $\bar{w}$, which gives

$$\bar{w} = \sqrt{\frac{1 + \sinh^2\left(\frac{\ell r_h}{2L^2}\right)}{\hat{\delta}^2 + \sinh^2\left(\frac{\ell r_h}{2L^2}\right)}}\,, \qquad \hat{\delta} = \frac{r_h \delta}{L^2}\,. \tag{5.36}$$

The UV divergences are regularized with the single cutoff prescription presented in Section 5.1. The natural choice of cutoff is found by performing a FG expansion of the metric to relate the asymptotic behavior of the deformed BTZ black hole with the non-deformed counterpart. Such asymptotic behavior is identified by

$$\frac{r}{r_h} \simeq \sqrt{(w^2-1)f(y)+1}\,. \tag{5.37}$$

The cutoff surface at $r = L^2/\delta$ induces the following value of y coordinate

$$y^*(w) = \frac{1}{2}\text{arcosh}\left(\frac{2 - \hat{\delta}^2\left(w^2+1\right)}{\hat{\delta}^2\left(w^2-1\right)\sqrt{1-2\gamma^2}}\right). \tag{5.38}$$

This in turn induces a cutoff in the w coordinate, which is found by maximizing the inverse of the previous function

$$w(y) = \sqrt{\frac{\frac{2}{\hat{\delta}^2} + \sqrt{1-2\gamma^2}\cosh(2y) - 1}{\sqrt{1-2\gamma^2}\cosh(2y)+1}}, \tag{5.39}$$

with respect to y. The maximum occurs at $y = 0$, and thus

$$w_{\text{max}} = \sqrt{\frac{\frac{2}{\hat{\delta}^2} + \sqrt{1-2\gamma^2} - 1}{\sqrt{1-2\gamma^2}+1}}\,. \tag{5.40}$$

This UV cutoff is the analog of z_{min} in the Janus AdS_3 case, see Eq. (5.15).

The extremal volume (5.4) for the static Janus BTZ geometry reads

$$\mathcal{V}(\gamma,\ell) = 2L^2\int_{\bar{w}}^{w_{\text{max}}} \mathrm{d}w \int_0^{y^*(w)} \mathrm{d}y \sqrt{\frac{f(y)}{w^2-1}}, \tag{5.41}$$

where we have included a factor of 2 due to the parity of the integrand in the y coordinate. After performing the following changes of variable

$$\tau = \frac{f(y)}{H^2}\,, \qquad z = \frac{L^4 - \delta^2 r_h^2}{H^2\delta^2 r_h^2(w^2-1)}\,, \qquad \bar{z} = \frac{L^4 - \delta^2 r_h^2}{H^2\delta^2 r_h^2(\bar{w}^2-1)}\,, \tag{5.42}$$

the integral reduces to the form

$$\mathcal{V}(\gamma,\ell) = \frac{L^2 H}{2}\int_1^{\bar{z}} \frac{\mathrm{d}z}{\sqrt{1+\alpha^2 z}} \int_1^z d\tau \sqrt{\frac{\tau}{(\tau-1)(\tau-m)}} \tag{5.43}$$

$$= \frac{L^2 H}{2}\int_1^{\bar{z}} \mathrm{d}\tau \sqrt{\frac{\tau}{(\tau-1)(\tau-m)}} \int_\tau^{\bar{z}} \frac{\mathrm{d}z}{z\sqrt{1+\alpha^2 z}}\,, \tag{5.44}$$

where we defined

$$\alpha \equiv \frac{H r_h\,\delta}{\sqrt{L^4 - \delta^2 r_h^2}}\,. \tag{5.45}$$

The integration over z yields three kind of terms, according to which we split the extremal volume as

$$\mathcal{V}(\gamma,\ell) = \mathcal{V}_1 + \mathcal{V}_2 + \mathcal{V}_3\,, \tag{5.46}$$

with the following definitions:

$$\mathcal{V}_1 \equiv L^2 H \int_1^{\bar{z}} \mathrm{d}\tau\, \log\left(1+\sqrt{1+\alpha^2\tau}\right)\sqrt{\frac{\tau}{(\tau-1)(\tau-m)}}\,, \tag{5.47}$$

$$\mathcal{V}_2 \equiv -\frac{L^2 H}{2}\int_1^{\bar{z}} \mathrm{d}\tau\, \log\tau\,\sqrt{\frac{\tau}{(\tau-1)(\tau-m)}}\,, \tag{5.48}$$

$$\mathcal{V}_3 \equiv -L^2 H \int_1^{\bar{z}} \mathrm{d}\tau\, \log\left(\frac{1+\sqrt{1+\alpha^2\bar{z}}}{\sqrt{\bar{z}}}\right)\sqrt{\frac{\tau}{(\tau-1)(\tau-m)}}\,. \tag{5.49}$$

The last two terms give (almost) exactly the same integral as in the Janus AdS_3 case, therefore, we refer to section 5.2 for their evaluation. The first term is slightly different but can be evaluated in a similar way: the trick is, again, to add and subtract the leading contibution to the divergence at infinity. In practice we have

$$\mathcal{V}_1 = LH^2\int_1^{\bar{z}} \mathrm{d}\tau\,\sqrt{\tau}\,\log\left(1+\sqrt{1+\alpha^2\tau}\right)\left[\left(\sqrt{\frac{1}{(\tau-1)(\tau-m)}}-\frac{1}{\sqrt{\tau}}\right)+\frac{1}{\sqrt{\tau}}\right]\,, \tag{5.50}$$

which can be evaluated as the previous integrals in the limit $\delta\to 0$. At the end of it all, the combined result is

$$\mathcal{V}(\gamma,\ell) = L^2\left\{\frac{\ell}{\delta}+\eta(\gamma)\log\left[\frac{2L^2}{H\delta r_h}\tanh\left(\frac{\ell r_h}{4L^2}\right)\right]+C(\gamma)\right\}+\mathcal{O}(\delta)\,, \tag{5.51}$$

where $\eta(\gamma)$ and $C(\gamma)$ were defined in euation (5.24).

The subregion volume in the BTZ background is still given by the AdS_3 result in eq. (5.29). This is because the subregion volume complexity of the BTZ background does not depend on temperature and it is topologically protected by the Gauss-Bonnet theorem [66]. This is however not the case for the Janus deformed geometry. In the small temperature regime $r_h\ell \ll 1$, we recover the Janus AdS result in Eq. (5.23).

Using the expression for temperature and the central charge

$$T = \frac{r_h}{2\pi L^2}\,, \qquad c = \frac{3L}{2G}\,. \tag{5.52}$$

we get that the subregion complexity, in terms of field theory quantities, is

$$\mathcal{C}(T,\gamma,\ell) = \frac{\mathcal{V}(\gamma\ell)}{LG} = \frac{2}{3}c\left\{\frac{\ell}{\delta}+\eta(\gamma)\log\left[\frac{H}{\pi T\delta}\tanh\left(\frac{\pi\ell T}{2}\right)\right]+C(\gamma)\right\}\,. \tag{5.53}$$

The temperature dependence of volume complexity is

$$\Delta\mathcal{C}(T,\gamma,\ell) \equiv \mathcal{C}(T,\gamma,\ell)-\mathcal{C}(0,\gamma,\ell) = \frac{2}{3}\,c\,\eta(\gamma)\Phi(\ell T) \tag{5.54}$$

where

$$\Phi(\ell T) = \log\left[\frac{2}{\pi\ell T}\tanh\left(\frac{\pi\ell T}{2}\right)\right]\,. \tag{5.55}$$

At zero temperature the contribution of the defect to $\mathcal{C}(\gamma,\ell)$ is proportional to the entanglement entropy of the segment without defect. However, the proportionality is spoiled at finite temperature. In fact, the BTZ entanglement entropy for a segment of length ℓ is

$$S_{\mathrm{BTZ}}(T,\ell) = \frac{c}{3}\log\left[\frac{2L^2}{r_h\,\delta}\sinh\left(\frac{\ell r_h}{2L^2}\right)\right] = \frac{c}{3}\log\left[\frac{1}{\pi\,T\,\delta}\sinh\left(\pi\ell T\right)\right]\,. \tag{5.56}$$

and is an increasing function of T. Instead $\Delta\mathcal{C}(\ell,\gamma)$ is a decreasing function of T.

Taking into account the two sides of the Kruskal diagram, the complexity relative to the formation of the static Janus BTZ backround starting from Janus AdS_3 is given by the $\ell \gg 1/T$ limit of $2\Delta\mathcal{C}$, i.e.,

$$\Delta\mathcal{C}_{\text{thermal}} = \frac{4}{3} c\, \eta(\gamma) \log\left(\frac{2}{\pi \ell T}\right) , \tag{5.57}$$

where, again, we interpret ℓ as an infrared regulator. In this limit, the complexity of formation is negative.

It is also interesting to consider the complexity of formation of the defect in the BTZ background. In this case, we subtract from Eq. (5.53) the $\gamma = 0$ result

$$\mathcal{C}(\gamma, T, \ell) - \mathcal{C}(0, T, \ell) = \frac{2}{3}\, c \left\{ \eta(\gamma) \log\left[\frac{1}{\pi H T \delta} \tanh\left(\frac{\pi \ell T}{2}\right)\right] + \chi(\gamma) + \pi \right\} . \tag{5.58}$$

Then, considering the $\ell T \gg 1$ limit and multiplying by an additional factor of two to account for the two sides of the Kruskal diagram, we obtain the complexity of formation of the defect starting from the static BTZ background

$$\Delta\mathcal{C}_{\text{defect}} = \frac{4}{3} c \left[\eta(\gamma) \log\left(\frac{1}{\pi a T \delta}\right) + \chi(\gamma) + \pi \right] . \tag{5.59}$$

Notice that, since the volume complexity in the BTZ black hole is topological, the above result can be also interpreted as the complexity of formation of the Janus static BTZ starting from the vacuum AdS_3 spacetime.

5.4 Volume of the Time-dependent Janus BTZ Geometry

We now consider CV-duality in the context of the time dependent Janus BTZ solution discussed in 5.4.

This gravity solution corresponds to a domain wall configuration for the dilaton field along the radial direction of AdS, which connects the left (L) and right (R) sides of the Penrose diagram 4.7. The dilaton does not divide each boundary into two halves, rather, it takes two different values on each boundary. Hence, the field theory dual of this solution is not an interface CFT, but it corresponds to a couple of entangled CFTs with two different and constant values of the dilaton source, e^{ϕ_-} and e^{ϕ_+}, on each side of the Penrose diagram.

As for the static Janus BTZ background, the arguments made in section 5.2.1 no longer hold. This is because the geometry is causally split by the event horizons, as a consequence we expect the volume to be time dependent.

5.4.1 Volume at Vanishing Boundary Time

In analogy to the cases of the previous Sections, we start by considering the scenario where the boundary times are $t_L = t_R = 0$ and the extremal volume sits on a time slice at constant $\tau = 0$. This can be interpreted as the complexity of formation of the Janus BTZ background starting from a simpler spacetime, which we can take to be either the simple BTZ black hole or a deformation of empty AdS space depending from the limit that we perform on the parameters of the geometry.

We consider the metric

$$ds^2 = dy^2 + f(y)\left(-d\tau^2 + r_h^2 \cos^2\tau\, d\theta^2\right) , \tag{5.60}$$

and by simply setting $\tau = 0$ we get the induced metric determinant

$$\sqrt{h} = r_h L^2 \sqrt{f(y)} . \tag{5.61}$$

In this way the extremal volume is simply given by

$$\mathcal{V}(\gamma, r_h) = 2r_h L^2 \int_0^{2\pi} \mathrm{d}\theta \int_0^{y^*} \mathrm{d}y \, \sqrt{f(y)}\,, \tag{5.62}$$

where we introduced a factor of 2 due to the symmetry of the problem and we also put a UV cutoff along the y coordinate.

In order to determine the value of the cutoff consistently with a FG expansion, we notice from [67] that near the conformal boundary, the metric approaches the AdS space in Poincaré coordinates with radial direction ξ and time coordinate t if we identify

$$\xi = \frac{2}{r_h \left(1-2\gamma^2\right)^{\frac{1}{4}}} e^{-|y|} \cosh\left(r_h t\right) . \tag{5.63}$$

If we set $\xi = \delta$ and we call the boundary values of the coordinates on the AdS_2 slice as $y = y_\infty$ and $t = t_\infty$, since everywhere $t = 0$ we get

$$\delta = \frac{2}{r_h \left(1-2\gamma^2\right)^{\frac{1}{4}}} e^{-y^*} \;\Rightarrow\; y^* = -\log\left(\frac{r_h(1-2\gamma^2)^{\frac{1}{4}}}{2}\,\delta\right) . \tag{5.64}$$

Notice from Eq. (5.62) that the angular part of the integral simply gives a factor of 2π and does not need to be regularized. For this reason, differently from the previous cases on the constant time slice $t = 0$, here we only have one meaningful regularization determined by the UV cutoff δ introduced with the FG expansion. The result of the integral is

$$\begin{aligned}
\mathcal{V}(\gamma, r_h) &= 4\pi r_h L^2 \int_0^{y^*} \mathrm{d}y \, \sqrt{f(y)} \\
&= 2\sqrt{2}\pi i r_h L^2 \sqrt{1+\sqrt{1-2\gamma^2}}\, \mathbb{E}\left(i \log\left[\frac{1}{2}(1-2\gamma^2)^{\frac{1}{4}} r_h\, \delta\right] \middle| 1-m \right) \\
&= \frac{4\pi L^2}{\delta} + 2\sqrt{2}\pi r_h L^2 \sqrt{1+\sqrt{1-2\gamma^2}}\, \left(\mathbb{K}(m) - \mathbb{E}(m)\right) + \mathcal{O}(\delta)\,,
\end{aligned} \tag{5.65}$$

where

$$m \equiv \frac{1-\sqrt{1-2\gamma^2}}{1+\sqrt{1-2\gamma^2}}\,. \tag{5.66}$$

We observe that both the finite and the divergent parts in δ are determined unambiguously.

Setting $\gamma = 0$ we recover the non-deformed BTZ solution, that is,

$$\mathcal{V}(\gamma = 0, r_h) = \frac{4\pi L^2}{\delta} + \mathcal{O}(\delta)\,, \tag{5.67}$$

If we subtract from the $\gamma \neq 0$ result the BTZ volume we get

$$\Delta\mathcal{V}(\gamma, r_h) \equiv \mathcal{V}(\gamma, r_h) - \mathcal{V}(\gamma = 0, r_h) = 2\pi r_h L^2 \eta(\gamma) + \mathcal{O}(\delta)\,. \tag{5.68}$$

We can indeed verify that this quantity is positive. The same result can be obtained if we set $r_h = 0$, which should correspond to considering a deformation of the empty AdS solution in the subtraction.

5.4.2 Growth Rate of the Volume

Let's now move to the case in which $t_L \neq 0$ and $t_R \neq 0$. In order to do that, we need to describe the codimension-one surface by expressing all the coordinates in terms of two parameters λ and ρ, meaning that

$$\tau = \tau(\lambda, \rho)\,, \qquad y = y(\lambda, \rho)\,, \qquad \theta = \theta(\lambda, \rho)\,. \tag{5.69}$$

However, we can simplify the situation by exploiting some of the symmetries inherent to the problem. First of all, we decide to take one of the parameters to be $\rho = \theta$; secondly, the fact that the metric is invariant under rotations along the angular direction implies that it is not restrictive to assume that the volume is independent of θ. For this reason, we parametrize the volume using $\theta, \tau(\lambda), y(\lambda)$, where λ is a kind of radial coordinate of the system. In this way we obtain the induced infinitesimal distance

$$ds^2_{\text{ind}} = L^2 \left[\left(\dot{y}^2 - f(y)\dot{\tau}^2 \right) d\lambda^2 + f(y)\, r_h^2 \cos^2\tau\, d\theta^2 \right] , \tag{5.70}$$

with determinant

$$\sqrt{h} = r_h L^2 \cos\tau \sqrt{f(y)\left(\dot{y}^2 - f(y)\dot{\tau}^2\right)} . \tag{5.71}$$

Consequently, the volume is given by

$$\mathcal{V} = 2\pi r_h L^2 \int_{\lambda_{\min}}^{\lambda_{\max}} \mathrm{d}\lambda\, \cos(\tau(\lambda)) \sqrt{\dot{y}^2 - f(y)\dot{\tau}^2} = 2\pi r_h L^2 \int_{\lambda_{\min}}^{\lambda_{\max}} \mathrm{d}\lambda\, \mathcal{L}(y, \dot{y}, \tau, \dot{\tau}) . \tag{5.72}$$

We impose the extremality condition by computing the Euler-Lagrange equations, which implies

$$2\sin\tau\dot{y}^3 - 3\cos\tau\, f'(y)\dot{y}^2\dot{\tau} + 2\cos\tau\, f(y)\dot{\tau}\left(f'(y)\dot{\tau}^2 + \ddot{y}\right) - 2f(y)\dot{y}\left(\sin\tau\,\dot{\tau}^2 + \cos\tau\,\ddot{\tau}\right) = 0 . \tag{5.73}$$

We exclude the trivial solution

$$\dot{\tau} = 0 , \qquad \dot{y} = 0 , \tag{5.74}$$

as it gives a vanishing volume at all times. At this point, one can use the invariance under reparametrization to normalize the integrand in a more convenient way. One possible choice is to take $\lambda = y$, which results in the following expression for the volume

$$\mathcal{V} = 2\pi r_h L^2 \int_{y_{\min}}^{y_{\max}} \mathrm{d}y\, f(y) \cos\left[\tau(y)\right] \sqrt{1 - f(y)\dot{\tau}^2} . \tag{5.75}$$

The differential equation (5.73) becomes

$$2\sin\tau - 3\cos\tau\, f'(y)\dot{\tau} + 2\cos\tau\, f(y) f'(y)\dot{\tau}^3 - 2f(y)\left(\sin\tau\,\dot{\tau}^2 + \cos\tau\,\ddot{\tau}\right) = 0 . \tag{5.76}$$

To solve the EOM we need to impose some kind of boundary conditions. We consider for simplicity[1] the case where the boundary times satisfy

$$\tau_B \equiv \tau_L = \tau_R . \tag{5.77}$$

In this case, the geometry is still symmetric between the left and right sides of the Penrose diagram, and it is reasonable to expect a turning point for the extremal volume slice (just as was found in [11].) For these reasons, we impose the boundary conditions

$$\tau(y_{\max}) = \tau_R , \qquad \tau(-y_{\max}) = \tau_L , \qquad \left.\frac{d\tau}{dy}\right|_{y=0} = 0 . \tag{5.78}$$

In particular, we define

$$\tau_{\min} \equiv \tau(y = 0) . \tag{5.79}$$

Changing the boundary time, also the value of $\tau_{\min}$ gets modified.

[1] Notice that in this case the assumption of taking the times symmetrically on the two boundaries is restrictive due to the absence of time translation invariance.

Numerical Solutions to the EOM

We approach the solution of the differential equation (5.73) numerically, as it seems not possible to solve it analytically.

First of all, we need an appropriate choice of the UV cutoff, which here is naturally determined by $y = y^*$ defined in equation (5.63) evaluated at $\xi = \delta$. We find

$$y_{\max}(\tau_B) = \log\left(\frac{2}{r_h\,\delta}\frac{1}{\cos\tau_B(1-2\gamma^2)^{\frac{1}{4}}}\right) . \tag{5.80}$$

This choice corresponds to the FG coordinates such that the metric on the boundary is the BTZ black hole solution, and, indeed, the cutoff is time-dependent as a result of the non-stationarity of the Janus deformation. Imposing the boundary conditions at these values of the y coordinate, we get the numerical solutions corresponding to a Janus deformation with $\gamma = 1/2$ in figure 5.3.

One may wonder which curves have turning point inside of the *shadow region*. This part of the spacetime is determined by the intersection of the curves at constant value of the null coordinates

$$w_1 = \frac{1}{2}(\tau+\mu) , \qquad w_2 = \frac{1}{2}(\tau-\mu) . \tag{5.81}$$

If we impose the condition that these null lines pass through the points

$$(\mu,\tau) = \left(-\mu_0, -\frac{\pi}{2}\right) , \qquad (\mu,\tau) = \left(\mu_0, \frac{\pi}{2}\right) , \tag{5.82}$$

then the curves of interest that determine the shadow region in the region of space with positive time are given by

$$-\mu+\mu_0 = \tau+\frac{\pi}{2} , \qquad \mu+\mu_0 = \tau+\frac{\pi}{2} . \tag{5.83}$$

The corresponding equation in the (y,τ) coordinate system is obtained after performing the transformation

$$\tanh y = \mathrm{sn}\left(\alpha_+\mu\middle|\frac{\alpha_-^2}{\alpha_+^2}\right) , \qquad \alpha_\pm^2 = \frac{1\pm\sqrt{1-2\gamma^2}}{2} , \tag{5.84}$$

and using the definition

$$\mu_0 = \frac{1}{\alpha_+}\mathbb{K}\left(\frac{\alpha_-^2}{\alpha_+^2}\right) \geq \frac{\pi}{2} . \tag{5.85}$$

The shadow region is shaded in red in fig. 5.3.

Divergent Part of the Volume

We can now numerically evaluate the integral corresponding to the extremal volume

$$\mathcal{V}(\gamma,\tau_B) = 4\pi r_h\int_0^{y_{\max}(\tau_B)} \mathrm{d}y\, f(y)\cos\left[\tau(y)\right]\,\sqrt{1-f(y)\dot{\tau}^2} , \tag{5.86}$$

by plugging in the numerical solutions for $\tau(y)$. The volume is expected to be divergent, as per our previous considerations. A typical feature of black hole solutions like the BTZ background is that the divergences are time-independent, while the finite part brings the information about the time evolution of the system. This can be heuristically understood from the fact that the turning point $\tau_{\min}$ is time-dependent, but it is determined at $y = 0$, which is far away from the boundary and then from the UV divergences. We suspect that the same phenomenon occurs for this non-stationary balck hole deformation, since the choice of the UV cutoff determined from the FG expansion is such that we recover the static BTZ background at the boundary.

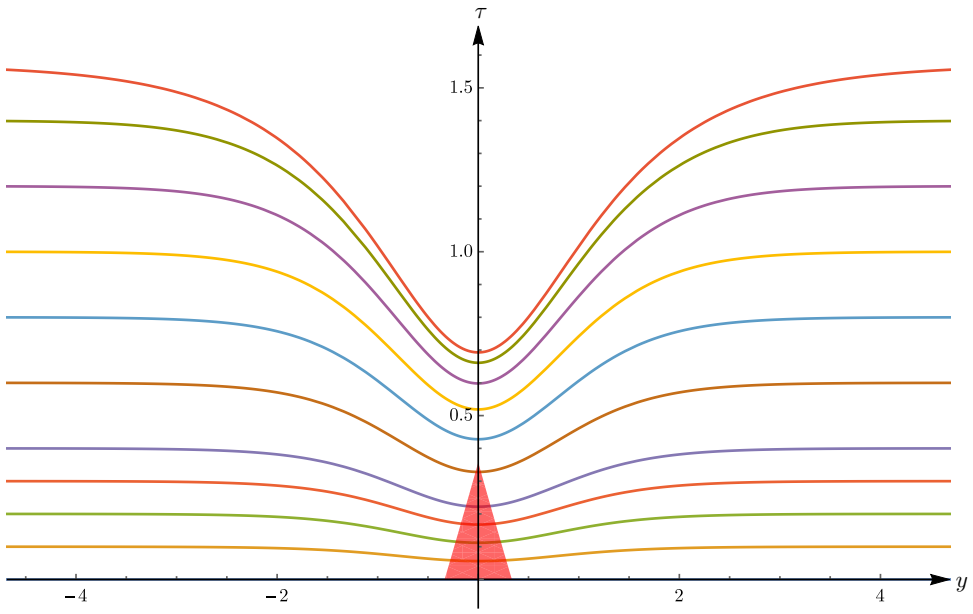

Figure 5.3: solutions of the EOM (5.73). each curve is attached to the boundary at a different time $\tau_B = \tau_L = \tau_R$. The shadow region is depicted in red.

Motivated by these observations, we shed light on the dependence of the volume from the UV cutoff by considering a fixed boundary time τ_B and choosing different values of

$$\delta_i = 10^{-\frac{i+2}{2}}\,, \tag{5.87}$$

with $i \in \{1, \dots, 10\}$. If we conjecture that the leading divergence of the extremal volume scales as

$$\mathcal{V}_i \equiv \mathcal{V}(\delta_i, \tau_B) = \frac{4\pi}{\delta_i} + \mathcal{O}(\delta_i^0)\,, \tag{5.88}$$

this would imply that the ratio between the volume evaluated for two consecutive values of the cutoff (5.87) is constant

$$\frac{\mathcal{V}_{i+1}}{\mathcal{V}_i} = \sqrt{10} \simeq 3.162\,. \tag{5.89}$$

We numerically tested this argument by computing these ratios for various choices of the boundary time: the result (see the table below) strongly suggests that the leading divergence indeed scales as δ^{-1}.

Boundary time τ_B	Ratio $\mathcal{V}_{i+1}/\mathcal{V}_i$
0.2	3.159 ± 0.006
0.4	3.158 ± 0.007
0.6	3.157 ± 0.010
0.8	3.154 ± 0.014
1.0	3.151 ± 0.020
1.2	3.144 ± 0.029

Table 5.1: Numerical value of the ratios $\mathcal{V}_{i+1}/\mathcal{V}_i$ evaluated at various boundary times τ_B. We determined the mean value and the standard deviation from the results obtained by varying $i \in \{1, \dots 10\}$ in the function $\delta = 10^{-\frac{i+2}{2}}$. The results must be compared with the analytic expectation $\sqrt{10} \simeq 3.162$.

We also notice that these ratios have a bigger error and deviate more from the analytic result as we increase the boundary time. We can explain this phenomenon in the following way. According to [16], the time-dependent metric originated by the Janus deformation should perturbe the black hole until the system reaches the thermal equilibrium at late times, going back to the original BTZ solution. From the analytic computation in Section 5.4.1, we found that the volume of the BTZ black hole solution is

$$\mathcal{V}_{\text{BTZ}}(\tau_B = 0) = \frac{4\pi}{\delta} + \mathcal{O}(\delta)\,, \tag{5.90}$$

without any finite part. On the other hand, we know from previous analysis [11] that the finite part of the volume monotonically grows with time. Putting all these considerations together, we expect that the finite part of the Janus deformation also increases with time, and this is responsible for the deviation of the ratios from the expected result obtained only from the estimation of the divergences.

Time Dependence of the Volume

First of all, we checked that the extremal volume computed numerically at $\tau_B = 0$ agrees with the exact result found in Eq. (5.65). To renormalize the diverging volume we subtract the $\gamma = 0$, i.e., the BTZ volume, volume at all times. Furthermore, to understand how the volume depends on the boundary time we have to relate τ with t, which can be done by means of the coordinate transformation

$$\tanh(r_h t) = \sin\tau\,, \tag{5.91}$$

which holds close to the boundary. In figure 5.4 we plot the volumes as a function of the boundary time for different values of the deformation parameter. The result is a monotonically increasing function of time, which reaches a linear growth for late times.

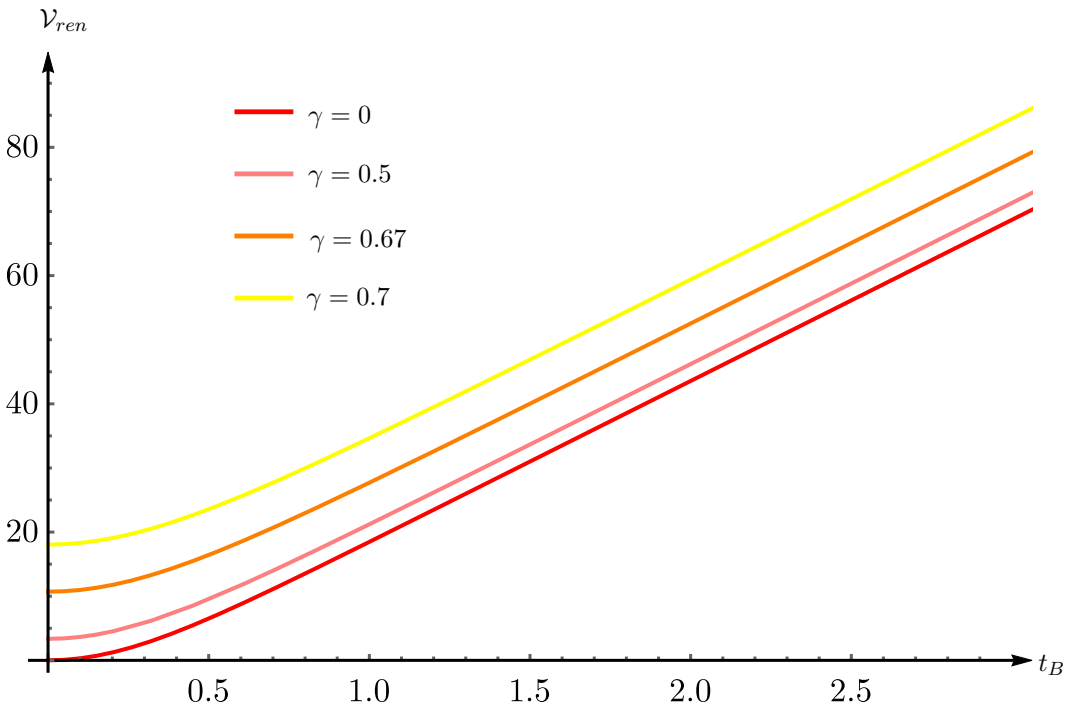

Figure 5.4: plot of the volume as a function of time for different values of γ.

It can be seen that, within numerical uncertainties, the growth rates of the volumes for different γ tend to the same value for late times. This should not come as a surprise, since we

expect that

$$\lim_{t_B\to\infty}\frac{\mathrm{d}\mathcal{V}_{\mathrm{ren}}}{\mathrm{d}t_B}\sim TS\,. \tag{5.92}$$

Indeed, we can verify numerically that this is precisely the case. According to [16], the time-dependent Janus deformation of the BTZ solution has a temperature given by

$$T=\frac{r_h}{2\pi}\,, \tag{5.93}$$

which is valid when the system reaches equilibrium. For arbitrary values of τ, as pointed out in [16], the time dependent Janus geometry represents an out of equilibrium system, and (5.93) is not valid. However, as the system reaches an equilibrium state for late times, we expect to be able to use (5.93) in this limit. In addition, the area of the horizon is given by [14]

$$\mathcal{A}(\tau)=2\pi r_h\frac{\alpha_+\sin\left(\pi/2-\tau\right)}{\mathrm{sn}\left(\alpha_+\left(\pi/2-\tau\right),k\right)}\underset{t_B\to\infty}{\longrightarrow}2\pi r_h\,. \tag{5.94}$$

This implies that at late times

$$TS=\frac{r_h^2}{4G}\,, \tag{5.95}$$

which is the same value that one gets for the BTZ background. We numerically checked that in the late time limit the growth rate of the volumes for all γ considered asyptotes to

$$\lim_{t_B\to\infty}\frac{d\mathcal{V}_{\mathrm{ren}}}{dt_B}=4\pi TS\,, \tag{5.96}$$

which matches with the volume rate at late times found in the literature [11]. A plot of the growth rate in function of the boundary time is shown below.

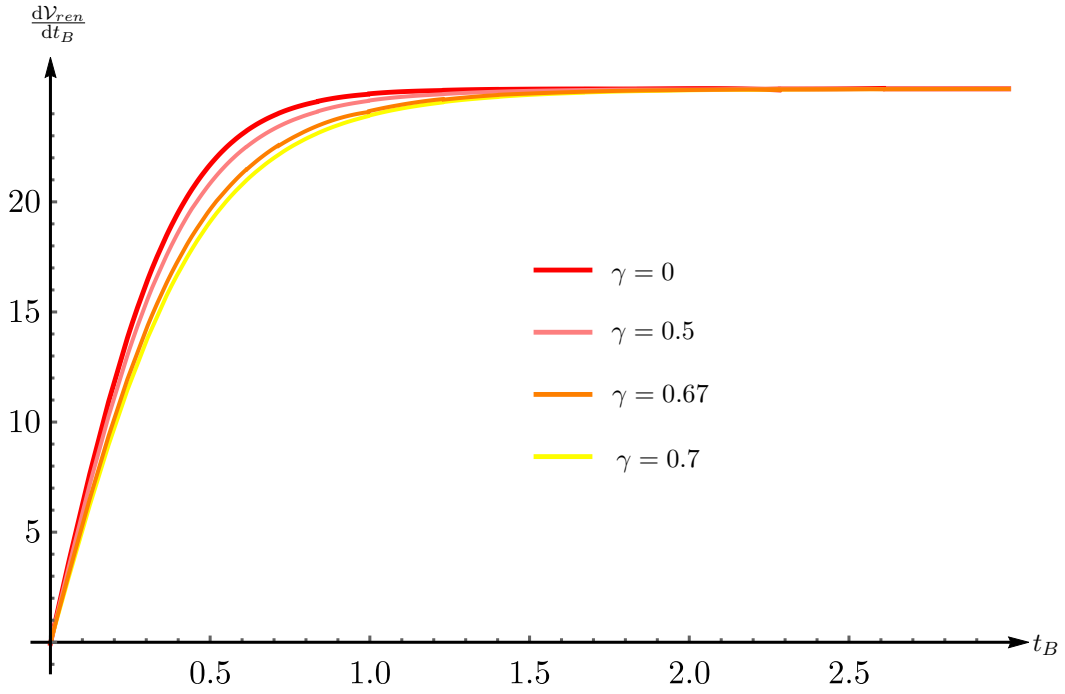

Figure 5.5: plot of the time derivative of the volume as a function of time for various values of the deformation parameter.

We remark that the divergence of the volume is universal because it does not depend on γ. For this reason, it is meaningfull to compare the finite part of the volume with different values of the Janus deformation. To that end, we define

$$\Delta\mathcal{V}(\gamma, t_B) = \mathcal{V}(\gamma, t_B) - \mathcal{V}(0, t_B)\,. \tag{5.97}$$

At $t_B = 0$, we have that $\Delta\mathcal{V} = \Delta\mathcal{V}_0$, given by eq. (5.68). The quantity $\Delta\mathcal{V}_0$ is positive and, in particular, for $\gamma \to \sqrt{2}/2$ it diverges. Since the time derivative of the volume is a decreasing function of γ, we have that $\Delta\mathcal{V}(\gamma, t_B)$ is a decreasing function of time. The asymptotic rate does not depend on γ and so $\Delta\mathcal{V}$ approaches a constant at late times.

For $\gamma \neq 0$ the system at $t_B = 0$ starts in a out-of-equilibrium state and then thermalizes at late times. The resulting rate of complexification is lower compared to the $\gamma = 0$ case: the computational power gets decreased by the time-dependent perturbation which brings the system out of equilibrium. The initial $\Delta\mathcal{V}_0$ is partially washed out at later times, but it does not approach zero asymptotically. It is surprising that the late-time volume rate is universal, in spite of the fact that different boundary values of the dilaton are dual to theories with different couplings.

Chapter 6

Volume Complexity for Janus AdS_5

In this chapter, we study holographic complexity according to the CV conjecture in the non-SUSY Janus deformed AdS_5 space. We will see that, compared with the lower dimensional counterpart, a different divergence structure appears. In [13] it is pointed out that for a boundary CFT the behavior of the divergent terms for the CV conjecture depends on the dimensionality of the space. Since a BCFT can be related to a CFT with a codimension-one defect or interface via the unfolding trick, we expect an analogous behavior also in the Janus interface case.

The strategies adopted in this chapter mirror those we have already discussed in the previous one, albeit with the extra caveats that come from extra dimensions. In section 6.1 we discuss the AdS_5 Janus extremal volume at vanishing boundary time, and in section 6.2 we discuss the subregion volume delimited by a ball-shaped geodesic dome. The material presented is based on [2].

6.1 Volume of the AdS_5 Janus Deformation

We evaluate the extremal volume using the metric in Eq. (4.35). Since the integral that defines the volume diverges near the asymptotic boundary, i.e., when $w \to \pm w_0$ and $z \to 0$, we have to regularize it introducing suitable cutoffs. In this section we adopt the single cutoff regularization procedure described in Section 5.1, which relates the UV cutoff along the w and the z directions.

6.1.1 Determination of the Cutoffs

First of all, re-write the metric of Janus AdS_5 space into the general form given in Eq. (5.1), where the coordinate y is non-compact and the prefactor of the dy^2 terms is the unity. This can be easily achieved by performing the following change of coordinates

$$dy = \gamma^{-1/2} h(w) dw \quad \Rightarrow \quad y = \gamma^{-1/2} \int_0^w \mathrm{d}w'\, h(w')\,, \tag{6.1}$$

which brings the metric (4.35) into the form

$$ds^2 = L^2 \left(dy^2 + h(y) ds^2_{\mathrm{AdS}_4} \right) . \tag{6.2}$$

The infinitesimal line element for Janus AdS_5 is now of the form expressed in (5.1), once we identify

$$A(y) = \sqrt{h(y)}\,, \quad \rho(y) = 1\,. \tag{6.3}$$

If we set the cutoff surface at$\xi = \delta$ we get the constraint

$$\delta = \frac{z}{\sqrt{h(y)}}\,, \tag{6.4}$$

which induces a lower bound on the z-variable, $z_{\min}$, that is,

$$z_{\min} = \delta \min_{y\in\mathbb{R}} \left(\sqrt{h(y)}\right) = \delta\,\sqrt{\gamma}\,, \tag{6.5}$$

where we used the fact that h takes minimum value at $y = 0$, where $h(0) = \gamma$. The previous prescription (which can be equivalently employed using the compact coordinate w) defines a cutoff $w_\pm$ such that

$$h(w_\pm) = \frac{z^2}{\delta^2} \quad \Rightarrow \quad w_\pm = h^{-1}\left(\frac{z^2}{\delta^2}\right)\,, \tag{6.6}$$

which regularizes the divergences stemming from the poles of the function $h(w)$ located at $w = \pm w_0$. In this way, the cutoff $w_\pm$ can be expanded in a power series of δ/z (see reference [61])

$$w_\pm\left(\frac{\delta}{z}\right) = \pm w_0 \mp \sum_{k=1}^{\infty} b_k\,\frac{\delta^{2k}}{z^{2k}}\,, \tag{6.7}$$

and all the coefficients of the series can be recursively determined order by order by imposing the condition (6.6). The previous expression only contains even powers of δ/z due to the parity of the function $h(w)$, and the first coefficients of the series are given by

$$b_1 = \frac{\sqrt{\gamma}}{2}\,, \qquad b_2 = \frac{\sqrt{\gamma}}{8}\,, \qquad b_3 = \frac{\sqrt{\gamma}}{16}\,, \qquad b_4 = \frac{5\sqrt{\gamma}}{128}\,, \qquad \dots \tag{6.8}$$

Whereas the location of the cvutoff is fixed via a Taylor expansion, the identity (6.6) is exact and formally re-sums all the coefficients of the series above.

6.1.2 Computation of the Volume

It is not restrictive to study the CV conjecture in the deformed AdS_5 background using a time slice at zero boundary time[1]. The extremal volume is computed by the integral

$$\mathcal{V} = \frac{2V_2}{\sqrt{\gamma}} \int_{\delta\sqrt{\gamma}}^{z_{\rm IR}} \frac{\mathrm{d}z}{z^3} \int_0^{w_+\left(\frac{\delta}{z}\right)} h(w)^{\frac{5}{2}}\,\mathrm{d}w\,, \tag{6.9}$$

where we introduced a factor of 2 because $\wp(w)$ is even in w, and we denoted with V_2 the two-dimensional infinite volume along the orthogonal spatial directions. Since the integral along the z direction is in principle divergent at infinity, we regularize it introducing a cutoff $z_{\rm IR}$. At the end we will remove this cutoff wherever possible.

We begin with the change of variables $\tau = h(w)$. The corresponding change of measure is evaluated using three identities:

- the inverse of the change of variables

$$\wp = \frac{\tau - 2\gamma(\gamma+\tau-1)}{\gamma-\tau}\,; \tag{6.10}$$

- the differential of Eq. (4.36)

$$h'(w) = -\frac{\gamma(4\gamma-3)}{(\wp+1-2\gamma)^2}\,\wp'(w)\,; \tag{6.11}$$

[1]It can be shown that the extremal slice at constant time is always a solution of the equations of motion at all times. By translational invariance along the time direction, we choose for convenience to study the case with vanishing boundary time.

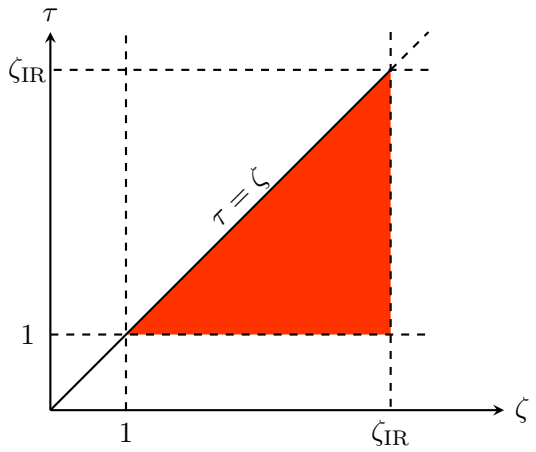

Figure 6.1: the domain of integration is depicted in red. We can swap the order of the integrals by adjusting the extremes of integration.

- and the following property of the Weierstrass $\wp-$function, which gets rid of all the $\wp'$ terms,

$$(\wp')^2 = 4\wp^3 - g_2\wp - g_3\,. \tag{6.12}$$

The extrema of integration are determined by the conditions $h(0) = \gamma$ and $h(w_\pm) = z^2/\delta^2$. In this way we get

$$\int_0^{w_+(\varepsilon)} \mathrm{d}w\, h^{5/2}(w) = \frac{\gamma^{5/2}}{2}\int_1^{\frac{z^2}{\gamma\delta^2}} \mathrm{d}\tau \sqrt{\frac{\tau^5}{\gamma(\tau^4-1)-(\tau^3-1)}}\,, \tag{6.13}$$

where we further rescaled $\tau \to \tau/\gamma$.

At this point, we perform another change of variables $\zeta = z^2/(\gamma\delta^2)$, which brings the volume (6.9) into the form

$$\mathcal{V} = \frac{\gamma V_2}{2\delta^2}\int_1^{\zeta_{\rm IR}} \frac{\mathrm{d}\zeta}{\zeta^2}\int_1^{\zeta} \mathrm{d}\tau\, \tau^{5/2} f(\tau)\,, \tag{6.14}$$

where we defined

$$f(\tau) \equiv \frac{1}{\sqrt{\gamma(\tau^4-1)-(\tau^3-1)}}\,, \qquad \zeta_{\rm IR} \equiv \frac{z_{\rm IR}^2}{\gamma\delta^2}\,. \tag{6.15}$$

A careful analysis of the integration region (see figure 6.1) reveals that we can swap the order of integration according to the rule

$$\int_1^{\zeta_{\rm IR}} \mathrm{d}\zeta \int_1^{\zeta} \mathrm{d}\tau\, F(\tau,\zeta) \to \int_1^{\zeta_{\rm IR}} \mathrm{d}\tau \int_\tau^{\zeta_{IR}} \mathrm{d}\zeta\, F(\tau,\zeta)\,, \tag{6.16}$$

for any given integrand function $F(\tau,\zeta)$. The evaluation of the ζ integration is trivial

$$\mathcal{V} = \frac{\gamma V_2}{2\delta^2}\int_1^{\zeta_{\rm IR}} \mathrm{d}\tau\, \tau^{5/2} f(\tau)\left(\frac{1}{\tau} - \frac{1}{\zeta_{\rm IR}}\right)\,. \tag{6.17}$$

The remaining integral is divergent in the limit $\delta \to 0$, which corresponds to the limit $\zeta_{\rm IR} \to \infty$. However, the integrand is well-behaved and we can series-expand $f(\tau)$ around infinity (where it is analytic). Thus, we can add and subtract the lowest orders of $f(\tau)$ expansion as follows:

$$\begin{aligned}\tau^{5/2} f(\tau)\left(\frac{1}{\tau} - \frac{1}{\zeta_{\rm IR}}\right) = {}& \tau^{3/2}\left[\left(f(\tau) - \frac{1}{\sqrt{\gamma}\tau^2} - \frac{1}{2\gamma^{3/2}\tau^3}\right) + \frac{1}{\sqrt{\gamma}\tau^2} + \frac{1}{2\gamma^{3/2}\tau^3}\right] \\ & - \frac{\tau^{5/2}}{\zeta_{\rm IR}}\left[\left(f(\tau) - \frac{1}{\sqrt{\gamma}\tau^2} - \frac{1}{2\gamma^{3/2}\tau^3}\right) + \frac{1}{\sqrt{\gamma}\tau^2} + \frac{1}{2\gamma^{3/2}\tau^3}\right]\,.\end{aligned} \tag{6.18}$$

In this way, the terms in the round parenthesis define a renormalized and finite integral where the limit $\delta \to 0$ can be performed directly (whatever the choice of $z_{\rm IR}$ is). The divergent parts of the integrals are trivially evaluated as

$$\int_1^{\zeta_{\rm IR}} \mathrm{d}\tau \left(\frac{1}{\sqrt{\gamma\tau}} + \frac{1}{2\gamma^{3/2}\tau^{3/2}} \right) = \frac{1}{\gamma^{3/2}} \left(2\gamma\sqrt{\zeta_{\rm IR}} - \frac{1}{\sqrt{\zeta_{\rm IR}}} + 1 - 2\gamma \right) , \tag{6.19}$$

$$\int_1^{\zeta_{\rm IR}} \mathrm{d}\tau \left(\sqrt{\frac{\tau}{\gamma}} + \frac{1}{2\gamma^{3/2}\sqrt{\tau}} \right) = \frac{1}{\gamma^{3/2}} \left(\frac{2\gamma}{3}\zeta_{\rm IR}^{3/2} + \sqrt{\zeta_{\rm IR}} - \frac{2}{3}\gamma - 1 \right) . \tag{6.20}$$

The non-trivial part is encoded by the renormalized integrals

$$A(\gamma) \equiv \int_1^{\infty} \mathrm{d}\tau\, \tau^{3/2} \left(f(\tau) - \frac{1}{\sqrt{\gamma}\tau^2} - \frac{1}{2\gamma^{3/2}\tau^3} \right) , \tag{6.21}$$

$$B(\gamma) \equiv \int_1^{\infty} \mathrm{d}\tau\, \tau^{5/2} \left(f(\tau) - \frac{1}{\sqrt{\gamma}\tau^2} - \frac{1}{2\gamma^{3/2}\tau^3} \right) , \tag{6.22}$$

where we have taken the limit $\delta \to 0$, which brings the upper extremum of integration to infinity. These functions are finite and well-defined for $\gamma \in (3/4, 1]$, whilst for $\gamma = 3/4$ they diverge, since $h(w) \to \gamma$ and the interval along which we integrate degenerates due to $w_0 \to \infty$. Furthermore, we can expand around $\gamma = 1$ (i.e., around the vacuum), since all the coefficients of the Taylor series can be computed analitically order by order. These functions are numerically displayed in figure 6.3. Summing all the contributions from the equations (6.19) and (6.22) with the

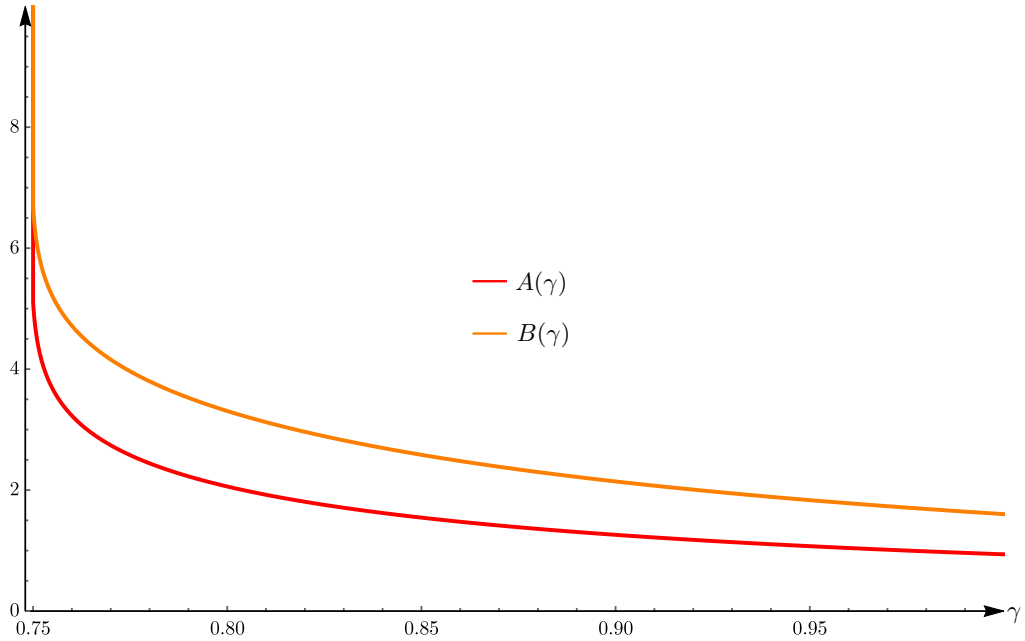

Figure 6.2: numerical plot of the functions $A(\gamma)$ and $B(\gamma)$ defined in Eqs. (6.21) and (6.22). The limit $\gamma \to 3/4$ is singular, while the limit $\gamma \to 1$ can be performed analitically from the Taylor expansion around that point, giving $A(1) = 1$ and $B(1) = 5/3$.

appropriate pre-factors, we obtain the extremal volume

$$\mathcal{V} = V_2 \left[\frac{2}{3}\frac{z_{\rm IR}}{\delta^3} + \mathcal{F}(\gamma)\frac{1}{\delta^2} - \frac{1}{z_{\rm IR}\delta} - \frac{1}{z_{\rm IR}^2}\mathcal{G}(\gamma) \right] + \mathcal{O}(\delta) . \tag{6.23}$$

where

$$\mathcal{F}(\gamma) \equiv \frac{\gamma A(\gamma)}{2} - \sqrt{\gamma} + \frac{1}{2\sqrt{\gamma}} , \qquad \mathcal{G}(\gamma) \equiv \frac{\gamma^2 B(\gamma)}{2} - \frac{\sqrt{\gamma}}{2} - \frac{1}{3}\gamma^{3/2} . \tag{6.24}$$

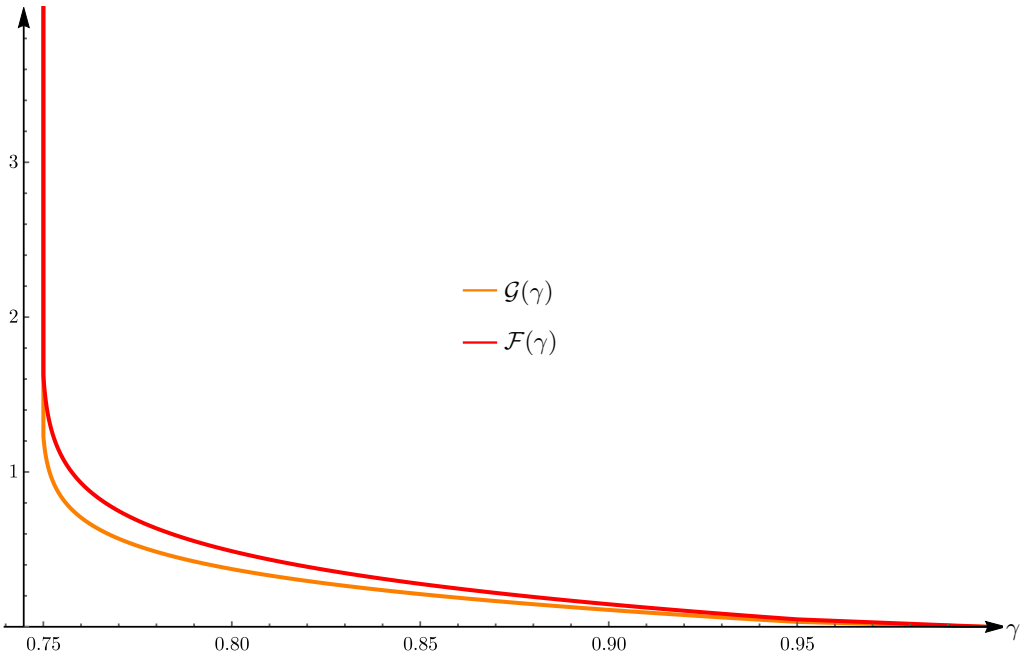

Figure 6.3: numerical plot of the functions $\mathcal{F}(\gamma)$ and $\mathcal{G}(\gamma)$ defined in (6.24).

Subtraction of Pure AdS$_5$

To identify the defect's contribution to the extremal volume, we need to subtract the result that stems from vacuum AdS$_5$. With this goal in mind, we proceed to set $\gamma = 1$ in (4.35), which results in

$$h(w) = \frac{1}{1-w^2}, \qquad w_0 = 1\ , \tag{6.25}$$

that is,

$$ds^2 = \frac{dw^2}{(1-w^2)^2} + \frac{1}{1-w^2} ds^2_{\text{AdS}_4}\ , \tag{6.26}$$

where $ds^2_{\text{AdS}_4}$ is the metric of a unit-radius AdS$_4$ in Poincaré slicing according to (5.3). Thus, the FG coordinates of empty AdS$_5$ are

$$\xi = z\sqrt{1-w^2}, \qquad \eta = zw\ . \tag{6.27}$$

The extremal volume at $t = 0$ for the AdS$_5$ vacuum is therefore given by

$$\mathcal{V}_{\text{AdS}_5} = 2V_2 \int_{z_{\text{min}}}^{z_{\text{IR}}} \frac{\mathrm{d}z}{z^3} \int_0^{w_*} \frac{\mathrm{d}w}{(1-w^2)^{5/2}}\ , \tag{6.28}$$

where the cutoff w_* can be derived from the FG coordinates in Eq. (6.27) setting $\xi = \delta$

$$w_* = \sqrt{1 - \frac{\delta^2}{z^2}}\ . \tag{6.29}$$

The value of z_{min} can be obtained as

$$z_{\text{min}} = \min\left(\frac{\delta}{\sqrt{1-\mathrm{w}^2}}\right) = \delta\ . \tag{6.30}$$

Computing the integral in Eq. (6.28), we get

$$\mathcal{V}_{\text{AdS}_5} = 2V_2 \left[\frac{1}{3}\frac{z_{\text{IR}}}{\delta^3} - \frac{1}{2}\frac{1}{z_{\text{IR}}\delta}\right] + \mathcal{O}(\delta)\ . \tag{6.31}$$

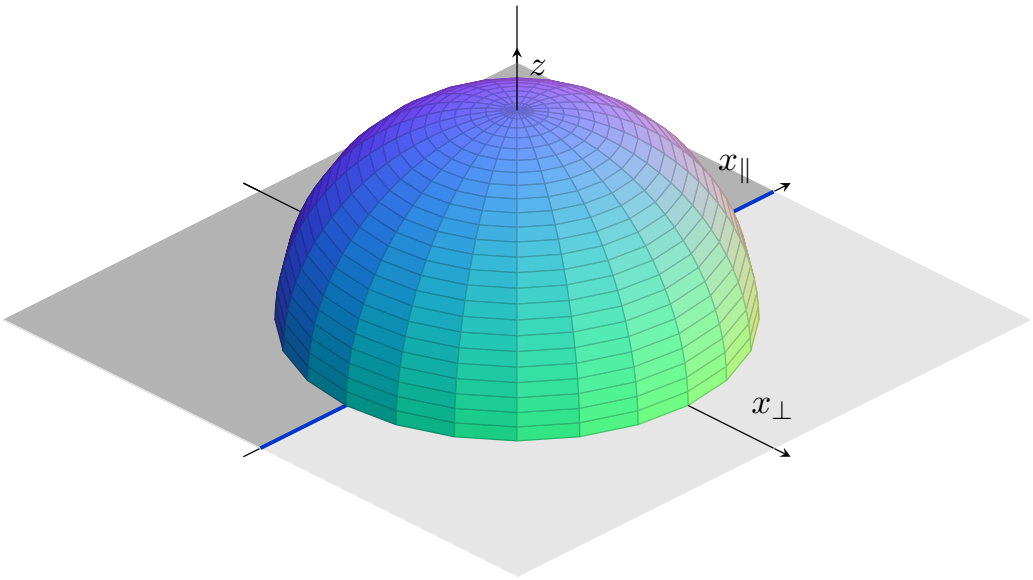

Figure 6.4: time slice of the Janus AdS_5 spacetime with a ball-shaped subregion centered on the interface. The Ryu-Takayanagi surface is represented by the spherical dome while the blue line represents the interface located at $x_\perp = 0$.

Subtracting the result for empty AdS space to Eq. (6.23), we obtain the complexity of formation of the Janus AdS_5 solution

$$\Delta\mathcal{C}(\gamma) = \frac{V_2}{G}\left(\frac{\mathcal{F}(\gamma)}{\delta^2} - \frac{\mathcal{G}(\gamma)}{z_{\text{IR}}^2}\right) + \mathcal{O}(\delta)\ . \tag{6.32}$$

It is interesting to compare this result with the double cutoff result discussed in B.3. One can promptly see that the finite term calculated in this section matches the finite term in (B.29) wilst the leading divergences don't match. This is a first suggestion that the universal information encoded by the complexity of formation is associated to the finite term, since a change of the energy scale does not affect it. We should also notice that the finite term is inversely proportional to the IR regulator, and then in the smooth limit $z_{\text{IR}} \to \infty$ the corresponding expression vanishes: so no universal information is contained in the complexity of formation for the entire geometry, except for the scaling of divergences proportionally to δ^{-2}.

6.2 Subregion Volume for the Janus AdS_5 Geometry

In this Section, we move to the case of subregion complexity with the hope of gaining further insight into the structure of the divergences. As we will see, as a result of the separation of the boundary into two regions an additional logarithmic divergence will appear .

6.2.1 Ball-shaped Subregion on the Boundary

Following ideas similar to those investigated for the entanglement entropy in [61, 64], a particularly convenient scenario in which we can study subregion complexity corresponds to considering a ball-shaped region of radius R centered on the interface, see figure 6.4. It is possible to show that the RT surface corresponding to this subregion is given by

$$z^2 + r^2 = R^2\ , \tag{6.33}$$

where this equation is written in terms of the metric (4.35) with the two-dimensional subspace parametrized with polar coordinates

$$d\vec{x}^2 = dr^2 + r^2 d\theta^2 \,. \tag{6.34}$$

Remarkably, this space-like geodesic is also a geodesic in vacuum AdS_5 space.

The RT surface delineates the region where the extremal codimension-one Cauchy slice extends. This will accordingly delineate the integration domain. Contrarily to what happens when considering the entire boundary, the resulting volume won't need IR regulators. The aforementioned subregion volume is computed by

$$\mathcal{V}(\gamma, R) = \frac{2}{\sqrt{\gamma}} \int_0^{2\pi} \mathrm{d}\theta \int_{z_{\min}}^{z_{\max}} \frac{\mathrm{d}z}{z^3} \int_0^{\sqrt{R^2-z^2}} \mathrm{d}r\, r \int_0^{w_+} \mathrm{d}w\, h^{\frac{5}{2}}(w) \,, \tag{6.35}$$

where a factor of 2 is included to account for symmetry in the w integration. The integral along the angular direction is trivial, while the one along the radial direction of the polar coordinates gives an additional factor that will modify the last integration along z. In other words,

$$\mathcal{V}(\gamma, R) = \frac{2\pi}{\sqrt{\gamma}} \int_{z_{\min}}^{R} \mathrm{d}z\, \frac{R^2 - z^2}{z^3} \int_0^{w_+} \mathrm{d}w\, h^{\frac{5}{2}}(w) \,. \tag{6.36}$$

Notice that the maximum value that can be reached by z is R, since the square root defining the maximum of radial coordinate r would otherwise be imaginary. On the other hand, the minimum of z is determined in the same way as for the total volume, that is, according to eqation (6.5) for the single cutoff prescription, and to $z_{\min} = \delta$ for the double cutoff.

6.2.2 Extremal Volume: Single Cutoff

Here we compute the extremal volume for the ball-spahed region in the Janus AdS_5 geometry using the single cutoff method. Once again, it is very useful to perfom the change of variables $\tau = \frac{h(w)}{\gamma}$, so that the integral we need to compute becomes

$$\mathcal{V}(\gamma, R) = \pi\gamma^2 \int_{\sqrt{\gamma}\delta}^{R} \mathrm{d}z\, \frac{R^2 - z^2}{z^3} \int_1^{\frac{z^2}{\gamma\delta^2}} \mathrm{d}\tau\, \tau^{5/2} f(\tau) \,, \tag{6.37}$$

where $f(\tau)$ is defined in equation (6.15). Performing a further change of variables $\zeta = z^2/(\gamma\delta^2)$, we are left with

$$\mathcal{V}(\gamma, R) = \pi\gamma^2 \int_1^{\frac{R^2}{\gamma\delta^2}} d\zeta\, \frac{R^2 - \gamma\delta^2\zeta}{2\gamma\delta^2\zeta^2} \int_1^{\zeta} \mathrm{d}\tau\, \tau^{5/2} f(\tau) \,. \tag{6.38}$$

As explained in equation (6.16), we can swap the integrals in ζ and τ being mindful to make suitable changes in the extremes of integration, getting

$$\mathcal{V}(\gamma, R) = \pi\gamma^2 \int_1^{\frac{R^2}{\gamma\delta^2}} \tau^{5/2} f(\tau) \int_\tau^{\frac{R^2}{\gamma\delta^2}} \mathrm{d}\zeta\, \frac{R^2 - \gamma\delta^2\zeta}{2\gamma\delta^2\zeta^2} \,. \tag{6.39}$$

At this point, it is possible to evaluate first the integral in the ζ variable as

$$\int_\tau^{\frac{R^2}{\gamma\delta^2}} d\zeta\, \frac{R^2 - \gamma\delta^2\zeta}{2\gamma\delta^2\zeta^2} = \frac{1}{2}\left(2\log\left(\frac{\sqrt{\gamma}\delta}{R}\right) - 1 + \frac{R^2}{\gamma\delta^2\tau} + \log\tau\right) \,. \tag{6.40}$$

Concerning the integration over τ, we have to compute three different types of integrals. The first one is

$$\int_1^{\frac{R^2}{\gamma\delta^2}} \mathrm{d}\tau\tau^{5/2} f(\tau) \,, \tag{6.41}$$

following the same steps of the computation for the total volume, we can write it as

$$B(\gamma)+\int_1^{\frac{R^2}{\gamma\delta^2}}\mathrm{d}\tau\left(\sqrt{\frac{\tau}{\gamma}}+\frac{1}{2\gamma^{3/2}\sqrt{\tau}}\right)=B(\gamma)+\frac{2R^3}{3\gamma^2\delta^3}+\frac{R}{2\gamma\delta^2}-\frac{1}{\gamma^{3/2}}-\frac{2}{3\sqrt{\gamma}}\,, \tag{6.42}$$

where $B(\gamma)$ is defined in Eq. (6.22) and we have taken the $\delta\to 0$ limit. The second integral in τ is given by

$$\int_1^{\frac{R^2}{\gamma\delta^2}}\mathrm{d}\tau\,\tau^{3/2}f(\tau), \tag{6.43}$$

which amounts to

$$A(\gamma)+\int_1^{\frac{R^2}{\gamma\delta^2}}\mathrm{d}\tau\left(\frac{1}{\sqrt{\gamma\tau}}+\frac{1}{2\gamma^{3/2}\tau^{3/2}}\right)=A(\gamma)+\frac{2R}{\gamma\delta}+\frac{1}{\gamma^{3/2}}-\frac{2}{\sqrt{\gamma}}-\frac{\delta}{\gamma R}\,. \tag{6.44}$$

Here, $A(\gamma)$ is defined in equation (6.21). The result is multiplied by a factor of $R^2/(\gamma\delta^2)$ coming from the ζ integral, so the result should be expanded up to order δ to keep track of the correct orders in the δ divergences. The last integral in τ that has to be taken into account is

$$\int_1^{\frac{R^2}{\gamma\delta^2}}\mathrm{d}\tau\,\tau^{5/2}\log\tau f(\tau)\,. \tag{6.45}$$

The integrand can be rewritten as

$$\tau^{5/2}\log\tau f(\tau)=\tau^{5/2}\log\tau\left[\left(f(\tau)-\frac{1}{\sqrt{\gamma}\tau^2}-\frac{1}{2\gamma^{3/2}\tau^3}\right)+\frac{1}{\sqrt{\gamma}\tau^2}+\frac{1}{2\gamma^{3/2}\tau^3}\right] \tag{6.46}$$

in such a way that the term in the round brackets gives a finite integral. Defining

$$C(\gamma)=\int_1^{\infty}\mathrm{d}\tau\,\tau^{5/2}\log\tau\left(f(\tau)-\frac{1}{\sqrt{\gamma}\tau^2}-\frac{1}{2\gamma^{3/2}\tau^3}\right)\,, \tag{6.47}$$

the integral presented in Eq. (6.45) becomes

$$C(\gamma)+\int_1^{\frac{R^2}{\gamma\delta^2}}\mathrm{d}\tau\left(\frac{\log\tau\sqrt{\tau}}{\sqrt{\gamma}}+\frac{\log\tau}{2\gamma^{3/2}\sqrt{\tau}}\right) \tag{6.48}$$

and finally gives

$$C(\gamma)-\log\left(\frac{\sqrt{\gamma}\delta}{R}\right)\left(\frac{4R^3}{3\gamma^2\delta^3}+\frac{2R}{\gamma^2\delta}\right)-\frac{4R^3}{9\gamma^2\delta^3}-\frac{2R}{\gamma^2\delta}+\frac{2}{\gamma^{3/2}}+\frac{4}{9\sqrt{\gamma}}\,. \tag{6.49}$$

Putting together all the terms, we get the following expression for the extremal subregion volume

$$\mathcal{V}(\gamma,R)=\frac{4\pi}{9}\frac{R^3}{\delta^3}-2\pi\frac{R}{\delta}+\pi\frac{R^2}{\delta^2}\mathcal{F}(\gamma)+2\pi\log\left(\frac{\sqrt{\gamma}\delta}{R}\right)\mathcal{G}(\gamma)+\mathcal{Q}(\gamma), \tag{6.50}$$

where $\mathcal{F}(\gamma)$ and $\mathcal{G}(\gamma)$ were defined in (6.24), and

$$\mathcal{Q}(\gamma)=\frac{\pi}{2}\left(\gamma^2C(\gamma)-\gamma^2B(\gamma)+3\sqrt{\gamma}+\frac{10}{9}\gamma^{3/2}\right)\,. \tag{6.51}$$

Subtraction of the Vacuum AdS Solution

Now, we can perform the subtraction of the AdS vacuum solution, which corresponds to set $\gamma = w_0 = 1$. The volume reads

$$\mathcal{V}_{\text{ball}}(w_0 = 1, \gamma = 1) = 2\pi \int_\delta^R \mathrm{d}z \, \frac{R^2 - z^2}{z^3} \int_0^{\sqrt{1-\frac{\delta^2}{z^2}}} \frac{\mathrm{d}w}{(1-w^2)^{\frac{5}{2}}} = \frac{4\pi}{9}\frac{R^3}{\delta^3} - 2\pi\frac{R}{\delta} + \frac{2\pi^2}{3} + \mathcal{O}(\delta)\,. \tag{6.52}$$

Subtracting the undeformed AdS_5 solution to the extremal volume obtained in Eq. (6.50), we get the complexity of formation in the Janus subregion case

$$\Delta\mathcal{C}_{sub}(\gamma, R) = \frac{\pi}{G}\left[\frac{R^2}{\delta^2}\mathcal{F}(\gamma) + 2\log\left(\frac{\sqrt{\gamma}\delta}{R}\right)\mathcal{G}(\gamma) + \frac{\mathcal{Q}(\gamma)}{\pi} - \frac{2\pi}{3}\right]\,. \tag{6.53}$$

A comment on the limit $R \to \infty$ is in order. The limit to corresponds to the case where the subregion coincides with the entire boundary, and hence, the result (6.53) should tend to the result found in (6.32). In order to verify that this is what actually happens, we notice that in polar coordinates the two-dimensional volume along the spatial directions $\vec{x} = (r, \theta)$ is

$$V_2 = \pi R^2\,, \tag{6.54}$$

which becomes infinite in the limit $R \to \infty$. For this reason, when comparing the two quantities we should check that

$$\frac{\Delta\mathcal{V}_{\text{AdS}_5}}{V_2} = \lim_{R\to\infty}\frac{\Delta\mathcal{V}_{\text{ball}}}{\pi R^2}\,. \tag{6.55}$$

The limit on the RHS of eq. (6.55) suppresses logarithmic and finite terms, and allows only to compare the divergent parts which are proportional to the volume of the subregion[2]. Employing Eq. (6.55), we immediatly recognize that the terms proportional to $1/\delta^2$ in Eq. (6.32) and (6.53) exactly match. In conclusion, the difference between the total and the subregion case for the complexity=volume conjecture involving the Janus deformation of AdS_5 spacetime, is given by the presence of an additional finite term and a logarithmic divergence. A similar difference also happens for the complexity=action computation involving the (2+1)-dimensional vacuum AdS or the BTZ black hole solutions.

Finally, we can compare the result attained in this section with the result attained from a different regularization scheme. In B.3.2, we employ the double cutoff procedure to compute the subregion volume; the result is displayed in eq. (B.34). Comparing the two results, it is clear that in the subregion case the universal contribution can be associated to the prefactor of the log divergence. This shouldn't surprise us: when a log divergence is present any ambiguity associated to the cutoff choice can be factored out of the logarithm (by using the most basic properties of logarithms) which then modifies the finite part. Hence, the log prefactor is universal while the finite part is ambiguous.

[2]Notice that the same observations held when comparing the complexity=action for the BTZ black hole when the subregion on the boundary is taken was sent to infinity [68].

Chapter 7

Closing Remarks

The main objective of this thesis has been to fill the gap in our understanding of complexity within the context of interface theories, by studying the CV proposal applied to Janus deformed theories. Let's summarize and comment our findings.

Three-dimensional Janus

In chapter 5 we examined three-dimensional Janus solutions. In particular, we studied subregion volume complexity for an interval of length ℓ centered around the Janus interface. At zero temperature, we found that the increment of subregion complexity compared to the vacuum CFT is

$$\Delta\mathcal{C}(\gamma,\ell) = \frac{2}{3}c\,\eta(\gamma)\,\log\left(\frac{l}{\delta}\right) + \text{finite terms}\,, \tag{7.1}$$

where c is the CFT central charge and $\eta(\gamma)$ is

$$\eta(\gamma) = 2\sqrt{\frac{1+\sqrt{1-2\gamma^2}}{2}}\,\left[\mathbb{K}(m) - \mathbb{E}(m)\right]\,, \qquad m = \frac{1-\sqrt{1-2\gamma^2}}{1+\sqrt{1-2\gamma^2}}\,. \tag{7.2}$$

A plot of $\eta(\gamma)$ is shown in figure 5.2. We can contrast this with the ground state degeneracy g of the Janus solution computed in [59], given by

$$\Delta S = \log g = \frac{c}{6}\kappa(\gamma)\,, \qquad \kappa(\gamma) = \log\frac{1}{\sqrt{1-2\gamma^2}}\,. \tag{7.3}$$

$\gamma \in [0, \sqrt{2}/2]$ parameterizes the excursion of the dilaton between the two sides of the interface, which diverges for $\gamma \to \frac{\sqrt{2}}{2}$.

It is interesting to compare $\Delta\mathcal{C}$ for the Janus interface with recent results found for other defect geometries, namely:

- the AdS_3 Randall-Sundrum, which was considered in [12, 59] . In this setup a two-dimensional brane of tension λ is embedded in AdS_3, resulting in the metric

$$ds^2 = L^2\left[dy^2 + \cosh^2(|y| - y^*)ds^2_{AdS_2}\right] \tag{7.4}$$

  where

$$\lambda = \frac{\tanh y^*}{4\pi GL}\,. \tag{7.5}$$

- and the BCFT model, considered in [13, 63, 69, 70]. In particular, the $BCFT_2$ defined on a half-line is dual to AdS_3 in Poincarè coordinares

$$ds^2 = \frac{L^2}{z^2}\left(-dt^2 + dz^2 + dx^2\right)\,, \tag{7.6}$$

where the geometry is restricted to the region $Q = \{(x, z) : x(z) = -z \cot \alpha\}$, and $\alpha \in (0, \pi/2]$. The parameter α is the angle at which the Q brane meets the boundary.

In the table 7.1 the resulting complexities of formation are displayed. By comparing the different entries we conclude that:

i. the leading divergence in $\Delta\mathcal{C}$ is always logarithmic, with a positive coefficient η that is a function of the deformation parameter of the model;

ii. in all three cases, the log divergence in $\Delta\mathcal{C}$ is not related in any universal way to the defect boundary entropy ΔS. Nonetheless, the two quantities share a similar behavior, that is, they diverge for the same critical value;

iii. for small values of the deformation parameters, in all the models η/κ is of order 1, i.e.,

$$\frac{\eta(\gamma)}{\kappa(\gamma)} = \frac{\pi}{4}\,, \qquad \frac{\eta_{\text{RS}}}{\kappa_{\text{RS}}} = \frac{\eta_{\text{BCFT}}}{\kappa_{\text{BCFT}}} = 1\,; \tag{7.7}$$

iv. in the Janus case η/κ remains very close to $\frac{\pi}{4}$ for the whole range of the deformation parameter γ. On the contrary, in the other two models $\eta \gg \kappa$ close to the critical values $y^* \to \infty$ and $\alpha \to 0$.

Theory	$\Delta\mathcal{C}$ (no finite terms)	η	κ
Janus	$\frac{2}{3} c\,\eta_{\text{J}}\, \log\left(\frac{\ell}{\delta}\right)$	$2\sqrt{\frac{1+\sqrt{1-2\gamma^2}}{2}}\,[\mathbb{K}(m) - \mathbb{E}(m)]$	$\log \frac{1}{\sqrt{1-2\gamma^2}}$
Randall-Sundrum	$\frac{2}{3} c\,\eta_{\text{RS}}\, \log\left(\frac{\ell}{\delta}\right)$	$2 \sinh y^*$	$2y^*$
BCFT	$\frac{2}{3} c\,\eta_{\text{BCFT}}\, \log\left(\frac{\ell}{\delta}\right)$	$\cot \alpha$	$\log\left(\cot \frac{\alpha}{2}\right)$

Table 7.1: comparison between different defect theories.

In absence of the interface, the subregion volume complexity for the BTZ background is topologically protected by the Gauss-Bonnet theorem [66] and, therefore, does not depend on temperature. This is no longer true in the presence of the Janus interface. The difference $\Delta\mathcal{C}_T$ between the finite and the zero temperature subregion complexity is:

$$\Delta\mathcal{C}(\gamma, \ell, T) = \frac{2}{3}\, c\, \eta(\gamma)\, \log\left[\frac{2}{\pi \ell T} \tanh\left(\frac{\pi \ell T}{2}\right)\right]\,. \tag{7.8}$$

This is a decreasing function of temperature. It would be interesting to compute this quantity also in the RS and in the BCFT models, in order to see if there is some universality property.

As the $\ell \to \infty$ limit covers the entire boundary timeslice, we can define the total complexity trough the $\ell \to \infty$ limit of subregion complexity. The complexity of formation for the defect is then defined as the difference between the total complexity and its value at $\gamma = 0$. At zero temperature, the result is given by (7.1), where ℓ is to be understood as an infrared regulator. At finite temperature, such expression generalizes to

$$\Delta\mathcal{C}_{\text{defect}} = \frac{4}{3} c\, \eta(\gamma)\, \log\left(\frac{1}{T\,\delta}\right) + \text{finite terms}\,, \tag{7.9}$$

which is still logarithmically divergent. Note that in this case there is no need of an infrared regulator. At finite temperature, it is also meaningful to consider the thermal complexity of

formation of the Janus BTZ black hole in a geometry which already contains a defect. In this case we compute the difference between the total complexity and its value at temperature $T = 0$, to obtain

$$\Delta\mathcal{C}_{\text{thermal}} = \frac{4}{3} c\, \eta(\gamma) \log\left(\frac{2}{\pi \ell T}\right) . \tag{7.10}$$

Compared to (7.9), this quantity is UV finite, but it requires an IR regulator ℓ.

We also numerically computed the time evolution of the volume complexity for the time-dependent Janus BTZ black hole. In this case the boundary theory is not an interface CFT, but corresponds to two entangled CFTs with different values of the dilaton field on each of the boundaries. At $t_B = 0$, the boundary theories start from an out-of-equilibrium state and the time-dependent Janus black hole background is the gravity dual of the thermalisation process. The rate of growth of the volume as a function of the boundary time t_B is shown in figure 5.5.

At late times, the growth rate of the volume saturates at the same constant value (proportional to TS) for all the values of γ. So the coupling does not influence the computational power of the CFT at equilibrium. This could come as a surprise given that γ determines the boundary values of the dilaton, which are dual to the couplings of the boundary CFTs. We find that at early times, where the dual field theory is in an out-of-equilibrium state for $\gamma \neq 0$, the Janus deformation always decreases the complexity growth rate compared to the BTZ case. Being out of equilibrium decreases the computational power of the CFT.

Non-SUSY Five-dimensional Janus

In chapter 6, we computed holographic complexity of formation for the Janus deformation of AdS_5 spacetime with respect to vacuum space both for the entire boundary and for the case of a symmetric ball-shaped subregion located symmetrically around the interface. We did so with two different prescriptions for regularizing the UV modes: the single cutoff prescription and the double cutoff prescription (see appendix B.3.) The coefficients of the UV divergences are collected in Table 7.2.

Complexity of formation	Single cutoff	Double cutoff
Entire boundary	$\frac{L^3}{G}\frac{V_2}{\delta^2}\mathcal{F}(\gamma)$	$\frac{L^3}{G}\frac{V_2}{\delta^2}\mathcal{G}(\gamma)$
Subregion: δ^{-2} term	$\frac{L^3}{G}\frac{\pi R^2}{\delta^2}\mathcal{F}(\gamma)$	$\frac{L^3}{G}\frac{\pi R^2}{\delta^2}\mathcal{G}(\gamma)$
Subregion: $\log\delta$ term	$\frac{2\pi L^3}{G}\log\left(\frac{\sqrt{\gamma}\delta}{R}\right)\mathcal{G}(\gamma)$	$\frac{2\pi L^3}{G}\log\left(\frac{\delta}{R}\right)\mathcal{G}(\gamma)$

Table 7.2: Coefficients of the divergences entering the complexity of formation for the non-SUSY Janus AdS_5 geometry.

First of all, we notice that the structure of the divergences differs between the subregion case and the setting in which we consider the entire boundary. The latter only admits a power-law divergence δ^{-2}, which is consistent with the result computed in [13] for a BCFT, while the former has a richer structure, where an additional logarithmic divergence and a non-vanishing finite terms appear. We suspect that this logarithmic term originates, as in the case of holographic entanglement entropy, from infinitely short correlations between degrees of freedom on each side of the subregion division. A similar difference is also present in the complexity = action computation involving the (2+1)-dimensional vacuum AdS or BTZ black hole solutions [68].

Comparing the entries in Table 7.2, the only result independent of the regularization scheme

is the coefficient of the logarithmic divergences in the subregion case[1]. In addition, the finite term in the total volume case also matches between single and double cutoff prescriptions – see equations (6.32) and (B.29) – but it vanishes once we take the limit $z_{\text{IR}} \to \infty$. This behavior suggests that similarly to the entanglement entropy computation, universal properties about complexity are encoded by logarithmic or finite terms since they are invariant under rescalings of the UV cutoff. When both terms are present, only the coefficient of the logarithm is universal. In fact, a transformation of the UV cutoff in the logarithm amounts to an additional finite part, which then becomes ambiguous. This remark is also consistent with the three-dimensional analysis considered above, given that the complexity of formation for Janus AdS_3 comprises a logarithmic divergence and a finite term – both at finite and at vanishing temperature – of which the finite term is the ambiguous one.

(Possible) Future Developments

There are some potential developments to the work presented in this thesis. The most natural step forward, would be to extend the analysis in chapter 5 and 6 to the CA case. This would ultimately allow us to compare the structure of the UV divergences in the two conjectures, and in so doing determine whether *holographic complexity for interfaces distinguishes CA from CV* or not. To date, the literature on defect theories seems to indicate that this should be the case in three dimensions [12] but not in higher dimensions [13]. We don't have much reason to believe that this pattern is broken in the case of Janus geometries, but only time will tell.

The work presented here only dealt with the gravitational side of the story. Therefore, another interesting avenue could be to consider holographic complexity for interfaces from the field theory side. Potentially there are a number of ways in which such study could be carried out. One possibility is to use the path integral approach [53], as done by [13]. Alternatively, one could generalize the method used in [52] to the case of interfaces, by studying the geometry that arises in a dual CFT where part of the original symmetry group is broken.

Finally, the computation of the extremal volume could also be pursued in the higher dimensional generalizations of the time-dependent Janus BTZ black hole proposed in [16].

[1]Notice that the results only differ by the term $\frac{\pi L^3}{G} \log \gamma$, which amounts to a finite part.

Appendix A

Useful Special Functions

A.1 Jacobi Elliptic Functions and Elliptic Integrals

We work with the standard Jacobi elliptic functions and elliptic integrals defined along the lines of [71]. We use the incomplete elliptic integrals

$$\mathbb{F}(x|m) = \int_0^x \frac{\mathrm{d}\theta}{\sqrt{1 - m\sin^2\theta}}\,, \tag{A.1}$$

$$\mathbb{E}(x|m) = \int_0^x \mathrm{d}\theta\sqrt{1 - m\sin^2\theta}\,, \tag{A.2}$$

$$\Pi\left(n; x\,|m\right) = \int_0^x \frac{\mathrm{d}\theta}{\left(1 - n\sin^2\theta\right)\sqrt{1 - m\sin^2\theta}}. \tag{A.3}$$

of the first, second and third kind, respectively. The complete elliptic integrals are defined as

$$\mathbb{F}\left(\frac{\pi}{2}\middle|m\right) = \mathbb{K}(m)\,, \quad \mathbb{E}\left(\frac{\pi}{2}\middle|m\right) = \mathbb{E}(m)\,, \quad \Pi\left(n; \frac{\pi}{2}\middle|m\right) = \mathbb{P}(n|m)\,. \tag{A.4}$$

We also use the Jacobi amplitude $\varphi = \mathrm{am}(x|m)$ which is the inverse of $\mathbb{F}(x|m)$

$$x = \mathbb{F}(\mathrm{am}(x|m)|m)\,. \tag{A.5}$$

The Jacobi elliptic functions are defined as

$$\mathrm{sn}\left(x|\,m\right) = \sin\varphi, \quad \mathrm{cn}\left(x|\,m\right) = \cos\varphi \quad \text{and} \quad \mathrm{dn}\left(x|\,m\right) = \sqrt{1 - m\sin^2\varphi}, \tag{A.6}$$

such that $\mathrm{sn}\left(\mathbb{K}(m)|\,m\right) = 1$ and $\mathrm{cn}\left(\mathbb{K}(m)|\,m\right) = 0$. The reciprocals of the latter functions are

$$\mathrm{ns}\left(x|\,m\right) := \frac{1}{\mathrm{sn}\left(x|\,m\right)}, \quad \mathrm{nc}\left(x|\,m\right) := \frac{1}{\mathrm{cn}\left(x|\,m\right)}, \quad \mathrm{nd}\left(x|\,m\right) := \frac{1}{\mathrm{dn}\left(x|\,m\right)}. \tag{A.7}$$

Periodicity:

- $\mathrm{sn}\left(x|\,m\right)$ is a doubly periodic function with respect to x with periods $2i\mathbb{K}(1-m)$ and $4\mathbb{K}(m)$.
- $\mathrm{cn}\left(x|\,m\right)$ is a doubly periodic function with respect to x with periods $4i\mathbb{K}(1-m)$ and $4\mathbb{K}(m)$.
- $\mathrm{dn}\left(x|\,m\right)$ is a doubly periodic function with respect to x with periods $4i\mathbb{K}(1-m)$ and $2\mathbb{K}(m)$.

Some useful identities between the various elliptic functions are

$$\mathrm{sn}^{-1}(x|m) = \mathbb{F}(\sin^{-1}(x)|m)\,, \tag{A.8}$$

$$\mathrm{sn}\,(x|\,m)^2 + \mathrm{cn}\,(x|\,m)^2 = 1\,. \tag{A.9}$$

The following asymptotic behavior is useful for $x \to \infty$

$$-\,i\,\mathbb{E}(ix|1-m) = \frac{\sqrt{1-m}}{2}e^x + (\mathbb{K}(m) - \mathbb{E}(m)) + O(e^{-x})\,. \tag{A.10}$$

A.2 Weierstrass Elliptic Functions

The Weierstrass $\wp$ is an elliptic function of order 2 defined by the series

$$\wp(z,\omega_1,\omega_2) = \frac{1}{z^2} + \sum_{(m,n)\neq(0,0)} \left[\frac{1}{(z-2m\omega_1-2n\omega_2)^2} - \frac{1}{(2m\omega_1+2n\omega_2)^2}\right]\,, \tag{A.11}$$

which is doubly periodic in the complex plane with half-periods ω_1, ω_2. It is a meromorphic and even function of z with double poles at the lattice point defined by its periods. One can alternatively define the elliptic $\wp$–function in terms of its invariants g_2, g_3, which can be computed as Eisenstein series involving the half-periods ω_1, ω_2. However, in this case it is simpler to define the $\wp$–function as the solution to the differential equation

$$(\partial_w \wp)^2 = 4\wp^3 - g_2\wp - g_3\,. \tag{A.12}$$

We also define the Weierstrass ζ and σ–functions as

$$\wp(z) = -\zeta'(z)\,, \qquad \zeta(z) = \frac{\sigma'(z)}{\sigma(z)}\,. \tag{A.13}$$

Appendix B

Alternative Regularizations

In the main text we performed the computations of the volume following the *single cutoff* prescription for regularizing the UV modes. In this appendix we discuss the alternatives presented in 5.1. We consider both the FG and the *double cutoff* regularizations for Janus AdS_3, in sections B.1 and B.2 respectively, whilst for Janus AdS_5 we focus solely on the double cutoff procedure.

B.1 Janus AdS_3 Volume: Fefferman-Graham Regularization

This method consists in using the FG expansion (5.5) to identify a UV cutoff in terms of the proper radial coordinate near the boundary. In particular, it is required that when $\xi \to 0$ the asymptotic behavior respects the limits

$$g_1(\xi/\eta) \to 1\,, \qquad g_2(\xi/\eta) \to 1\,. \tag{B.1}$$

The change of coordinates from (y, z) to (ξ, η) breaks down when $\xi/\eta \gg 1$, which corresponds to approaching the interface. This condition is equivalent to the statement that there exists a value of $y = y_0$ such that the FG expansion breaks down. Since $f(y)$ is a monotonically increasing function in the region $y \geq 0$, this equivalently implies that there exists a value of $\alpha \geq 1$ such that

$$A(y_0) = \alpha\, A(0)\,, \tag{B.2}$$

where $A(y)$ was introduced in Eq. (5.1). This criterion selects a particular $y = y_0$ such that the FG expansion breaks down:

$$y_0 = A^{-1}(\alpha A(0))\,. \tag{B.3}$$

There exist universal quantities that do not depend on the choice of the curve connecting the two FG patches [61]. For this reason, in the region where $y \in [-y_0, y_0]$ we can introduce an arbitrary curve interpolating between the two regions. As proposed in [12], we will select an interpolating curve connecting smoothly the two patches.

In the following, we show that this prescription gives the same result as the single cutoff method applied in Section 5.2, except for an ambiguity in the finite part.

B.1.1 Integration in the FG Patches

We consider the FG expansion defined in Eq. (4.26) with a UV cutoff located at $\xi = \delta$ and the condition $y \gg 1$. In this way we find

$$\frac{\delta}{z} = \frac{1}{\sqrt{f(y)}}\,, \quad \Rightarrow \quad y^* = \frac{1}{2}\,\text{arccosh}\left(\frac{\frac{2z^2}{\delta^2} - 1}{\sqrt{1 - 2\gamma^2}}\right)\,, \tag{B.4}$$

which is equivalent to the single cutoff prescription (5.10) after using the dictionary (5.13). According to Eq. (B.3), we determine the minimal value of $y = y_0$ such that the FG expansion is valid by solving

$$\sqrt{f(y_0)} = \alpha\sqrt{f(0)} \quad \Rightarrow \quad y_0 = \frac{1}{2}\,\text{arccosh}\left(\frac{2\alpha^2 f(0) - 1}{\sqrt{1-2\gamma^2}}\right). \tag{B.5}$$

Therefore, the integration in the FG patch region is given by

$$\mathcal{V}_1(\gamma,\ell) = 2\int_{z_{\min}^{\text{FG}}}^{\bar{z}} \frac{\mathrm{d}z}{z}\int_{y_0}^{y} \mathrm{d}y\,\sqrt{f(y)}\,, \tag{B.6}$$

where $\bar{z}$ was defined in (5.12), and we include a factor of 2 due to the symmetry of the problem. The minimal value $z = z_{\min}^{\text{FG}}$ is determined as

$$z_{\min}^{\text{FG}} = \delta \min_{y\in[y_0,y^*]}\left(\sqrt{f(y)}\right) = \alpha\,\delta\sqrt{\frac{1+\sqrt{1-2\gamma^2}}{2}}\,, \tag{B.7}$$

where we used the fact that in a single FG patch the function $f(y)$ is monotonically increasing. Notice that this value of $z_{\min}^{\text{FG}}$ differs from $z_{\min}$ in Eq. (5.15) (determined for the single cutoff prescription) only by the factor α.

B.1.2 Interpolation in the Middle Region

Now we consider the middle region where we do not have access to a FG expansion. We show that the surfaces at constant y and the ones at constant z are orthogonal to each others. Since the normal one-forms to such surfaces are given by

$$\mathbf{v} = \mathrm{d}y\,, \qquad \mathbf{w} = \mathrm{d}z\,, \tag{B.8}$$

one can easily show that $\mathbf{v}\cdot\mathbf{w} = 0$. Even though the coordinates (ξ,η) are not defined in the middle region, the original variables (y,z) are still a valid coordinate choice. According to [12], the curve interpolating the FG patches should be chosen in such a way to be perpendicular to the surface located at $y = y_0$. On the time slice $t = 0$, this condition entails that we need to select curves at constant z.

The integral in this region reads

$$\mathcal{V}_2(\gamma,\ell) = 2\int_{z_{\min}^{\text{FG}}}^{\bar{z}} \frac{\mathrm{d}z}{z}\int_{0}^{y_0} \mathrm{d}y\,\sqrt{f(y)}\,. \tag{B.9}$$

Despite the distinction between the FG patches and the middle region, the additivity property of integrals allow us to write

$$\mathcal{V}(\gamma,\ell) \equiv \mathcal{V}_1(\gamma,\ell) + \mathcal{V}_2(\gamma,\ell) = 2\int_{z_{\min}^{\text{FG}}}^{\bar{z}} \frac{\mathrm{d}z}{z}\int_{0}^{y^*} \mathrm{d}y\,\sqrt{f(y)}\,, \tag{B.10}$$

which is exactly the integral (5.16) that we evaluated for the single cutoff prescription, except that now we integrate from $z_{\min}^{\text{FG}} \geq z_{\min}$. However, it can be shown by explicit computation that this change only amounts to a shift of the finite part, while the leading divergences are the same. Subtracting vacuum AdS_3, the result is

$$\Delta\mathcal{V}(\gamma,\ell) = \eta(\gamma)\log\left(\frac{\ell}{2\alpha H\,\delta}\right) + C(\gamma) + \pi + \mathcal{O}(\delta)\,. \tag{B.11}$$

This procedure also shows that the value $y = y_0$ where the FG patch ends does not play any special role.

B.2 Janus AdS$_3$ Volume: Double Cutoff Regularization

In this Appendix, we compute the extremal volume for a symmetric subregion of length ℓ at vanishing time for the Janus AdS$_3$ geometry using the double cutoff regularization scheme. Following the procedure described in Section 5.1, we take one cutoff at $z = \delta$, whereas the other one is determined as

$$f(y) = \frac{1}{\varepsilon^2} \,. \tag{B.12}$$

Solving the previous equations for $y = y^*$, we find

$$y^*(\varepsilon) = f^{-1}\left(\frac{1}{\varepsilon^2}\right) \,. \tag{B.13}$$

This value is the same as the one in Eq. (5.15), once we identify $\varepsilon = \delta/z$. The main difference in using this method is that ε does not depend on z. Thus, the two integrals defining the volume are independent and factorize. Therefore, the extremal volume for the subregion is given by

$$\mathcal{V}(\gamma, \ell) = 2 \int_\delta^{\bar{z}} \frac{\mathrm{d}z}{z} \int_0^{y^*(\varepsilon)} \mathrm{d}y \, \sqrt{f(y)} \,, \tag{B.14}$$

where we have included a symmetry factor of 2. Following the analysis in Section 5.2 and performing the change of variables

$$\tau = \frac{f(y)}{H^2} \,, \tag{B.15}$$

the integral computing the volume reads

$$\mathcal{V}(\gamma, \ell) = L^2 H \log\left(\frac{\bar{z}}{\delta}\right) \int_1^{\frac{1}{H^2\varepsilon^2}} \mathrm{d}\tau \sqrt{\frac{\tau}{(\tau-1)(\tau-m)}} \,. \tag{B.16}$$

A direct evaluation gives

$$\mathcal{V}(\gamma, \ell) = L^2 \left(\eta(\gamma) + \frac{2}{\varepsilon}\right) \log\left(\frac{\bar{z}}{\delta}\right) \,, \tag{B.17}$$

where $\eta(\gamma)$ is defined in Eq. (5.24). Subtracting the volume of pure AdS_3 space which is given by

$$\mathcal{V}(0, \ell) = L^2 \frac{2}{\varepsilon} \log\left(\frac{\bar{z}}{\delta}\right) + \mathcal{O}(\varepsilon) \,, \tag{B.18}$$

we get the volume relative to the defect

$$\Delta\mathcal{V}(\gamma, \ell) = L^2 \, \eta(\gamma) \log\left(\frac{\ell}{2\,\delta}\right) + \mathcal{O}(\delta) \,. \tag{B.19}$$

We observe that the dependence on ε disappears after the subtraction of the empty AdS$_3$ solution, consistently with what we expected [64]. The remaining logarithmic divergence matches with the single cutoff computation (5.30), which differs only in the finite part. This is to be expected given that the leading divergence is logarithmic.

B.3 Janus AdS$_5$: Double Cutoff Regularization

We employ the double cutoff prescription to regularize the UV divergences of the extremal volume. The advantage of this procedure is that the integrals are not nested, since we introduce two different regulators for the z and w directions. Specifically, we put a cutoff at the radial direction $z = \delta$ along one of the AdS$_4$ slicings, and following the logic of section 6.1.2 we impose

$$h(w_\pm) = \frac{1}{\varepsilon^2} \,. \tag{B.20}$$

This result comes from the FG expansion of the metric where in addition we set $\varepsilon = \delta/z$. In this way the Taylor expansion (6.7) defining the location of the cutoff becomes

$$w_{\pm}(\varepsilon) = \pm w_0 \mp \sum_{k=1}^{\infty} b_k \, \varepsilon^{2k} \,, \tag{B.21}$$

with the same coefficients determined in Eq. (6.8).

B.3.1 Computation of the Volume

The extremal volume at vanishing boundary time is determined by

$$\mathcal{V} = \frac{2V_2}{\sqrt{\gamma}} \int_{\delta}^{z_{\rm IR}} \frac{\mathrm{d}z}{z^3} \int_0^{w_+(\varepsilon)} h(w)^{\frac{5}{2}} \mathrm{d}w \,. \tag{B.22}$$

It is evident that in this case the integrations are independent. We start with the simplest one

$$\int_{\delta}^{\infty} \frac{\mathrm{d}z}{z^3} = -\left[\frac{1}{2z^2}\right]_{\delta}^{\infty} = \frac{1}{2\delta^2} - \frac{1}{2z_{\rm IR}^2} \,. \tag{B.23}$$

Following the same steps described in section 6.1.2, we change variables into $\tau = h(w)$ to obtain

$$\mathcal{V} = \frac{\gamma^2 V_2}{2\delta^2} \int_1^{\frac{1}{\gamma\varepsilon^2}} \mathrm{d}\tau \, \tau^{5/2} f(\tau) \,. \tag{B.24}$$

The last integration is performed, again, by renormalizing the integrand at infinity, and evaluating the divergent parts separately. In this way the volume contains the function $B(\gamma)$ defined in Eq. (6.22). Now, the $\varepsilon \to 0$ limit is regular and can be taken immediately. The non-trivial reminders of this manipulation are evaluated using the identity

$$\int_1^{\frac{1}{\gamma\varepsilon^2}} \mathrm{d}\tau \left(\sqrt{\frac{\tau}{\gamma}} + \frac{1}{2\gamma^{3/2}\sqrt{\tau}}\right) = \frac{1}{\gamma^2}\left(\frac{2}{3\varepsilon^3} + \frac{1}{\varepsilon} - \sqrt{\gamma} - \frac{2}{3}\gamma^{3/2}\right) , \tag{B.25}$$

which gives

$$\mathcal{V} = \frac{V_2}{2}\left(\frac{1}{\delta^2} - \frac{1}{z_{\rm IR}^2}\right)\left(\frac{2}{3\varepsilon^3} + \frac{1}{\varepsilon} + \gamma^2 B(\gamma) - \sqrt{\gamma} - \frac{2}{3}\gamma^{3/2}\right) + \mathcal{O}(\varepsilon) \,. \tag{B.26}$$

In order to subtract the extremal volume of a spacelike slice anchored at the boundary of the vacuum AdS_5 geometry, we repeat the steps explained in Section 6.1.2, with the difference that the cutoff along the y coordinate is located at

$$y^* = \operatorname{arccosh}\left(\frac{1}{\varepsilon}\right) \quad \Rightarrow \quad w^* = \sqrt{1-\varepsilon^2} \,. \tag{B.27}$$

In this way the volume reads

$$\begin{aligned} \mathcal{V}_{AdS_5} &= 2V_2 \int_{\delta}^{\infty} \frac{\mathrm{d}z}{z^3} \int_0^{\sqrt{1-\varepsilon^2}} \frac{\mathrm{d}w}{(1-w^2)^{5/2}} = \frac{V_2}{\delta^2}\left[\frac{w(3-2w^2)}{3(1-w^2)^{3/2}}\right]_0^{\sqrt{1-\varepsilon^2}} \\ &= \frac{V_2}{\delta^2}\left(\frac{1}{3\varepsilon^3} + \frac{1}{2\varepsilon}\right) + \mathcal{O}(\varepsilon) \,. \end{aligned} \tag{B.28}$$

After subtracting the vacuum solution from the extremal volume (B.26) in the presence of the defect, we get the complexity of formation

$$\Delta\mathcal{C}_{AdS_5} = \frac{V_2}{2G}\mathcal{G}(\gamma)\left(\frac{1}{\delta^2} - \frac{1}{z_{\rm IR}^2}\right) , \tag{B.29}$$

where $\mathcal{G}(\gamma)$ is defined in 6.24. Comparing this result with Eq. (6.32), we notice that the divergent part is different, while the finite part matches. This is a first suggestion that the universal information encoded by the complexity of formation is associated to the finite term, since a change of the energy scale does not affect it. We should also notice that the finite term is inversely proportional to the IR regulator, so that in the limit $z_{\rm IR} \to \infty$ it actually vanishes.

B.3.2 Subregion Volume

We can also evaluate the ball-shaped subregion volume in Eq. (6.36) using the double cutoff prescription. In this case we have to choose $z_{\text{min}} = \delta$. Since, again, the integrals along the z and w directions factorize, we can evaluate them separately. First of all we have

$$\int_{\delta}^{R} \mathrm{d}z \, \frac{R^2 - z^2}{z^3} = \frac{R^2}{2\delta^2} + \log\left(\frac{\delta}{R}\right) - \frac{1}{2} \,. \tag{B.30}$$

The integration along w simplifies using the change of variables $\tau = \gamma^{-1} h(w)$, and therefore we need to evaluate

$$\mathcal{V}_{\text{ball}} = \pi\gamma^2 \left(\frac{R^2}{2\delta^2} + \log\left(\frac{\delta}{R}\right) - \frac{1}{2}\right) \int_1^{\frac{1}{\gamma\varepsilon^2}} \mathrm{d}\tau \, \tau^{5/2} f(\tau) \,. \tag{B.31}$$

On the other hand, this integral is now completely equivalent to the one considered in section B.3, hence,

$$\mathcal{V}_{\text{ball}} = \pi \left(\frac{R^2}{2\delta^2} + \log\left(\frac{\delta}{R}\right) - \frac{1}{2}\right) \left(\gamma^2 B(\gamma) + \frac{2}{3\varepsilon^3} + \frac{1}{\varepsilon} - \sqrt{\gamma} - \frac{2}{3}\gamma^{3/2}\right) + \mathcal{O}(\varepsilon) \,. \tag{B.32}$$

The corresponding volume in the empty AdS geometry is easily obtained by considering the following

$$\mathcal{V}_{\text{AdS}_5} = 2\pi \int_{\delta}^{R} \mathrm{d}z \, \frac{R^2 - z^2}{z^3} \int_0^{\sqrt{1-\varepsilon^2}} \frac{\mathrm{d}w}{(1-w^2)^{5/2}} = 2\pi \left(\frac{R^2}{2\delta^2} + \log\left(\frac{\delta}{R}\right) - \frac{1}{2}\right) \left(\frac{1}{3\varepsilon^3} + \frac{1}{2\varepsilon}\right) + \mathcal{O}(\varepsilon) \,. \tag{B.33}$$

After subtracting the vacuum solution from the full result (B.32), we get the complexity of formation

$$\Delta\mathcal{C}_{\text{ball}} = \frac{\pi}{G} \left(\frac{R^2}{\delta^2} + 2\log\left(\frac{\delta}{R}\right) - 1\right) \mathcal{G}(\gamma) + \mathcal{O}(\delta) \,, \tag{B.34}$$

where, again, $\mathcal{G}(\gamma)$ is defined in (6.24). We can easily check that in the limit $R \to \infty$, we obtain a correct comparison with the case considered in section B.3, since

$$\lim_{R\to\infty} \frac{V_2}{\pi R^2} \Delta\mathcal{C}_{\text{ball}} = \frac{V_2}{2G\delta^2} \mathcal{G}(\gamma) \,, \tag{B.35}$$

which matches with Eq. (B.29).

Bibliography

[1] Roberto Auzzi et al. "Volume complexity for Janus AdS_3 geometries". In: (May 2021). arXiv: 2105.08729 [hep-th].

[2] Stefano Baiguera, Sara Bonansea, and Kristian Toccacelo. "Volume complexity for the non-supersymmetric Janus AdS_5 geometry". In: (May 2021).

[3] Juan Martin Maldacena. "The Large N limit of superconformal field theories and supergravity". In: *Adv. Theor. Math. Phys.* 2 (1998), pp. 231–252. DOI: 10.1023/A:1026654312961. arXiv: hep-th/9711200.

[4] Jacob D. Bekenstein. "Black Holes and Entropy". In: *Phys. Rev. D* 7 (8 1973), pp. 2333–2346. DOI: 10.1103/PhysRevD.7.2333. URL: https://link.aps.org/doi/10.1103/PhysRevD.7.2333.

[5] Stephen W Hawking. "Particle creation by black holes". In: *Communications in mathematical physics* 43.3 (1975), pp. 199–220.

[6] Shinsei Ryu and Tadashi Takayanagi. "Holographic derivation of entanglement entropy from AdS/CFT". In: *Phys. Rev. Lett.* 96 (2006), p. 181602. DOI: 10.1103/PhysRevLett.96.181602. arXiv: hep-th/0603001.

[7] Leonard Susskind. "Entanglement is not enough". In: *Fortsch. Phys.* 64 (2016), pp. 49–71. DOI: 10.1002/prop.201500095. arXiv: 1411.0690 [hep-th].

[8] Adam R. Brown et al. "Holographic Complexity Equals Bulk Action?" In: *Phys. Rev. Lett.* 116.19 (2016), p. 191301. DOI: 10.1103/PhysRevLett.116.191301. arXiv: 1509.07876 [hep-th].

[9] Douglas Stanford and Leonard Susskind. "Complexity and Shock Wave Geometries". In: *Phys. Rev. D* 90.12 (2014), p. 126007. DOI: 10.1103/PhysRevD.90.126007. arXiv: 1406.2678 [hep-th].

[10] Adam R. Brown et al. "Complexity, action, and black holes". In: *Phys. Rev. D* 93.8 (2016), p. 086006. DOI: 10.1103/PhysRevD.93.086006. arXiv: 1512.04993 [hep-th].

[11] Dean Carmi et al. "On the Time Dependence of Holographic Complexity". In: *JHEP* 11 (2017), p. 188. DOI: 10.1007/JHEP11(2017)188. arXiv: 1709.10184 [hep-th].

[12] Shira Chapman, Dongsheng Ge, and Giuseppe Policastro. "Holographic Complexity for Defects Distinguishes Action from Volume". In: *JHEP* 05 (2019), p. 049. DOI: 10.1007/JHEP05(2019)049. arXiv: 1811.12549 [hep-th].

[13] Yoshiki Sato and Kento Watanabe. "Does Boundary Distinguish Complexities?" In: *JHEP* 11 (2019), p. 132. DOI: 10.1007/JHEP11(2019)132. arXiv: 1908.11094 [hep-th].

[14] Dongsu Bak, Michael Gutperle, and Shinji Hirano. "Three dimensional Janus and time-dependent black holes". In: *JHEP* 02 (2007), p. 068. DOI: 10.1088/1126-6708/2007/02/068. arXiv: hep-th/0701108.

[15] Dongsu Bak, Michael Gutperle, and Romuald A. Janik. "Janus Black Holes". In: *JHEP* 10 (2011), p. 056. DOI: 10.1007/JHEP10(2011)056. arXiv: 1109.2736 [hep-th].

[16] Dongsu Bak, Michael Gutperle, and Andreas Karch. "Time dependent black holes and thermal equilibration". In: *JHEP* 12 (2007), p. 034. DOI: 10.1088/1126-6708/2007/12/034. arXiv: 0708.3691 [hep-th].

[17] Dongsu Bak, Michael Gutperle, and Shinji Hirano. "A Dilatonic deformation of AdS(5) and its field theory dual". In: *JHEP* 05 (2003), p. 072. DOI: 10.1088/1126-6708/2003/05/072. arXiv: hep-th/0304129.

[18] Eric D'Hoker, John Estes, and Michael Gutperle. "Ten-dimensional supersymmetric Janus solutions". In: *Nucl. Phys. B* 757 (2006), pp. 79–116. DOI: 10.1016/j.nuclphysb.2006.08.017. arXiv: hep-th/0603012.

[19] Luis Fernando Alday. *Conformal Field Theory*. URL: https://mmathphys.physics.ox.ac.uk/sites/default/files/CFTlectures.pdf.

[20] John McGreevy. *8.821 String Theory*. 2008. URL: https://ocw.mit.edu/courses/physics/8-821-string-theory-fall-2008/.

[21] Hong Liu. *8.821 String Theory and Holographic Duality*. 2014. URL: https://ocw.mit.edu/courses/physics/8-821-string-theory-and-holographic-duality-fall-2014/.

[22] Kazunori Akiyama et al. "First M87 Event Horizon Telescope Results. I. The Shadow of the Supermassive Black Hole". In: *Astrophys. J. Lett.* 875 (2019), p. L1. DOI: 10.3847/2041-8213/ab0ec7. arXiv: 1906.11238 [astro-ph.GA].

[23] W. G. Unruh. "Notes on black-hole evaporation". In: *Phys. Rev. D* 14 (4 1976), pp. 870–892. DOI: 10.1103/PhysRevD.14.870. URL: https://link.aps.org/doi/10.1103/PhysRevD.14.870.

[24] Raphael Bousso. "The Holographic principle". In: *Rev. Mod. Phys.* 74 (2002), pp. 825–874. DOI: 10.1103/RevModPhys.74.825. arXiv: hep-th/0203101.

[25] Daniel Harlow. "TASI Lectures on the Emergence of Bulk Physics in AdS/CFT". In: *PoS* TASI2017 (2018), p. 002. DOI: 10.22323/1.305.0002. arXiv: 1802.01040 [hep-th].

[26] Alberto Zaffaroni. "Introduction to the AdS-CFT correspondence". In: *Classical and Quantum Gravity* 17 (Aug. 2000), p. 3571. DOI: 10.1088/0264-9381/17/17/306.

[27] Horatiu Nastase. "Introduction to AdS-CFT". In: (2007). arXiv: 0712.0689 [hep-th].

[28] Martin Ammon and Johanna Erdmenger. *Gauge/gravity duality: Foundations and applications*. Cambridge University Press, 2015.

[29] Edward Witten. "Anti-de Sitter space and holography". In: *Adv. Theor. Math. Phys.* 2 (1998), pp. 253–291. DOI: 10.4310/ATMP.1998.v2.n2.a2. arXiv: hep-th/9802150 [hep-th].

[30] S. S. Gubser, Igor R. Klebanov, and Alexander M. Polyakov. "Gauge theory correlators from noncritical string theory". In: *Phys. Lett. B* 428 (1998), pp. 105–114. DOI: 10.1016/S0370-2693(98)00377-3. arXiv: hep-th/9802109.

[31] Mark Van Raamsdonk. "Building up spacetime with quantum entanglement". In: *Gen. Rel. Grav.* 42 (2010), pp. 2323–2329. DOI: 10.1142/S0218271810018529. arXiv: 1005.3035 [hep-th].

[32] Pasquale Calabrese and John L. Cardy. "Entanglement entropy and quantum field theory". In: *J. Stat. Mech.* 0406 (2004), P06002. DOI: 10.1088/1742-5468/2004/06/P06002. arXiv: hep-th/0405152.

[33] Shinsei Ryu and Tadashi Takayanagi. "Aspects of Holographic Entanglement Entropy". In: *JHEP* 08 (2006), p. 045. DOI: 10.1088/1126-6708/2006/08/045. arXiv: hep-th/0605073.

[34] Nabil Iqbal. "Entanglement Entropy in Field Theory and Gravity". In: *PoS* Modave2015 (2016), p. 002. DOI: 10.22323/1.271.0002.

[35] Juan Martin Maldacena. "Eternal black holes in anti-de Sitter". In: *JHEP* 04 (2003), p. 021. DOI: 10.1088/1126-6708/2003/04/021. arXiv: hep-th/0106112.

[36] Veronika E. Hubeny, Mukund Rangamani, and Tadashi Takayanagi. "A Covariant holographic entanglement entropy proposal". In: *JHEP* 07 (2007), p. 062. DOI: 10.1088/1126-6708/2007/07/062. arXiv: 0705.0016 [hep-th].

[37] Dmitri V. Fursaev and Sergey N. Solodukhin. "On the description of the Riemannian geometry in the presence of conical defects". In: *Phys. Rev. D* 52 (1995), pp. 2133–2143. DOI: 10.1103/PhysRevD.52.2133. arXiv: hep-th/9501127.

[38] John Watrous. *Quantum Computational Complexity*. 2008. arXiv: 0804.3401 [quant-ph].

[39] Leonard Susskind. *Three Lectures on Complexity and Black Holes*. 2018. arXiv: 1810.11563 [hep-th].

[40] Mark R Dowling and Michael A Nielsen. "The geometry of quantum computation". In: *Quantum Information & Computation* 8.10 (2008), pp. 861–899.

[41] Michael A. Nielsen et al. "Quantum Computation as Geometry". In: *Science* 311.5764 (2006), pp. 1133–1135. ISSN: 0036-8075. DOI: 10.1126/science.1121541. eprint: https://science.sciencemag.org/content/311/5764/1133.full.pdf. URL: https://science.sciencemag.org/content/311/5764/1133.

[42] Michael A. Nielsen. "A geometric approach to quantum circuit lower bounds". In: *arXiv e-prints*, quant-ph/0502070 (Feb. 2005), quant–ph/0502070. arXiv: quant-ph/0502070 [quant-ph].

[43] Dean Carmi, Robert C. Myers, and Pratik Rath. "Comments on Holographic Complexity". In: *JHEP* 03 (2017), p. 118. DOI: 10.1007/JHEP03(2017)118. arXiv: 1612.00433 [hep-th].

[44] Bartlomiej Czech et al. "The Gravity Dual of a Density Matrix". In: *Class. Quant. Grav.* 29 (2012), p. 155009. DOI: 10.1088/0264-9381/29/15/155009. arXiv: 1204.1330 [hep-th].

[45] Matthew Headrick et al. "Causality \& holographic entanglement entropy". In: *JHEP* 12 (2014), p. 162. DOI: 10.1007/JHEP12(2014)162. arXiv: 1408.6300 [hep-th].

[46] Mohsen Alishahiha. "Holographic Complexity". In: *Phys. Rev. D* 92.12 (2015), p. 126009. DOI: 10.1103/PhysRevD.92.126009. arXiv: 1509.06614 [hep-th].

[47] Ro Jefferson and Robert C. Myers. "Circuit complexity in quantum field theory". In: *JHEP* 10 (2017), p. 107. DOI: 10.1007/JHEP10(2017)107. arXiv: 1707.08570 [hep-th].

[48] Arpan Bhattacharyya, Arvind Shekar, and Aninda Sinha. "Circuit complexity in interacting QFTs and RG flows". In: *JHEP* 10 (2018), p. 140. DOI: 10.1007/JHEP10(2018)140. arXiv: 1808.03105 [hep-th].

[49] Pablo Bueno, Javier M. Magan, and C. S. Shahbazi. "Complexity measures in QFT and constrained geometric actions". In: (Aug. 2019). arXiv: 1908.03577 [hep-th].

[50] Pawel Caputa and Javier M. Magan. "Quantum Computation as Gravity". In: *Phys. Rev. Lett.* 122.23 (2019), p. 231302. DOI: 10.1103/PhysRevLett.122.231302. arXiv: 1807.04422 [hep-th].

[51] Johanna Erdmenger, Marius Gerbershagen, and Anna-Lena Weigel. "Complexity measures from geometric actions on Virasoro and Kac-Moody orbits". In: *JHEP* 11 (2020), p. 003. DOI: 10.1007/JHEP11(2020)003. arXiv: 2004.03619 [hep-th].

[52] Nicolas Chagnet et al. "Complexity for Conformal Field Theories in General Dimensions". In: (Mar. 2021). arXiv: 2103.06920 [hep-th].

[53] Pawel Caputa et al. "Liouville Action as Path-Integral Complexity: From Continuous Tensor Networks to AdS/CFT". In: *JHEP* 11 (2017), p. 097. DOI: 10.1007/JHEP11(2017)097. arXiv: 1706.07056 [hep-th].

[54] A. B. Clark et al. "Dual of the Janus solution: An interface conformal field theory". In: *Phys. Rev. D* 71 (2005), p. 066003. DOI: 10.1103/PhysRevD.71.066003. arXiv: hep-th/0407073.

[55] Dongsu Bak et al. "Unitarity of Entanglement and Islands in Two-Sided Janus Black Holes". In: *JHEP* 01 (2021), p. 155. DOI: 10.1007/JHEP01(2021)155. arXiv: 2006.11717 [hep-th].

[56] D. Z. Freedman et al. "Fake supergravity and domain wall stability". In: *Phys. Rev. D* 69 (2004), p. 104027. DOI: 10.1103/PhysRevD.69.104027. arXiv: hep-th/0312055.

[57] Ioannis Papadimitriou and Kostas Skenderis. "Correlation functions in holographic RG flows". In: *JHEP* 10 (2004), p. 075. DOI: 10.1088/1126-6708/2004/10/075. arXiv: hep-th/0407071.

[58] Marco Chiodaroli, Michael Gutperle, and Ling-Yan Hung. "Boundary entropy of supersymmetric Janus solutions". In: *JHEP* 09 (2010), p. 082. DOI: 10.1007/JHEP09(2010)082. arXiv: 1005.4433 [hep-th].

[59] Tatsuo Azeyanagi et al. "Holographic calculation of boundary entropy". In: *JHEP* 03 (2008), p. 054. DOI: 10.1088/1126-6708/2008/03/054. arXiv: 0712.1850 [hep-th].

[60] Michael Gutperle and John D. Miller. "Entanglement entropy at holographic interfaces". In: *Phys. Rev. D* 93.2 (2016), p. 026006. DOI: 10.1103/PhysRevD.93.026006. arXiv: 1511.08955 [hep-th].

[61] John Estes et al. "On Holographic Defect Entropy". In: *JHEP* 05 (2014), p. 084. DOI: 10.1007/JHEP05(2014)084. arXiv: 1403.6475 [hep-th].

[62] Maximo Banados et al. "Geometry of the (2+1) black hole". In: *Phys. Rev. D* 48 (1993). [Erratum: Phys.Rev.D 88, 069902 (2013)], pp. 1506–1525. DOI: 10.1103/PhysRevD.48.1506. arXiv: gr-qc/9302012.

[63] Paolo Braccia, Aldo L. Cotrone, and Erik Tonni. "Complexity in the presence of a boundary". In: *JHEP* 02 (2020), p. 051. DOI: 10.1007/JHEP02(2020)051. arXiv: 1910.03489 [hep-th].

[64] Michael Gutperle and Andrea Trivella. "Note on entanglement entropy and regularization in holographic interface theories". In: *Phys. Rev. D* 95.6 (2017), p. 066009. DOI: 10.1103/PhysRevD.95.066009. arXiv: 1611.07595 [hep-th].

[65] Cesar A. Agón, Matthew Headrick, and Brian Swingle. "Subsystem Complexity and Holography". In: *JHEP* 02 (2019), p. 145. DOI: 10.1007/JHEP02(2019)145. arXiv: 1804.01561 [hep-th].

[66] Raimond Abt et al. "Topological Complexity in AdS_3/CFT_2". In: *Fortsch. Phys.* 66.6 (2018), p. 1800034. DOI: 10.1002/prop.201800034. arXiv: 1710.01327 [hep-th].

[67] Yuki Nakaguchi, Noriaki Ogawa, and Tomonori Ugajin. "Holographic Entanglement and Causal Shadow in Time-Dependent Janus Black Hole". In: *JHEP* 07 (2015), p. 080. DOI: 10.1007/JHEP07(2015)080. arXiv: 1412.8600 [hep-th].

[68] Roberto Auzzi et al. "On subregion action complexity in AdS_3 and in the BTZ black hole". In: *JHEP* 01 (2020), p. 066. DOI: 10.1007/JHEP01(2020)066. arXiv: 1910.00526 [hep-th].

[69] Tadashi Takayanagi. "Holographic Dual of BCFT". In: *Phys. Rev. Lett.* 107 (2011), p. 101602. DOI: 10.1103/PhysRevLett.107.101602. arXiv: 1105.5165 [hep-th].

[70] Mitsutoshi Fujita, Tadashi Takayanagi, and Erik Tonni. "Aspects of AdS/BCFT". In: *JHEP* 11 (2011), p. 043. DOI: 10.1007/JHEP11(2011)043. arXiv: 1108.5152 [hep-th].

[71] M. Abramowitz and I. Stegun. *Handbook of Mathematical Functions*. fifth edition, Dover (1964), New York.